NASA Contractor Report 195026

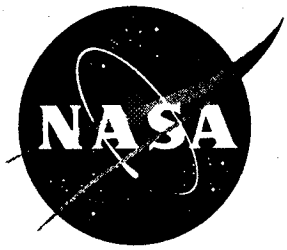

Guidance and Control Requirements for High-Speed Rollout and Turnoff (ROTO)

Steve H. Goldthorpe, Alan C. Kernik, Larry S. McBee, and Orv W. Preston
McDonnell Douglas Corporation, McDonnell Douglas Aerospace Transport Aircraft, Long Beach, California

Contract NAS1-19703 Task 3

January 1995

National Aeronautics and Space Administration
Langley Research Center
Hampton, Virginia 23681-0001

TABLE OF CONTENTS

1.0 SUMMARY 1

2.0 INTRODUCTION 2

OBJECTIVES 2

ASSUMPTIONS 3

3.0 MODELING 4

ROTO EXIT GEOMETRY 4

AIRCRAFT SIMULATION 5

AIRCRAFT ACTUATION SYSTEMS 6

TIRE-RUNWAY COEFFICIENT OF FRICTION MODEL 7

FORCES ON THE AIRCRAFT 8

AIRCRAFT EQUATIONS OF MOTION 13

NAVIGATION 16

WINDS 16

AUTOBRAKING CONTROL LAW 16

STEERING CONTROL LAW 17

SIMULATION DATA 19

4.0 RESULTS 22

REQUIREMENTS 22

5.0 DESCRIPTION OF TEST DATA 26

6.0 CONCLUSIONS AND RECOMMENDATIONS 31

7.0 REFERENCES 32

APPENDIX A I

SURVEY OF RUNWAY COEFFICIENT OF FRICTION MEASUREMENT I

1.0 SUMMARY

Braking and steering requirements for a high speed Rollout and Turnoff (ROTO) system applicable to transport class aircraft are developed and described herein. These requirements were developed with the aid of a non-real time simulation program incorporating airframe and gear dynamics as well as candidate steering and braking guidance algorithms. An objective of a ROTO system meeting these requirements is to assure that the target aircraft can land with an interarrival spacing of 2 nautical miles. Turnoff speeds of 70 knots are allowed with dry and wet surface conditions.

Time history data from the ROTO simulation are documented herein. Parameters which were treated as variables in the simulation study include aircraft weight and CG, runway friction, sensor noise, longitudinal touchdown conditions, runway geometry, and rudder actuator type.

Runway occupancy time is measured from the time the aircraft crosses the runway threshold until its wing tip clears the near side of the runway. 30 degree exit geometries are assumed. Auto-asymmetric braking (steering) is required for aft C.G. aircraft. It also allows for less symmetric braking (deceleration) on the exit until the wing tip clears the runway side, thereby improving runway occupancy times.

The dispersion certified for MD-11 CATIIIB is acceptable (longitudinal dispersion from 250 to 2500 feet past threshhold). Using this longitudinal dispersion, seven ROTO exits are required at and between 3000 and 9000 feet past the runway threshhold (spaced 1000 feet apart), to satisfy runway occupancy time for 2 nautical mile spacing.

Requirements documented in this report are valid for the assumptions/models used in this simulation. It is believed that the results will apply to the general class of transport aircraft; however further effort is required to validate this assumption for the general case.

2.0 INTRODUCTION

OBJECTIVES

The objective of this study is to define the initial requirements for designing a research ROTO guidance and control system which will be used to develop operational ROTO requirements for both automatic and manual piloted operation under normal and reduced visibility conditions.

The study addresses:

Nose wheel/rudder steering requirements,
Braking/reverse thrust requirements,
Touchdown dispersion requirements, and
Navigation system requirements.

Another objective is to assess the state-of-the-art in the measurement of the runway coefficient of friction for various runway conditions, and identify operational limits and concerns in achieving the coefficient of friction measurement.

ASSUMPTIONS

Surface Conditions

For the initial ROTO requirements only dry and wet surface conditions were considered valid. Further investigations are required to determine the possibilities for conducting ROTO operations during slushy, snow-packed, and icy runway conditions. It is assumed that ROTO exits contain embedded surface sensors which would guarantee dry or wet conditions.

Navigation

This report does not make an assumption about the navigation source. The navigation data dynamics were however modeled using GPS characteristics. It is assumed that available ROTO exit locations/geometries are uploaded to the aircraft during approach.

Guidance

It is assumed that auto-ROTO (steering and braking) will be used with autoland approaches, otherwise manual-ROTO will be used.

Runway Occupancy Time

An overall goal of NASA/FAA research is to reduce aircraft inter-arrival spacing to a distance of 2 nautical miles. For zero-wind approach speeds of 130 and 140 knots, the time to travel 2 nautical miles is, respectively, 55.4 and 51.4 seconds. This study will therefore assume that the runway occupancy time (clearing threshold to wing tip clearing side of main runway) should not exceed 53 seconds. Because autobraking did not meet the 53 second criteria for wet runway conditions, it is assumed that reverse thrust will be used in this situation.

CATIIIB

CATIIIB specifications determined the crosswind (15 kts) and tailwind (10 kts)/headwind (25 kts) magnitudes used in the simulation.

Nose Gear Control

It is assumed that the nose gear dynamics did not include hysteresis due to a cable system. This would reflect a fly-by-wire type nose gear command rather than follow up mechanical cables from the rudder.

3.0 MODELING

ROTO EXIT GEOMETRY

Two exit geometries were investigated in this study. The first exit geometry has an initial constant radius of 2900 ft which transitions tangentially (30 degrees) into a final constant radius of 1500 ft. Theoretically, the lateral G's should not exceed 0.15 if the exit speed is 70 knots or less. The second exit geometry is described in Reference 1. It has a gradually decreasing radius (spiral) which transitions tangentially (30 degrees) into a final constant radius of 800 ft. Both exit footprints are approximately 2200 ft by 600 ft. Figure 3.1 overlays both exits as a comparison.

AIRCRAFT SIMULATION

The aircraft simulation is a 3 degree of freedom (yaw, forward, lateral) computer model of an MD-11. It calculates aerodynamic, thrust and tire forces on the airplane and solves the resulting equations of motion to determine aircraft accelerations, velocities and positions during a simulated turnoff. The simulation also includes hydraulic models of the nosewheel steering, rudder and autobrakes. A flowchart of the computer program is shown in Figure 3.2.

The simulation is started by specifying initial aircraft forward, lateral and yaw positions and velocities. During the run, the ROTO controller subroutine reads in input parameters and sends back nosewheel, rudder and braking commands. The program uses this information to calculate aircraft positions, velocities, accelerations and jerk. Time histories of the output parameters are saved throughout the run for later plotting.

AIRCRAFT ACTUATION SYSTEMS

When the turnoff controller commands a nosewheel position, rudder position or deceleration rate, the command goes to some aircraft actuation system which carries out the command. For example, in the case of the nosewheel, a steering command from the controller goes to a hydraulic valve that ports fluid to a pair of actuators that rotate the nosewheel to the commanded position. This section describes those aircraft systems that convert controller commands to mechanical responses.

Nosewheel Actuation

A block diagram of the nosewheel actuation model is shown in Figure 3.3. The model inputs commanded nosewheel position and outputs nosewheel position. The effects of ground moment on the steering rate are included. Nosewheel steering deadband and rate limit effects result from valve flow characteristics.

Rudder Actuation

The simulated aircraft (MD-11) has both a upper and lower rudder. Each rudder has a tandem actuator with control valve operated either by pilot input or by autopilot input. The dynamics of the actuator is similar for the two modes and a simplified model is used for the simulated aircraft as shown in figure 3.4.

Autobrake Actuation

A block diagram of the autobrake control system is shown in Figure 3.5. the model inputs commanded deceleration and outputs brake pressure. The actuation system is identical to the existing MD11 autobrake system except that instead of 3 available settings (high, medium, low), the actuation model allows the setting to be continuously varied by the turnoff controller. As in the existing system, the model delays all braking until after spoiler deployment to ensure adequate vertical loading of the gear. Full braking ramp rates and gains are only available after nose wheel touchdown.

TIRE-RUNWAY COEFFICIENT OF FRICTION MODEL

The tire-runway coefficient of friction is required to calculate maximum possible runway friction for the lateral and drag tire force calculations. The following method is used to calculate the coefficient for any velocity, runway condition and tire pressure.

1) The tire-runway friction coefficient for dry runways is calculated with the following equation.

$$\mu_{MAX} = (0.93 - 0.0011p) \times (1.0 - 0.0013V_{KTS})$$

where,

p = tire bearing pressure (psi)
V_{KTS} = ground speed (knots)

This is an empirical equation given in Reference 2 with a modification to include the effect of velocity.

2) The friction coefficient for other runway conditions is found by multiplying the dry coefficient by velocity dependent runway condition factors. The equation for wet runway conditions is shown below.

$$\mu_{WET} = \mu_{MAX} \times f_{WET}(V_{KTS})$$

A similar equation is used for icy, snow covered and flooded runway conditions. A simulation run using icy conditions is listed in section 5.

FORCES ON THE AIRCRAFT

The aerodynamic, thrust and tire forces acting on the aircraft are shown in Figure 3.6. The methods used to calculate these forces are given in this section.

Aerodynamic Forces

The aerodynamic forces are calculated using the aerodynamic lift, drag, pitching moment, yaw moment and side force equations given below.

$$ALIFT = lift = q \cdot C_L \cdot S_W$$

$$ADRAG = drag = q \cdot C_D \cdot S_W$$

$$AMOM = \text{pitching moment} = \cdot C_M \cdot S_W \cdot L_{MAC}$$

$$FYAERO = \text{side slip force} = q \cdot C_{Y\beta} \cdot \beta \cdot S_W$$

$$MNAERO = \text{side slip yaw moment} = q \cdot C_{N\beta} \cdot \beta \cdot S_W \cdot B_W$$

$$TR = \text{rudder yaw moment} = q \cdot C_{MR} \cdot \delta_R \cdot S_W \cdot B$$

where,

q = dynamic pressure

β = side slip angle

S_W = wing area

δ_R = rudder angle

L_{MAC} = length of mean aerodynamic chord

B_W = wing span

$C_D, C_L, C_M, C_{Y\beta}, C_{N\beta}, C_{MR}$ = aerodynamic coefficients

The aero coefficients used in the above equations are for an aircraft with gear down and in ground effect. The effects of flaps, slats, spoilers and elevator are included.

Thrust

Thrust can be defined within the program as function of velocity or time. It is determined directly from engine thrust data and is input from look-up tables.

Idle thrust was used for landings with dry surface conditions, while maximum reverse thrust was used for wet conditions. The time histories display the thrust values for each run. Idle and reverse thrust are dependent on airspeed, as is shown in Figures 3.7 and 3.8 respectively. Maximum reverse thrust is achieved within the first 10 seconds of landing. Reverse thrust is stowed at an airspeed of 60 knots and below.

Vertical Tire Forces

Tire vertical forces do not directly affect any of the three degrees of freedom used in the model (lateral, longitudinal, yaw). They are calculated because they affect maximum possible runway friction and therefore affect the lateral and drag tire forces. The following method is used to approximate vertical tire forces.

1)The wing and center gears are lumped together as a single equivalent main gear.
2)The following static equilibrium calculation is used to find loads on the nose gear and the lumped main gear. Refer to Figure 3.9 for variable definitions.

$$P_M = \frac{W \cdot A + AMOM - ALIFT \cdot (A - C) - BDRAG \cdot HCG}{A + B} = \text{lumped main gear load}$$

$$P_N = W - P_M - ALIFT = \text{weight on nose gear}$$

3)A look-up table $\gamma(P_M)$ is used to determine how the lumped main gear load is shared by the wing gears and the center gear. The equations used are shown below.

$$P_{MC} = \gamma(P_M) \cdot P_M$$

$$P_{MW} = (1 - \gamma(P_M)) \cdot P_M$$

The table $\gamma(P_M)$ is based on the relative stiffness of the center and wing gear.

4)The distribution of vertical load on the left and right gear are approximated using the following equilibrium calculation based on the aircraft centripetal acceleration.

$$P_{MR} = \frac{P_{MW}}{2} - \frac{W \cdot HCG}{g \cdot TREAD} \cdot A_C$$

$$P_{ML} = P_{MW} - P_{MR}$$

where,

TREAD=distance between left and right main gears

g = gravitational constant

A_C = aircraft centripetal acceleration (positive right)

Braking Drag Forces

A block diagram of the braking drag loads model is shown in Figure 3.10. Inputs for the model are brake pressure (differential and symetric), tire vertical load and runway friction coefficient. The model outputs total drag force.

The model first calculates the maximum drag force that the brakes can develop at the input pressure assuming no tire slip. An empirical relation based on brake dynamometer data is used for this calculation. This maximum braking drag is then compared with the maximum available runway friction drag. Maximum available runway friction drag depends on the friction coefficient, the vertical tire load, and the tire side force. The smaller of the braking drag and the available runway friction drag is used as the actual brake drag per wheel. Brake drag per wheel is then multiplied by the number of wheels to give total brake drag on the aircraft.

Tire Side Forces

If a tire is yawed with respect to its direction of motion, the ground will react with a side force perpendicular to the wheel plane as illustrated in Figure 3.11. The first step to determine tire side force is to calculate the tire yaw angle. The calculation sequence is listed below. Refer to Figure 3.12 for variable descriptions.

1) Calculate velocity components of the tires.

$\dot{X}_N$ = nosegear forward velocity = $\dot{X} - A \cdot \dot{\psi} \cdot sin\psi$

$\dot{Y}_N$ = nosegear lateral velocity = $\dot{Y} + A \cdot \dot{\psi} \cdot cos\psi$

$\dot{X}_C$ = center gear forward velocity = $\dot{X} + BC \cdot \dot{\psi} \cdot sin\psi$

$\dot{Y}_C$ = center gear lateral velocity = $\dot{Y} - BC \cdot \dot{\psi} \cdot cos\psi$

$\dot{X}_{ML}$ = left wing gear forward velocity = $\dot{X} + R \cdot \dot{\psi} \cdot sin(\alpha_0 + \psi)$

$\dot{Y}_{ML}$ = left wing gear lateral velocity = $\dot{Y} - R \cdot \dot{\psi} \cdot cos(\alpha_0 + \psi)$

$\dot{X}_{MR}$ = right wing gear forward velocity = $\dot{X} - R \cdot \dot{\psi} \cdot sin(\alpha_0 - \psi)$

$\dot{Y}_{MR}$ = right wing gear lateral velocity = $\dot{Y} - R \cdot \dot{\psi} \cdot cos(\alpha_0 - \psi)$

2) Find angle of velocity vector.

ψ_{NV} = nose gear velocity angle = $arctan\left(\frac{\dot{Y}_N}{\dot{X}_N}\right)$

ψ_{CV} = center gear velocity angle = $arctan\left(\frac{\dot{Y}_C}{\dot{X}_C}\right)$

ψ_{MVL} = left wing gear velocity angle = $arctan\left(\frac{\dot{Y}_{ML}}{\dot{X}_{ML}}\right)$

ψ_{MVR} = right wing gear velocity angle = $arctan\left(\frac{\dot{Y}_{MR}}{\dot{X}_{MR}}\right)$

3) Find tire yaw angle.

ψ_N = nose gear yaw angle = $\sigma + \psi - \psi_{NV}$

ψ_C = center gear yaw angle = $\psi - \psi_{CV}$

ψ_{MR} = right wing gear yaw angle = $\psi - \psi_{MVR}$

ψ_{ML} = left wing gear yaw angle = $\psi - \psi_{MVL}$

Due to the relative importance of the nose gear on steering, a more sophisticated model is used for the nose gear than for the wing and center gears. The following describes the differences between the two methods.

Wing and Center Gears

The side loads for the wing and center gear are determined as follows.

$$F_{MR} = \text{right gear side force} = \begin{cases} (4 \text{ wheels}) \cdot N_{MR} \cdot \psi_{MR} & 4 \cdot N_{MR} \cdot \psi_{MR} \le \mu_{MAX} \cdot P_{MR} \\ \mu_{MAX} \cdot P_{MR} & 4 \cdot N_{MR} \cdot \psi_{MR} > \mu_{MAX} \cdot P_{MR} \end{cases}$$

$$F_{ML} = \text{left gear side force} = \begin{cases} (4 \text{ wheels}) \cdot N_{ML} \cdot \psi_{ML} & 4 \cdot N_{ML} \cdot \psi_{MRL} \le \mu_{MAX} \cdot P_{ML} \\ \mu_{MAX} \cdot P_{ML} & 4 \cdot N_{ML} \cdot \psi_{ML} > \mu_{MAX} \cdot P_{ML} \end{cases}$$

$$F_C = \text{center gear side force} = \begin{cases} (2 \text{ wheels}) \cdot N_C \cdot \psi_C & 2 \cdot N_C \cdot \psi_C \le \mu_{MAX} \cdot P_{MC} \\ \mu_{MAX} \cdot P_{MC} & 2 \cdot N_C \cdot \psi_C > \mu_{MAX} \cdot P_{MC} \end{cases}$$

where,

N_{MR} = cornering power per right wing gear tire

N_{ML} = cornering power per left wing gear tire

N_C = cornering power per center gear tire

μ_{MAX} = maximum ground coefficient of friction

Tire relaxation length effects are included. The tire relaxation length is proportional to the distance a yawed tire must be rolled forward before full side force is developed. It is modeled in the simulation by lagging the side force with a time constant based on ground speed.

Nose Gear

Unlike the main gear model, the nose gear model continuously recalculates cornering power during the simulation. Cornering power is calculated from vertical tire loads and the tire properties listed in the data section.

The cornering power calculation is complicated by the fact the nose gear is not vertical due to its forward cant relative to the aircraft body axes. Therefore, as it is steered left of right from neutral, the vertical load (and cornering power) on one tire increases and that on the other tire decreases. The model accounts for this and calculates cornering power individually for the right and left tire.

The nosewheel model accounts for side force reductions due to lateral tire skidding. The skidding model is based on the results of Reference 3. Also, ground moment about the nosewheel strut is calculated for use in the nosewheel actuation model.

AIRCRAFT EQUATIONS OF MOTION

The forces acting on the aircraft and the reference frames used to derive the equations of motion are shown in Figure 3.13. The equations of motion in terms of the stationary reference axes x-y are given below.

$$\ddot{X} = \frac{1}{m} \cdot \sum F_X$$

$$\ddot{Y} = \frac{1}{m} \cdot \sum F_Y$$

$$\ddot{\psi} = \frac{1}{I_{YAW}} \cdot \sum M_Z$$

where,

m = aircraft mass

I_{YAW} = aircraft yaw moment of inertia

$\sum F_X$ = sum of forces in X direction

$\sum F_Y$ = sum of forces in Y direction

$\sum M_Z$ = sum of yaw moments

Since forces are derived in terms of the aircraft body axes, it is convenient to make the following substitutions.

$$\sum F_X = \cos\psi \cdot \sum F_U - \sin\psi \cdot \sum F_V$$

$$\sum F_Y = \sin\psi \cdot \sum F_U + \cos\psi \cdot \sum F_V$$

$$\ddot{X} = \frac{d}{dt}(U \cdot \cos\psi - V \cdot \sin\psi)$$

$$\ddot{Y} = \frac{d}{dt}(U \cdot \sin\psi + V \cdot \cos\psi)$$

Taking derivatives, substituting and rearranging gives the following equations of motion in terms of aircraft body axes U-V.

Aircraft Accelerations

$$\dot{V} = \frac{1}{m} \cdot \sum F_V - U \cdot \dot{\psi}$$

$$\dot{U} = \frac{1}{m} \cdot \sum F_U + V \cdot \dot{\psi}$$

$$\ddot{\psi} = \frac{1}{I_{YAW}} \cdot \sum M_Z$$

where,

$$\sum F_V = F_{NOSE} \cdot cos\sigma + F_{ML} + F_{MR} - \frac{T_R}{L_{TAIL}} + FYAERO + F_C$$

$$\sum F_U = -F_{NOSE} \cdot sin\sigma - BDRAGR - BDRAGL - BDRAGC - ADRAG + THRUST$$

$$\sum M_Z = F_{NOSE} \cdot A \cdot cos\sigma - (F_{ML} + F_{MR}) \cdot B - F_C * BC + TR + MNAERO + \frac{TREAD}{2} \cdot (BDRAGR - BDRAGL)$$

Aircraft velocities and positions are found by integrating accelerations as follows.

Aircraft Velocities (body axes)

$$V = \int \dot{V} dt$$

$$U = \int \dot{U} dt$$

$$\dot{\psi} = \int \ddot{\psi} dt$$

Aircraft Velocities (reference axes)

$$\dot{X} = U \cdot cos\psi - V \cdot sin\psi$$

$$\dot{Y} = V \cdot cos\psi + U \cdot sin\psi$$

$$\dot{\psi} = \int \ddot{\psi} dt$$

Aircraft Positions (reference axes)

$$X = \int \dot{X} dt$$

$$Y = \int \dot{Y} dt$$

$$\psi = \int \dot{\psi} dt$$

NAVIGATION

This simulation did not combine the navigation source with inertial guidance, which might improve performance. Gusting/noise simulation runs combined the navigation position signal X and Y with noise having the characteristic of 4 feet * N(0 mean ,1 unity variance) lagged with a 30 second time constant. The time histories of gust/noise simulation runs show an accuracy of +/- 2 feet. Navigation velocity data was not used. The navigation position data dropout was simulated as 2% using a uniformly distributed random number. When data was dropped out, the last good data was used in its place. It is assumed that data marked as valid is in fact valid.

WINDS

Steady longitudinal winds ranged from a 10 knot tailwind to a 25 knot headwind, depending on the run. A steady crosswind of 15 knots was used for non-gusting simulation runs. It was found that a positive steady crosswind, blowing in a positive Y to negative Y direction, is worst case for a right hand turn used in these studies. The gusting/noise simulation runs used a dryden filter with a sigma of 22.5 for the crosswind. The gusting crosswind reached values of 15 knots in the simulation runs.

AUTOBRAKING CONTROL LAW

The autobraking control law provides a variable deceleration command to the autobrake system. The purpose is to decelerate the aircraft as it approaches the available ROTO exits and on the ROTO exit so that the aircraft may stop prior to the taxiway. The deceleration command is rate limited so as to minimize longitudinal jerk. The autobrake control law is updated at 20 Hz. Inputs to the autobraking control law are the aircraft ground speed and the position/geometry of all available exits. It is assumed that current available exit information is uploaded to the aircraft during approach.

At nose gear touchdown the autobrake logic calculates the <u>minimum</u> deceleration needed to exit at the first available ROTO exit at the desired exit speed (70 knots). The deceleration command is calculated as such:

$$\text{deceleration command} = \frac{-\left(\left(\text{desired exit speed}\right)^2 - \left(\text{current ground speed}\right)^2\right)}{\text{braking distance} * 2.0}$$

If the required deceleration is greater than the <u>maximum</u> allowed value (i.e. 9 feet/sec**2), the control law recalculates the required deceleration using the next available ROTO exit as the exit goal (braking distance would change). The deceleration calculation is ongoing in case the aircraft is not decelerating as expected due to unexpected friction conditions. The deceleration command is smoother if braking distance is calculated as actual braking distance * fraction (0.85). This creates a buffer distance at which the aircraft should have already reached the desired speed. The buffer distance decreases in size as the exit nears. As noted

earlier, under wet runway conditions maximum reverse thrust (manual) was used to decelerate the aircraft which results in little, if any, requirement for autobraking.

On the ROTO exit the control law decelerates the aircraft to a stop without exceeding 9 feet/sec**2. The stopping position may be prior to the aircraft reaching the taxiway, if desired. If asymmetrical braking is used for steering, it is possible to brake minimally on the exit until the aircraft wing tip clears the side of the runway.

STEERING CONTROL LAW

The steering control law used for this study started with the proportional/integral MD-11 rollout control law as a baseline. A general diagram of the steering control law is shown in Figure 3.18. The inputs and outputs of this control law are as follows:

Inputs
X and Y position of aircraft. X and Y position of runway centerline.
(used to create lateral displacement and displacement rate inputs)
Aircraft yaw rate (yaw damping).
Ground speed (gain scheduling).

Output
Rudder command.
Nose gear steering command (follow up mechanical cables from rudder).

The modified ROTO control law added these inputs and outputs.

Additional Inputs
X and Y position of centerline as it continues onto the ROTO exit(s).
(need all available exit centerline(s), i.e. exit geometries.)
Centerline radius, derived from exit centerline data.
(additional feedback to minimize lateral displacement error)
Aircraft CG, derived from trim horizontal stabilizer setting during approach.
(used to command elevator)

Additional Outputs
Nose gear steering command (direct command, no cable hysteresis).
Elevator command.
Right and left main gear asymmetric deceleration commands (steering).

The steering control law is updated at 20 Hz. Two main features were added to the control law. One was to use the exit centerline radius as an added feedback to minimize the lateral displacement error (lean into exit curve). The second feature was for exits with a constant radius entrance. These exits cause a large jerk because there is an instantaneous change in centrifugal force as the radius begins. To prevent a large lateral jerk, the control law was modified to smoothly increase the lateral acceleration to nominal lateral acceleration as

defined by ROTO exit radius and desired exit speed (i.e. easy-on the nominal lateral acceleration). The lateral acceleration is increased at maximum allowable lateral jerk. This procedure is begun at a distance prior to the exit based on the aircraft speed and how many seconds are required to ramp up the lateral acceleration. This feature is not needed for spiral exits and causes the entrance of a constant radius exit to mimic a spiral exit. During the pre-exit lateral acceleration, the lateral position of the aircraft changes less than a foot due to the commanded lateral acceleration.

SIMULATION DATA

Aircraft Geometry Data

Variable Name	Description	Value	Units
A	distance -- nose gear to center of gravity (CG)	72.982 (fwd cg) 78.256 (aft cg)	feet
B	distance -- main gear to CG	7.732 (fwd cg) 2.457 (aft cg)	feet
BC	distance -- center gear to CG	10.284 (fwd cg) 5.009 (aft cg)	feet
BW	wing span	165.37	feet
C	distance -- lift moment arm to CG	-3.056 (fwd cg) 2.218 (aft cg)	feet
HCG	CG height	15.476 (fwd cg) 15.466 (aft cg)	feet
LMAC	length of mean aerodynamic chord	24.648	feet
LTAIL	distance -- CG to tail center of pressure	83.739	feet
SW	wing area	3647.5	$feet^2$
TREAD	distance between wing landing gears	34.677	feet

Note: fwd cg = 12.6% mean aerodynamic chord (MAC), aft cg = 34% MAC.

Aircraft Weight and Inertia

Variable Name	Description	Value	Units
IYAW	aircraft yaw moment of inertia	2.56E7	$slug\text{-}ft^2$
W	aircraft weight	480,000 (heavy) 340,000 (light)	lbs

Aerodynamic Coefficients

Variable Name	Description	Value	Units
CDRAG	aircraft drag coefficient	.1746 (fwd cg) .1651 (aft cg)	-
CLIFT	aircraft lift coefficient	.123 (fwd cg) .226 (aft cg)	-
CMOM	aircraft pitch moment coefficient	.515 (fwd cg) .216 (aft cg)	-
CMR	rudder yaw moment coefficient	-.00262	1/degree
CNB	aircraft side slip moment coefficient	.0037	-
CYB	aircraft side slip force coefficient	-.024	-

Elevator effect: add .008 per elevator deg to CLIFT, -.025 per elevator deg to CMOM

Wing and Center Gear Tire Properties

Variable Name	Description	Value	Units
NC	center gear cornering power per tire	4426	lbs/deg
NM	wing gear cornering power per tire	4806	lbs/deg
SPM	wing and center gear tire static pressure	188	psi

Constants Used to Calculate Nose gear Cornering Power and Strut Moment

Variable Name	Description	Value	Units
DELB	nose gear tire deflection at load RB	1.1	inch
DELS	nose gear tire rated deflection	3.4	inch
HS	nose gear tire section height	9.8	inch
OD	nose gear tire outside diameter	39.6	inch
RB	nose gear tire vert. load at deflection DELB	8000	lbs
RP	nose gear tire rated pressure (loaded)	203	psi
RS	nose gear tire rated load	39500	lbs
S	nosewheel spacing	25	feet
SP	nose gear tire static pressure (loaded)	167	psi
THETA	nosewheel forward cant angle	9.5	degrees
WS	nose gear tire section width	15.5	inch

Nosewheel Actuation

Variable Name	Description	Value	Units
KS1	(steering valve spool displacement) / (steering error)	.00873	in/degree
KS2	(steering rate)/(valve flow)	.676	$(deg/s)/(in^3/sec)$
KS3	(steering actuator pressure) / (strut ground moment)	.00842	psi/in-lb

Autobrake Actuation

Variable Name	Description	Value	Units
RRPHASE1	phase 1 brake pressure ramp rate	400	psi/sec
RRPHASE2	phase 2 brake pressure ramp rate	1200	psi/sec
KBPHASE1	phase 1 brake pressure gain	600	$(psi/sec)/(ft/sec^2)$
KBPHASE2	phase 2 brake pressure gain	1800	$(psi/sec)/(ft/sec^2)$
TMGD	main gear touchdown time	0	sec
TNGD	nose gear touchdown time	6	sec
TSPOIL	time between main gear touchdown and spoiler deployment	1.3	sec
TDELAY	time between spoiler deployment and start of brake ramp	3	sec

Hydraulic System

Variable Name	Description	Value	Units
PSUP	hydraulic supply pressure	3000	psi
PRET	hydraulic return pressure	60	psi

Functions

Function	Figure
idle thrust vs. aircraft velocity	3.7
reverse thrust vs. time, velocity	3.8
runway condition factors for friction coefficient vs. velocity	3.14
nosewheel max side mu vs. side slip velocity	3.15
fraction of main gear load supported by center gear vs. main gear load	3.16
steering valve flow gain curve	3.17

4.0 RESULTS

REQUIREMENTS

The approach taken to develop steering and braking requirements for the high speed rollout and turnoff system was to first develop a candidate steering and braking control system and evaluate the performance thereof using a high fidelity simulation. Nominal values were defined for the parameters of interest. Second, the critical parameters were varied until the limiting values were determined which still satisfied the performance requirements.

The simulation has been described in section 3.0 and the simulation data which forms the basis of the requirements is contained in section 5.0. A description of the specific requirements developed using the simulation follows.

A. Nose Wheel/Rudder Steering Requirements:

Minimum parameter values for the rudder actuators are:

Position limit:	23 degrees
Rate limit:	
upper:	63 deg/sec
lower:	43 deg/sec
Deadband:	0.091 degrees (of rudder)
Actuator bandwidth:	
upper:	19.5 radians/sec
lower:	13.5 radians/sec

Minimum parameter values for the nose gear actuator are:

Position limit:	8 degrees
Rate limit:	11.1 deg/sec
Deadband:	1.15 degrees (of nose gear)
Actuator bandwidth:	2.9 rad/sec

B. Braking/Reverse Thrust Requirements (deceleration):

No unique requirements were identified for the aircraft braking system other than a limitation on the rate at which the braking action is modified. This is for passenger comfort and was set at .05 g/sec based on results of previous studies. The algorithms for application of braking pressure are of course critical and must be designed to minimize the maximum deceleration that is required to achieve the desired exit speed at the high speed turnoff.

The simulation determined that a high speed turnoff can not be achieved with braking alone for non-dry surface conditions; reverse thrust is a requirement in this case. However, it was determined that the use of maximum reverse thrust for some cases results in a deceleration greater than the nominal value required to decelerate the aircraft to the desired exit velocity. Therefore, the aircraft may be slowed below the desired exit speed which could result in a runway occupancy time greater than expected.

C. Asymmetric Braking Requirements (steering):

Auto asymmetric braking is required to assist in steering aft C.G. aircraft and to allow for minimal deceleration (symmetrical braking) on the exit until the aircraft wing tip clears the runway side.

D. Touchdown Dispersion Requirements:

Due to a limitation of time available, a definitive assessment of touchdown point sensitivity on ROTO performance capabilities was not possible. The simulation data collected and reported herein used the two sigma extremes of allowable touchdown dispersion accepted by the FAA autoland criteria for the test cases. The shortest landing point used was 250 feet beyond runway threshold and the longest point was 2500 feet beyond runway threshold.

The worst cases are: i) a light (therefore slow) aircraft in a headwind condition which lands short and barely reaches the first ROTO exit within the time window; and ii) a heavy (fast) aircraft landing with a tail wind which lands long and nearly misses the last ROTO exit.

The two extreme longitudinal dispersions used are as follows:

Landing Type	Touchdown past Threshold (feet)	Airspeed (knots)	Tailwind (knots)	Crosswind (knots) steady or gusting
early, slow, light	250	130	-25	15
late, fast, heavy	2500	166	10	15

All test cases following these requirements (runs 1-16) satisfied the ROTO runway occupancy time criteria (< 52.6 seconds).

E. Runway Coefficient of Friction
[See section entitled Runway Coefficient of Friction Measurement]

F. Navigation Requirements:

The accuracy of the navigation source is critical. The requirements for navigation accuracy are interactive with the other system requirements.

Steering and braking requirements defined herein are compatible with a navigation accuracy of +/- two feet.

The source of position data on which the steering and braking control laws are based can be updated as slow as 10 samples/sec. No inertial smoothing is assumed in this study.

G. General System Requirements:

Maximum levels of acceleration and jerk are set by passenger comfort requirements.

Acceleration and jerk:

Lateral acceleration and jerk should not be allowed to exceed +/- 0.15 G and +/- 0.05 G/sec respectively.

Longitudinal acceleration and jerk should not be allowed to exceed +/- 0.25 G and +/- 0.05 G/sec respectively.

ROTO exit selection and speed:

An available ROTO exit will be bypassed and the next available ROTO exit selected if the aircraft requires a deceleration greater than 9 ft/sec/sec to reach a selected exit at its desired exit speed (70 knots for both dry and wet surface conditions). The autobraking strategy is described in section 3 (Modeling) under the Autobraking Control Law heading. The commanded deceleration is the minimum necessary to arrive at an exit at a desired speed. The deceleration may creep upwards as needed as the aircraft approaches the exit.

ROTO exit geometry:

The exit should be designed such that, at any given point along the exit radius, if the aircraft is at the design ground speed and tracking the curve accurately, lateral acceleration should not exceed 0.15 G. Similarly, the exit geometry, when traversed as designed, should not induce a lateral jerk value in excess of 0.05 G. This latter requirement essentially imposes a requirement for a spiral exit geometry since a constant radius exit normally results in the aircraft experiencing relatively large jerk values. Is it possible however, for a control law to give a constant radius exit the entrance jerk characteristics of a spiral exit.

ROTO exit locations:

Seven ROTO exits are required at and between 3000 and 9000 feet past the runway threshhold, spaced 1000 feet apart. Strategies may exist to decrease the number of exits to three, beginning at approx. 5000 ft from the runway threshhold and spaced 2000 feet apart. Possible approaches may be to require a smaller longitudinal touchdown dispersion (requiring improved glideslope guidance) allowing for exits to be spaced further apart, use auto reverse thrust (minimizing premature manual deceleration prior to the first exit) thereby

not needing the first two exits, and delaying initial commanded deceleration until all aircraft are out of the dispersion box (attempt to minimize the affects of dispersion and normalize the deceleration profile for all aircraft). Each of these approaches has costs, safety and operational issues associated with them in an attempt to minimize the cost of ROTO exit construction and maintenance.

ROTO control laws:

The algorithms implemented in the developmental simulation were found to function adequately with iteration rates at a minimum of 20 Hz.

The only general constraints on control laws are to impose the appropriate command limits that allow staying within the stated lateral and longitudinal acceleration limits.

Specifically, lateral steering commands are limited such that the product of turn rate and ground speed is less than 0.15 G; and the braking command is constrained to limit the commanded longitudinal deceleration to less than 0.25 G.

Reverse Thrust:

Reverse thrust must be available for ROTO execution on non-dry surface conditions.

Surface Conditions:

Conditions other than dry or wet runways (i.e., ice, snow, slush) prohibit the use of high speed ROTO use. For example, simulation run 23 in the test data section shows that a heavy aircraft landing late and fast on an untreated icy surface was not able to decrease its speed to below 70 knots (using maximum reverse thrust) prior to the last ROTO exit at 9000 feet past the runway threshold. For this study, dry and wet conditions represent friction coefficients. Other meteorological conditions may also be treated to meet the minimum required wet friction coefficient. However the friction coefficient must be uniform along the aircraft path, especially on the ROTO exit. Uniformity may be more difficult for treated non-dry/wet conditions (i.e. patches of untreated ice, squall (flooding) conditions on different areas of the runway, etc.).

5.0 DESCRIPTION OF TEST DATA

24 MD-11 ROTO time histories using a spiral exit are documented while varying weight, CG, runway friction, noise inputs, and longitudinal touchdown conditions. In order to show extreme cases for this study, a heavy weight MD-11 at 480,000 lbs lands late (2500 feet) at high speed (166 knots) with a tailwind of 10 knots. A light weight MD-11 at 340,000 lbs lands early (250 feet) at low speed (130 knots) with a headwind of 25 knots. These two cases are repeated for a total of 16 runs with combinations of 12/34 % CG, dry/wet surface and clear/noise conditions. The 'clear' runs had a steady positive 15 knot crosswind from the left (negative to positive y direction) while the 'noise' runs had a gusting 15 knot crosswind. All runs are summarized in Table 1 and documented in Figures 5.1 through 5.48 (2 pages/run, run number in title).

The first 16 runs used auto-asymmetric braking, with the maximum runway occupancy time being 52.6 seconds. Runs 17-19 repeat earlier runs but do not use auto-asymmetric braking. Of these three runs, run 17 has the greatest runway occupancy time of 59.1 seconds, due to its required 55 knot exit speed for adequate steering of aft C.G. aircraft without auto-asymmetric braking. Auto-asymmetric braking also allows for minimal deceleration on the exit prior to the wing tip clearing the near side of the runway. Minimizing initial deceleration on the exit cuts about 1.5 seconds from the runway occupancy time (compare runs 18 and 19 with runs 10 and 9).

Run 20 illustrates the aircraft stopping on the exit prior to the taxiway. Runs 21 and 22 illustrate the need for ROTO exits to be spaced 1000 feet apart (only exits spaced 2000 feet apart were available during these runs). The dispersion box is 2250 feet long. When an aircraft lands in the middle of the box, approximately 1000 feet from either end, many seconds may elapse before the aircraft reaches the next available exit. This situation is worst for slow aircraft as seen with run 22 having a runway occupancy time of 63.6 seconds. The placement of the ROTO exits in this study, spaced 2000 feet apart, was optimized for touchdown at the beginning and end of the dispersion box.

Run 23 simulates a heavy aircraft landing late and fast on untreated icy surface conditions. The aircraft was not able to slow to the 70 knot ROTO exit speed prior to the last ROTO exit at 9000 feet past the runway threshold. Run 24 simulates the use of the constant 2900 ft radius exit, with acceptable results. Run 24 has a runway occupancy time 3 seconds less than run 2 using the spiral exit because the constant radius veers away from the runway more quickly.

Simulation runs which include the gusting crosswind do not display lateral and longitudinal jerk because their large magnitude impaired the visibility of the other time traces. The non-gust simulation runs 1-16 show that longitudinal jerk is greater than the desired 0.05 G/sec at the onset of autobrakes after touchdown and during the exit when auto-asymmetric brakes are used for steering. The first situation is due to the autobrake torque having a threshold breakout pressure, as seen in figure 3.10. The autobrake control law has a deceleration command rate limit, but it does not correct the sudden increase of torque at the pressure

breakout. To overcome the pressure breakout when auto-asymmetric braking is active, a minimal symmetric braking command is summed with the asymmetric command so that the brake pressure is always above the breakout. Runs 1-16 show that longitudinal jerk is still a problem with auto-asymmetric braking, unlike runs 17-19 without auto-asymmetric braking, necessitating further study.

Table 1

Run #	Dry or Wet Conditions	Slow or Fast Touchdown	Clear or Gust Conditions	Weight %CG	Runway Time (sec)
1	Dry	Fast	Clear	480klb, 34	52.1
2	Wet	Fast	Clear	480klb, 34	52.1
3	Dry	Fast	Gust	480klb, 34	52.1
4	Wet	Fast	Gust	480klb, 34	52.6
5	Dry	Slow	Clear	340klb, 34	31.8
6	Wet	Slow	Clear	340klb, 34	33.3
7	Dry	Slow	Gust	340klb, 34	31.8
8	Wet	Slow	Gust	340klb, 34	33.8
9	Dry	Fast	Clear	480klb, 12	52.1
10	Wet	Fast	Clear	480klb, 12	52.1
11	Dry	Fast	Gust	480klb, 12	52.1
12	Wet	Fast	Gust	480klb, 12	52.6
13	Dry	Slow	Clear	340klb, 12	32.3
14	Wet	Slow	Clear	340klb, 12	42.7
15	Dry	Slow	Gust	340klb, 12	32.3
16	Wet	Slow	Gust	340klb, 12	43.2
17	Repeat run 2 without auto-asymmetric braking (steering).				59.1
18	Repeat run 10 without auto-asymmetric braking (steering).				53.6
19	Repeat run 9 without auto-asymmetric braking (steering).				53.6
20	Repeat run 2 but stop on the exit prior to the taxiway.				52.1
21	Repeat run 4 but land 1000 feet earlier, ~ dispersion center. (shows need for spacing ROTO exits 1000 feet apart)				54.2
22	Repeat run 8 but land 1250 feet later, ~ dispersion center. (shows need for spacing ROTO exits 1000 feet apart)				63.6
23	Repeat run 2 but with untreated icy conditions				>100
24	Repeat run 2 but with constant radius (2900 ft) ROTO exit				49.1

Each simulation run is documented with two pages of time histories. When a plot shares more than one variable, the second variable is usually plotted on the right hand Y axis. The zero origin of the left and right axis are usually offset so that the variable time histories do not cross each other. The X axis of all plots is the runway longitudinal axis in feet. -3000 feet is the runway threshold. The first ROTO exit is at position 0. ROTO exits are positioned every 2000 feet thereafter in these simulation runs. A 1000 foot exit separation is listed as a requirement in this report.

Page 1; Bottom Plot
This plot shows two views of the aircraft position relative to the runway with a right hand ROTO turnoff. The left axis shows the aircraft Y position in feet. The runway centerline is

along the top of the plot. The desired path is along the centerline and then curves to the right as the right-handed ROTO exit. A solid line tracks the (dashed) exit path.

The right axis shows the aircraft Y lateral displacement (solid line) in feet from the runway centerline and exit path. The straight-lined funnel shape represents the allowable lateral width in which the aircraft can move without running off the pavement. The funnel width is the runway and ROTO exit widths minus the aircraft main gear offset (in this case 20 feet per side).

Page 1; 2nd from Bottom Plot
The left axis plots the aircraft ground speed in knots (decreasing trace). This is a summation of airspeed (not including gusts) and tailwind/headwind. The right axis plots the aircraft runway occupancy time in seconds. The runway occupancy time at touchdown begins at a value greater than zero because it begins counting at the runway threshold. The runway occupancy time flattens when the aircraft wing tip clears the near side of the runway.

Page 1; Middle Plot
The left axis plots the aircraft lateral acceleration in G's (lower trace). The right axis plots the aircraft lateral jerk in G/sec. Gust cases do not plot the lateral jerk.

Page 1; 2nd from Top Plot
The left axis plots the aircraft longitudinal acceleration in G's (lower trace). The right axis plots the aircraft longitudinal jerk in G/sec. Gust cases do not plot the longitudinal jerk.

Page 1; Top Plot
The left axis plots the percentage of available aircraft braking in use (lower trace). The right axis plots the aircraft total thrust in pounds. Non-dry conditions use reverse thrust.

Page 2; Bottom Plot
The left axis plots the aircraft rudder position in degrees (lower trace). The right axis plots the nose gear position in degrees.

Page 2; 2nd from Bottom Plot
The left axis plots the aircraft nose gear μ (lower trace). The right axis plots the available aircraft nose gear μ.

Page 2; 3rd from Bottom Plot
The left axis plots the aircraft main right gear μ (lower trace). The right axis plots the available aircraft main right gear μ.

Page 2; 4th from Bottom Plot
The left axis plots the aircraft main center gear μ (lower trace). The right axis plots the available aircraft main center gear μ.

Page 2; 3rd from Top Plot

The left axis plots the aircraft yaw angle with respect to the aircraft track angle in degrees. The right axis plots the aircraft elevator angle in degrees (gradually rising trace).

Page 2; 2nd from Top Plot
The left axis plots the steady tailwind (10) in knots. A headwind would have a negative value (-25). The right axis plots the crosswind in knots. If the crosswind is steady it will have a value of 15. A positive crosswind blows in a negative Y to positive Y direction. Gust cases will show a varying crosswind.

Page 2; Top Plot
The left axis plots the navigation X position data noise content (lower trace). The right axis plots the navigation Y position data noise content.

6.0 CONCLUSIONS AND RECOMMENDATIONS

The requirements listed in this report satisfy the aircraft inter-arrival spacing of 2 nautical miles. For zero-wind approach speeds of 130 and 140 knots, the time to travel 2 nautical miles is, respectively, 55.4 and 51.4 seconds. The maximum runway occupancy time using the requirements in this study is 53 seconds with runway occupancy time measured from the runway threshold until the aircraft wing tip clears the runway side. See Table 1 in the results section of this report. Auto-asymmetric braking (steering) is required for aft C.G. MD-11 type aircraft. It also allows for less symmetric braking (deceleration) on the exit until the wing tip clears the runway side, thereby improving runway occupancy times.

The dispersion certified for MD-11 CATIIIB is acceptable (longitudinal dispersion from 250 to 2500 feet past threshhold). Seven ROTO exits are required at and between 3000 and 9000 feet past the runway threshhold, spaced 1000 feet apart.

Two exit geometries were investigated in this study. The first exit geometry has an initial constant radius of 2900 ft (allowing for .15 lateral G's with 70 knot exit speed) which transitions tangentially (30 degrees) into a final constant radius of 1500 ft. The second exit geometry is described in Reference 1. Spiral and constant radius exits have trade-offs. The spiral exit may be exited at a higher speed and has a smoother transition onto the exit. Its drawback is that it takes more exit length for the aircraft wing tip to clear the runway side and has a smaller secondary radius. All of the simulation runs described in this report, except run 24, used the spiral exit because it was a documented ROTO exit shape. Run 24 uses the constant radius exit with acceptable ROTO performance. The constant radius exit is acceptable when allowances are made for it in the steering control law to minimize lateral jerk at the exit entrance.

This study did not investigate other operational airport factors which may not allow for an interarrival spacing of 2 nautical miles.

The initial requirements for designing a research ROTO guidance and control system was defined. The results of this study can be used to develop operational ROTO requirements. Accordingly the recommendation is made that the ROTO concept be further explored by defining the operational ROTO concepts while conducting a variety of landings on a 6 degree of freedom moving base simulator. Evaluation and comparison can be made of the results for both automatic and manual pilot-in-the-loop operations.

7.0 REFERENCES

1. Anon, AIRPORT DESIGN STANDARDS - AIRPORTS SERVED BY AIR CARRIERS - TAXIWAYS, Advisory Circular AC No. 150/5300 - B, U S Department of Transportation, Federal Aviation Administration, Washington DC, 5/9/80.

2. Smiley, R. F., Horne, W. B., MECHANICAL PROPERTIES OF PNEUMATIC TIRES WITH SPECIAL REFERENCE TO MODERN AIRCRAFT TIRES, NASA Technical Report R-64, 1960.

3. Horne, W. B. , Leland, T. J. W., INFLUENCE OF TREAD PATTERN AND RUNWAY SURFACE CONDITIONS ON BRAKING AND ROLLING RESISTANCE OF A MODERN AIRCRAFT TIRE, NASA Technical Note D-1376, September 1962.

FIGURE 3.1.

ROTO Exit Comparison

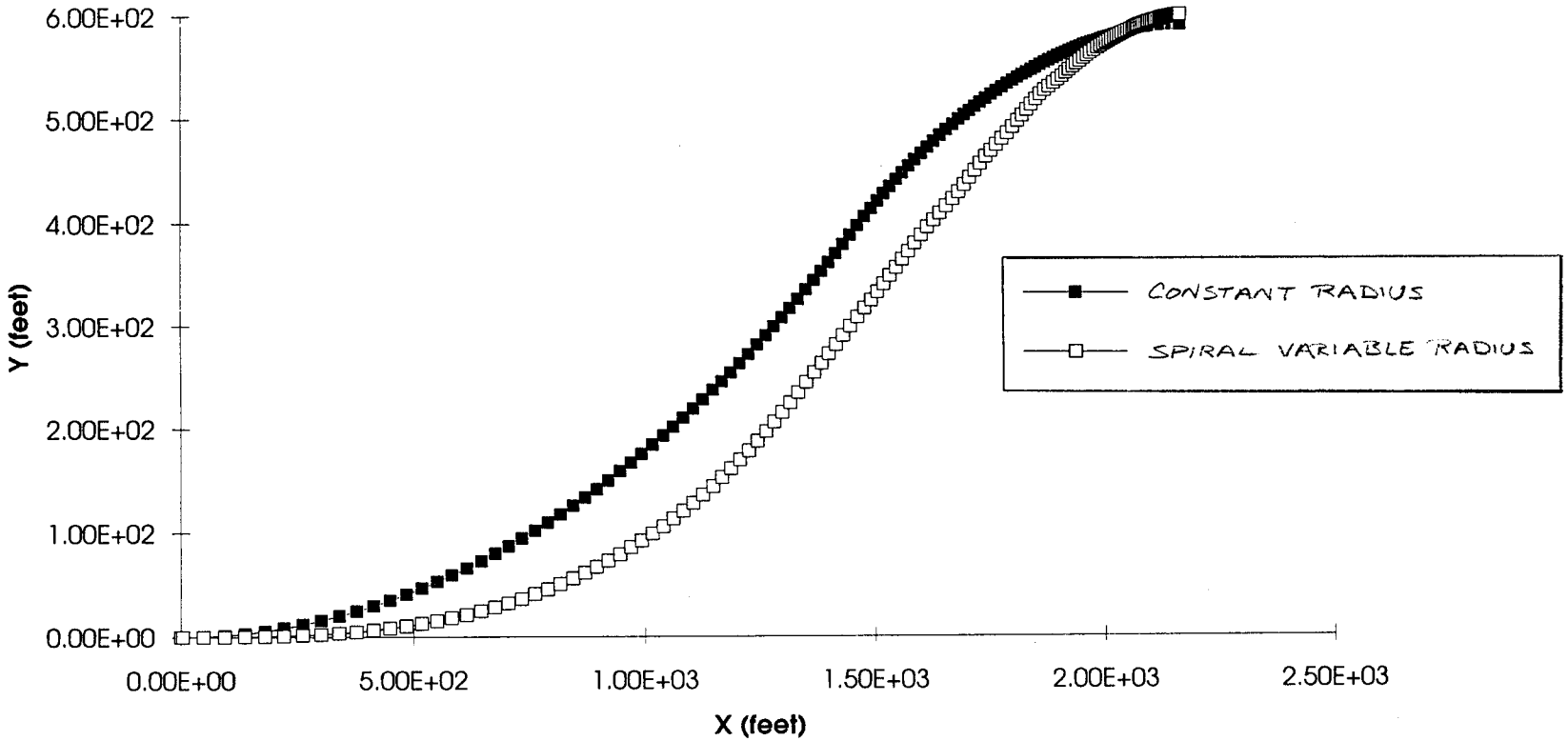

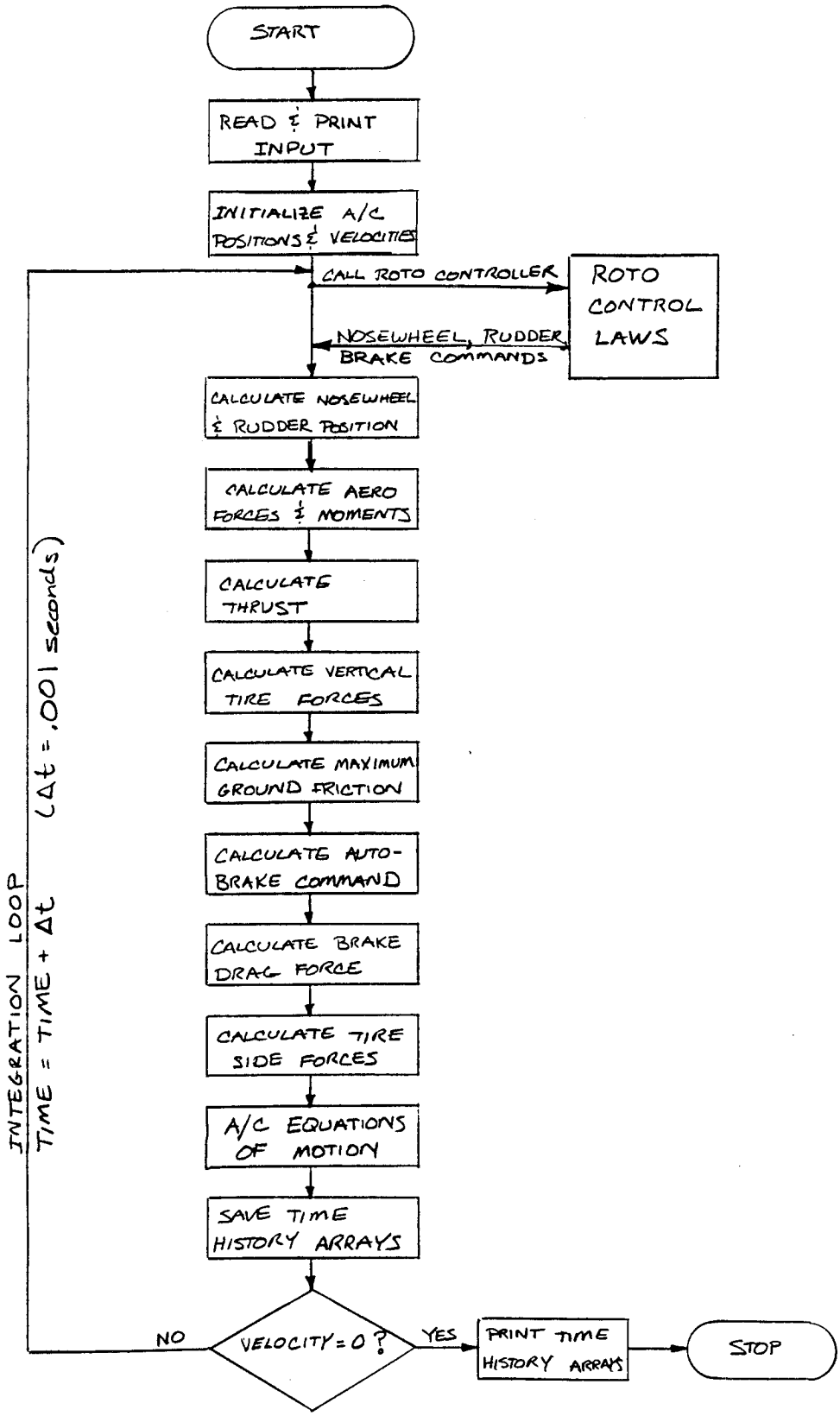

FIGURE 3.2 COMPUTER SIMULATION FLOWCHART

FIGURE 3.3. NOSEWHEEL ACTUATION BLOCK DIAGRAM

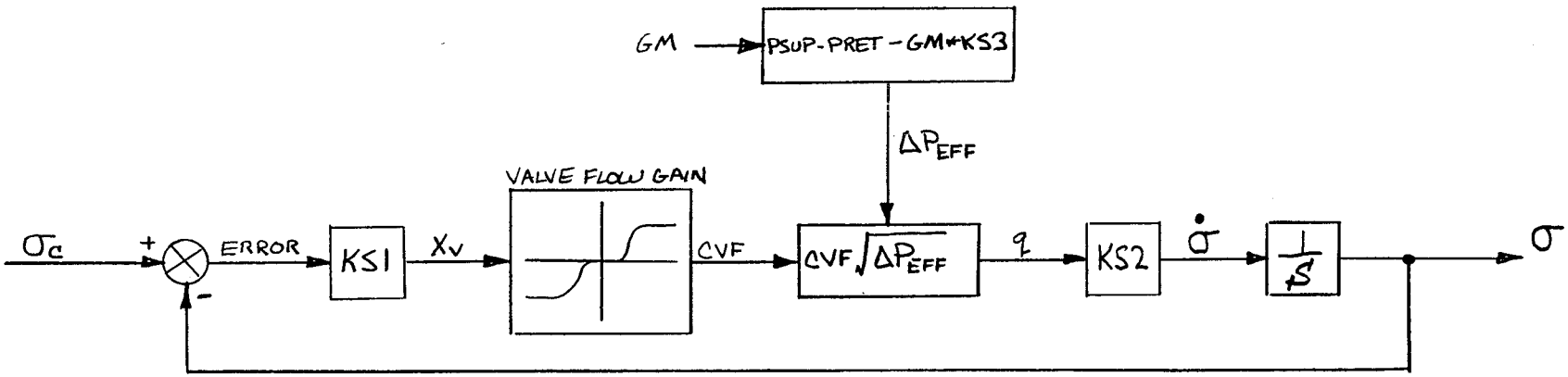

INPUT

σ_c = commanded nosewheel angle (deg)
GM = ground moment on nosewheel strut (in-lbs)

CONSTANTS

KS1 = (valve spool displacement)/error (in/deg)
KS2 = (steering rate)/(valve flow) (deg/sec)/(in^3/sec)
PSUP = hydraulic supply pressure (psi)
PRET = hydraulic return pressure (psi)

INTERNAL VARIABLES

ERROR = error (deg)
CVF = valve flow coefficient (in^3/sec)/$\sqrt{psi}$
$q_{\dot{\sigma}}$ = valve flow (in^3/sec)
$\dot{\sigma}$ = steering rate (deg/sec)
ΔP_{EFF} = effective hydraulic pressure (psi)

OUTPUT

σ = nosewheel angle (deg)

FUNCTION

VALVE(X_V) = CVF (in^3/sec)/$\sqrt{psi}$

CONSTANT VALUES AND FUNCTION GIVEN IN SIMULATION DATA SECTION.

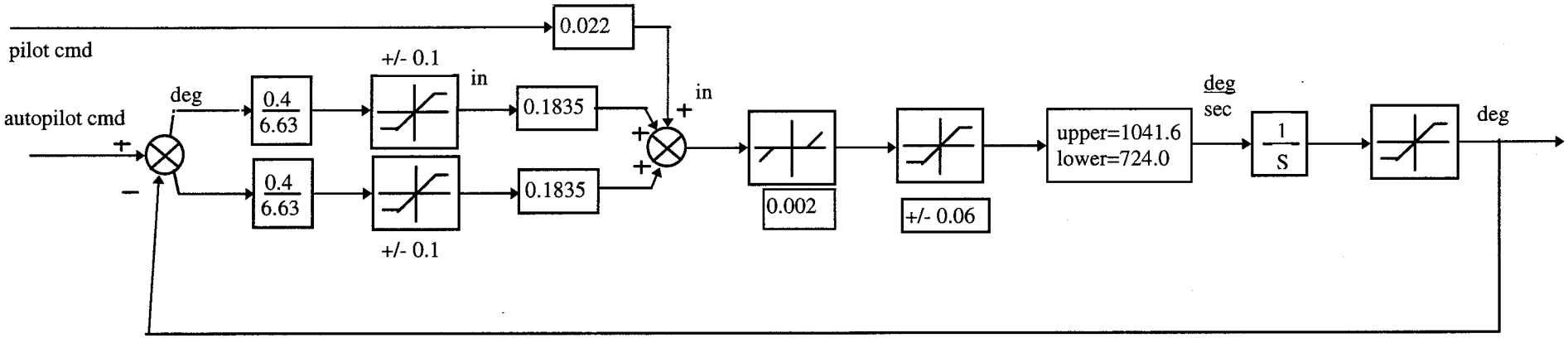

MD-11 RUDDER ACTUATOR

Figure 3.4

FIGURE 3.5. AUTOBRAKE ACTUATION BLOCK DIAGRAM

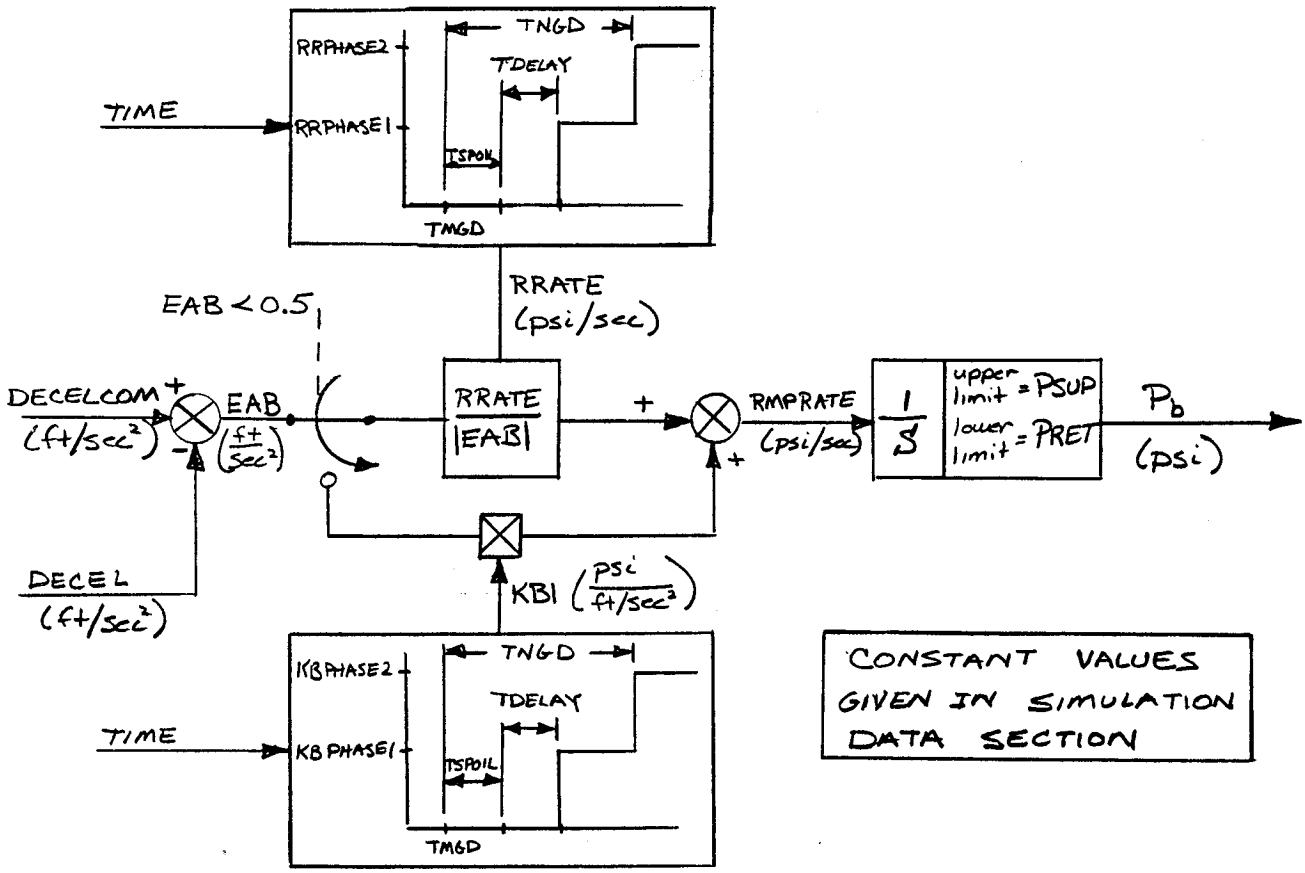

INPUTS

DECELCOM = commanded A/C deceleration
DECEL = actual A/C deceleration

OUTPUTS

P_b = brake pressure command (symetric part)

CONSTANTS

TMGD = main gear touchdown time
TSPOIL = time between main gear touchdown & spoiler deployment
TDELAY = delay time between spoiler deployment and brake ramp-up
TNGD = time between main gear touchdown & nose gear touchdown
RRPHASE1 = phase 1 brake pressure ramp rate (psi/sec)
RRPHASE2 = phase 2 " " " " "
KBPHASE1 = phase 1 brake pressure gain (psi/(ft/sec²))
KBPHASE2 = phase 2 " " " "
PSUP = hydraulic supply pressure (psi)
PRET = hydraulic return pressure (psi)

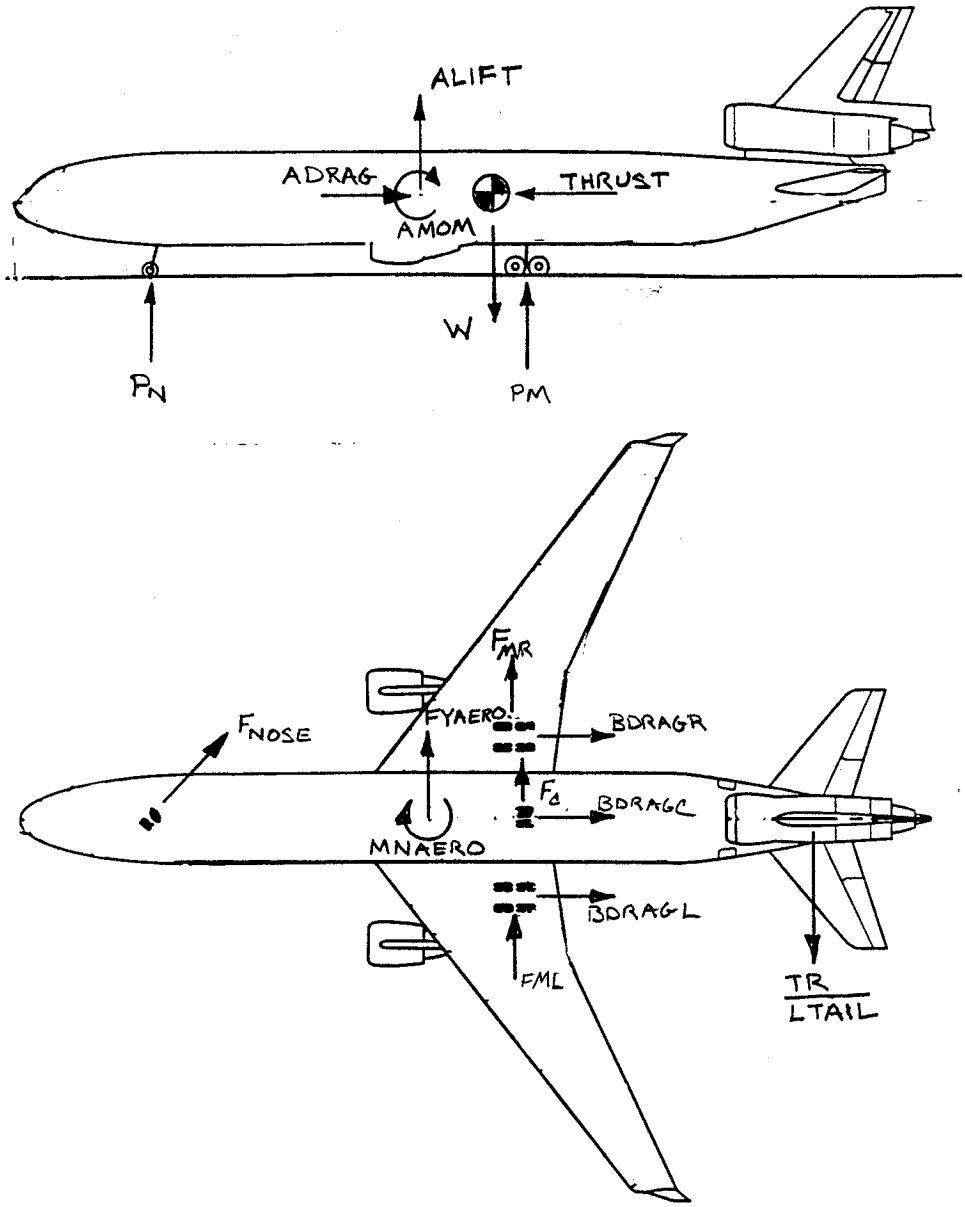

FIGURE 3.6 FORCES ACTING ON AIRCRAFT

FIGURE 3.7

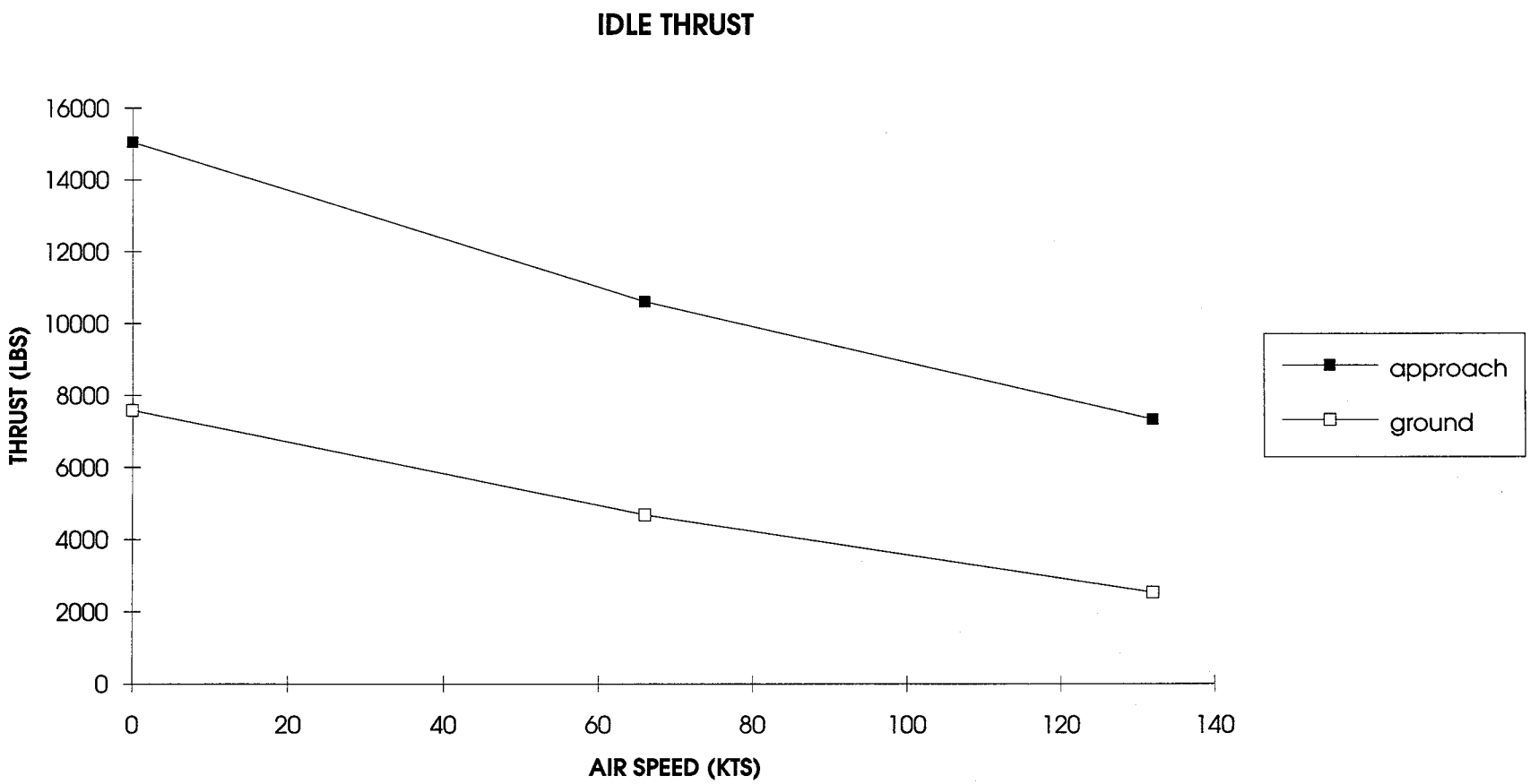
IDLE THRUST
THRUST (LBS)
16000
14000
12000
10000
8000
6000
4000
2000
0
0
20
40
60
80
100
120
140
AIR SPEED (KTS)
approach
ground

FIGURE 3.8

REVERSE THRUST

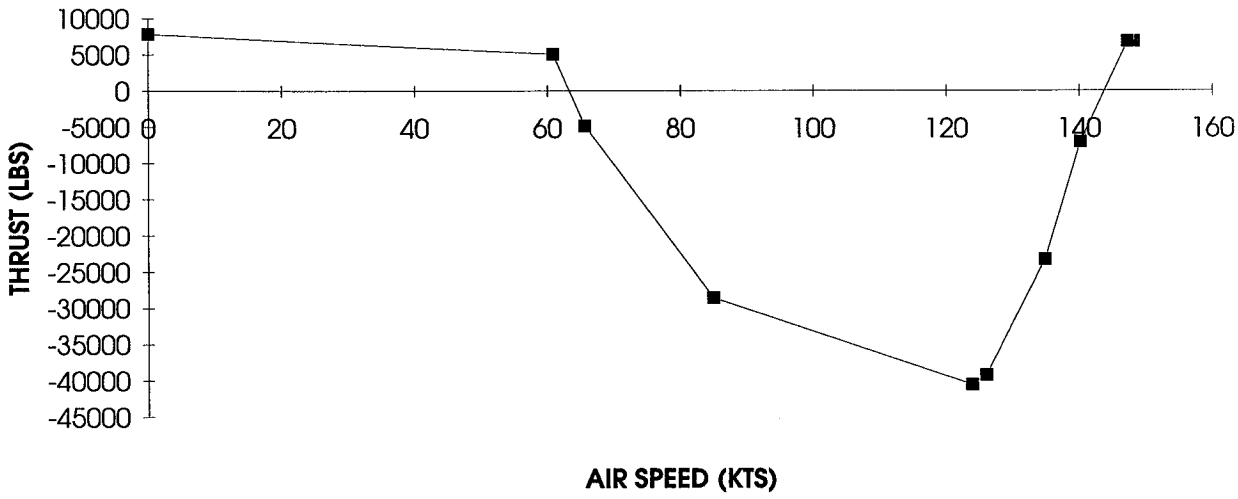

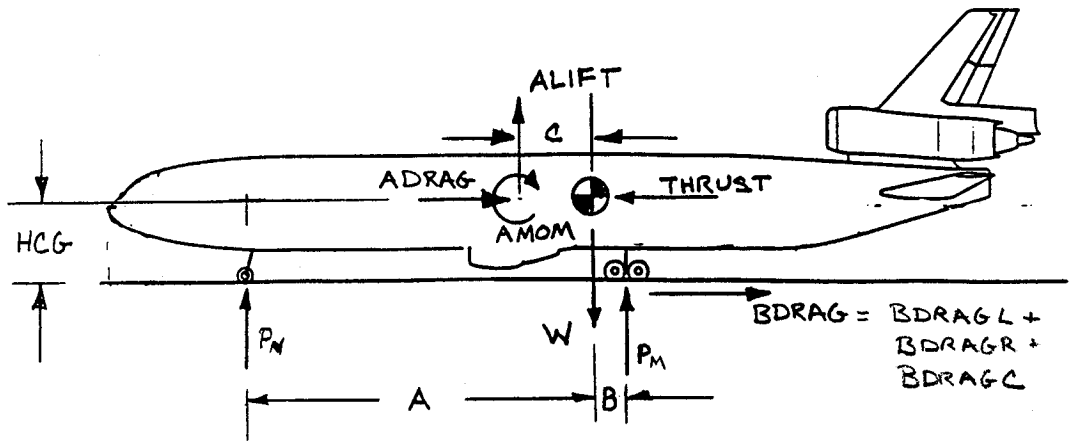

FIGURE 3.9 VARIABLE DEFINITIONS FOR STATIC EQUILIBRIUM CALCULATION

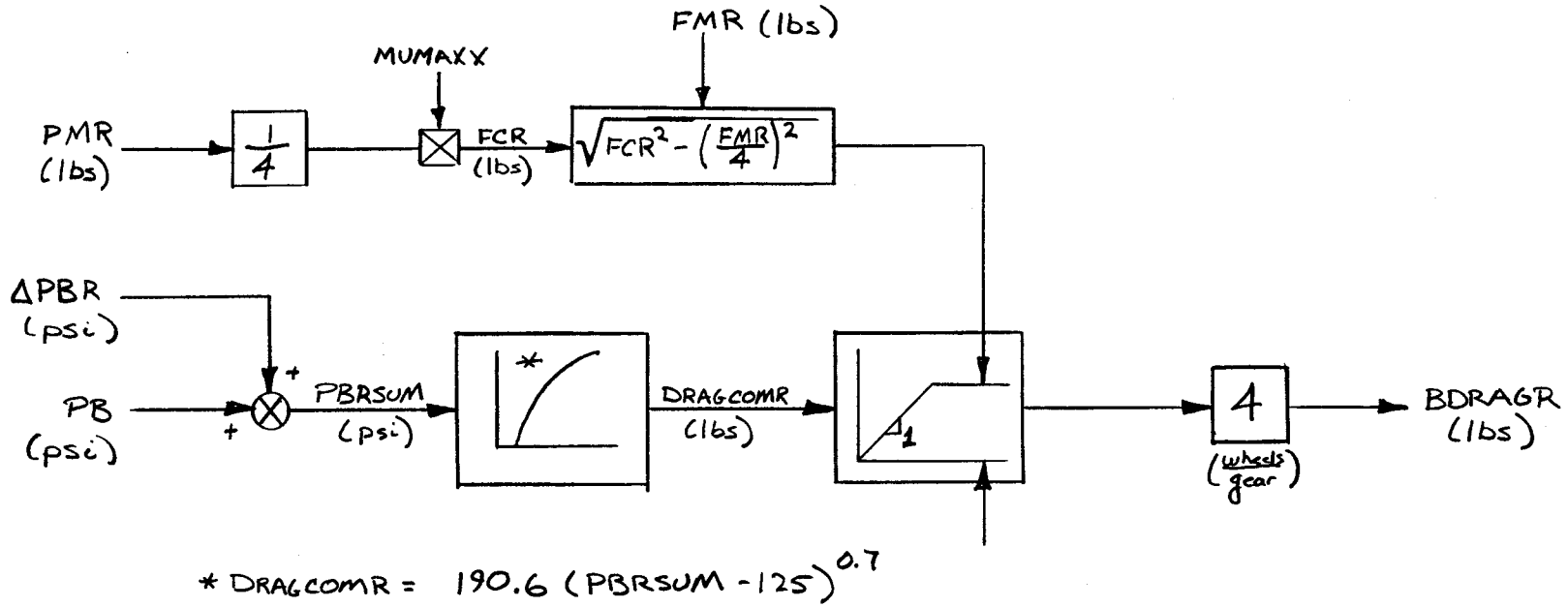

NOTE: BLOCK DIAGRAM FOR RIGHT GEAR IS SHOWN. LEFT & CENTER GEAR ARE SIMILAR

INPUTS

PB = SYMETRIC PART OF BRAKE PRESSURE COMMAND
ΔPBR = ASYMETRIC PART OF BRAKE PRESSURE COMMAND
PMR = VERTICAL LOAD ON RIGHT GEAR
MUMAXX = MAXIMUM RUNWAY COEFFICIENT OF FRICTION
FMR = SIDE FORCE ON RIGHT GEAR

OUTPUT

BDRAGR = BRAKE DRAG FORCE ON RIGHT GEAR

FIGURE 3.10 BRAKING DRAG LOADS MODEL

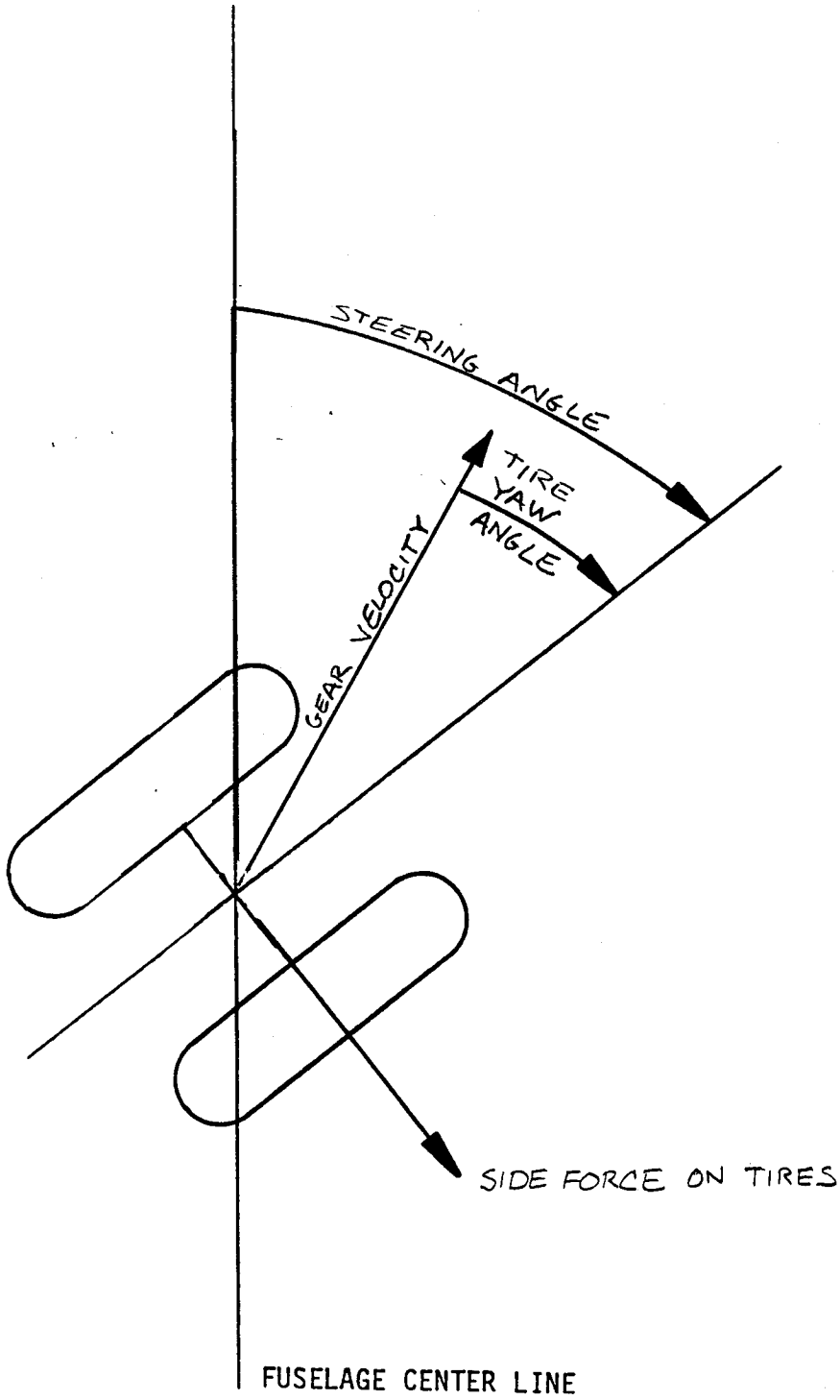

FIGURE 3.11 SIDE FORCE ON YAWED TIRES

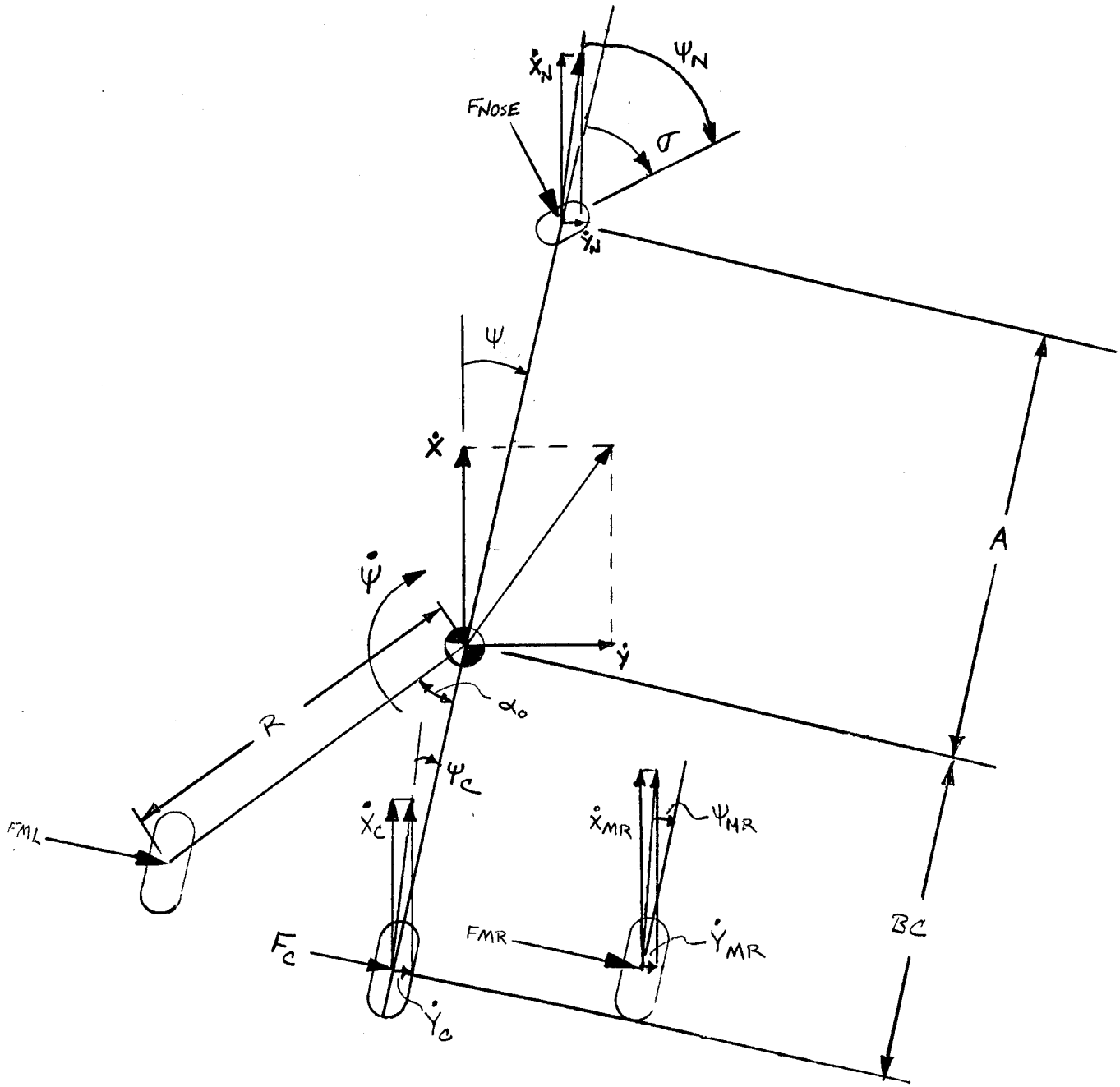

FIGURE 3.12 TIRE YAW ANGLE GEOMETRY

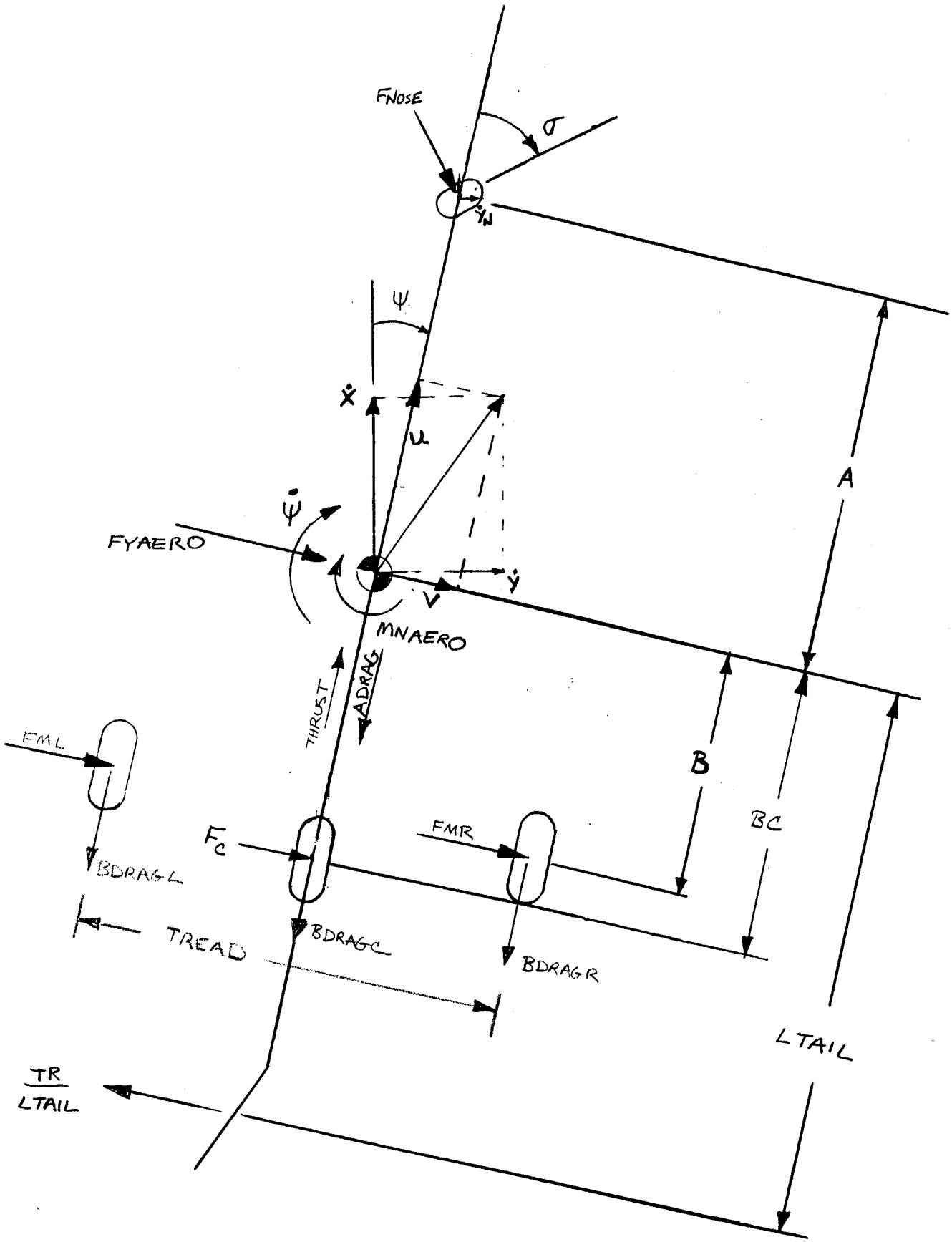

FIGURE 3.13 FORCES AND REFERENCE FRAMES

FIGURE 3.14.

WET RUNWAY FRICTION FACTOR

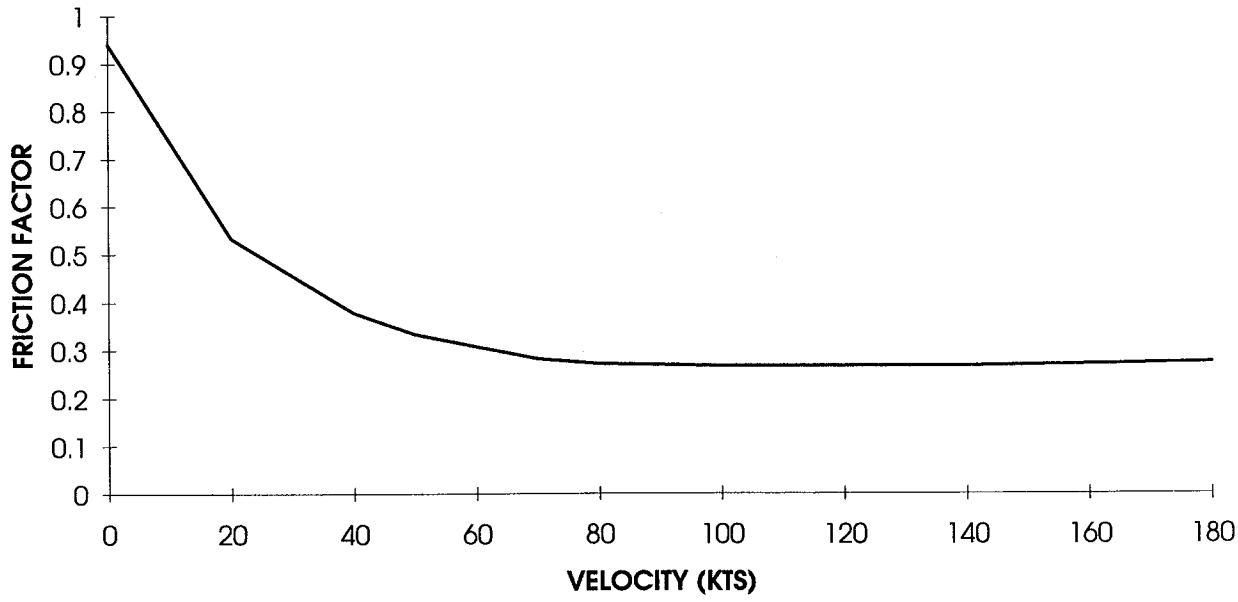

FIGURE 3.15.

NOSEWHEEL FRICTION FACTOR VS. SIDE SLIP VELOCITY

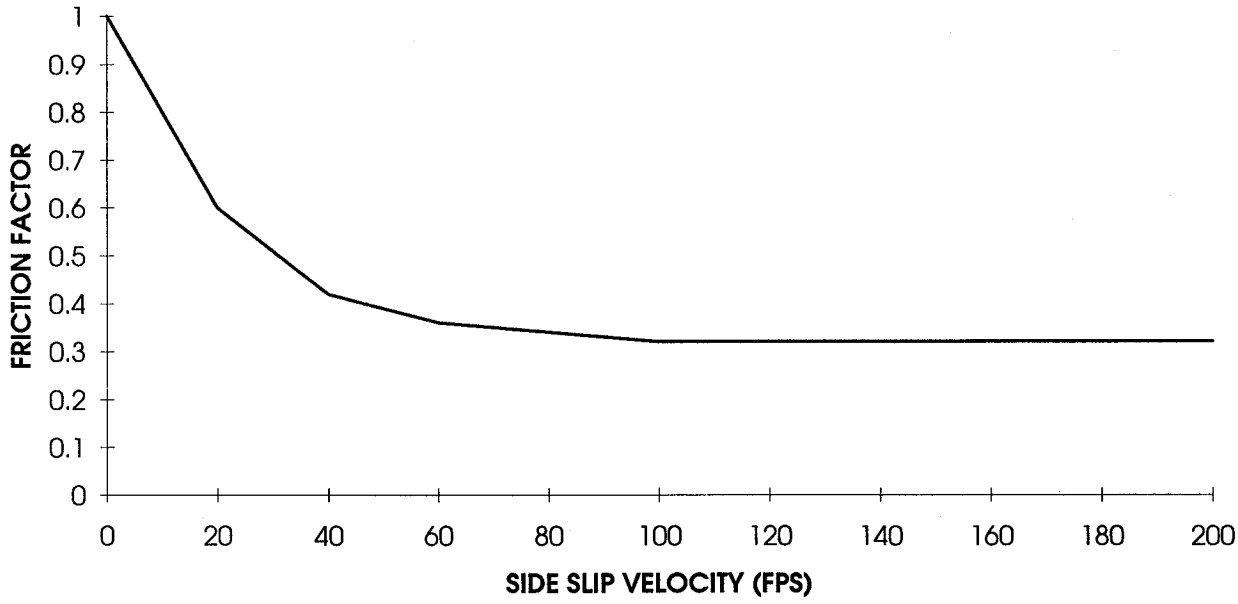

FIGURE 3.16

FRACTION OF MAIN GEAR LOAD SUPPORTED BY CENTER GEAR

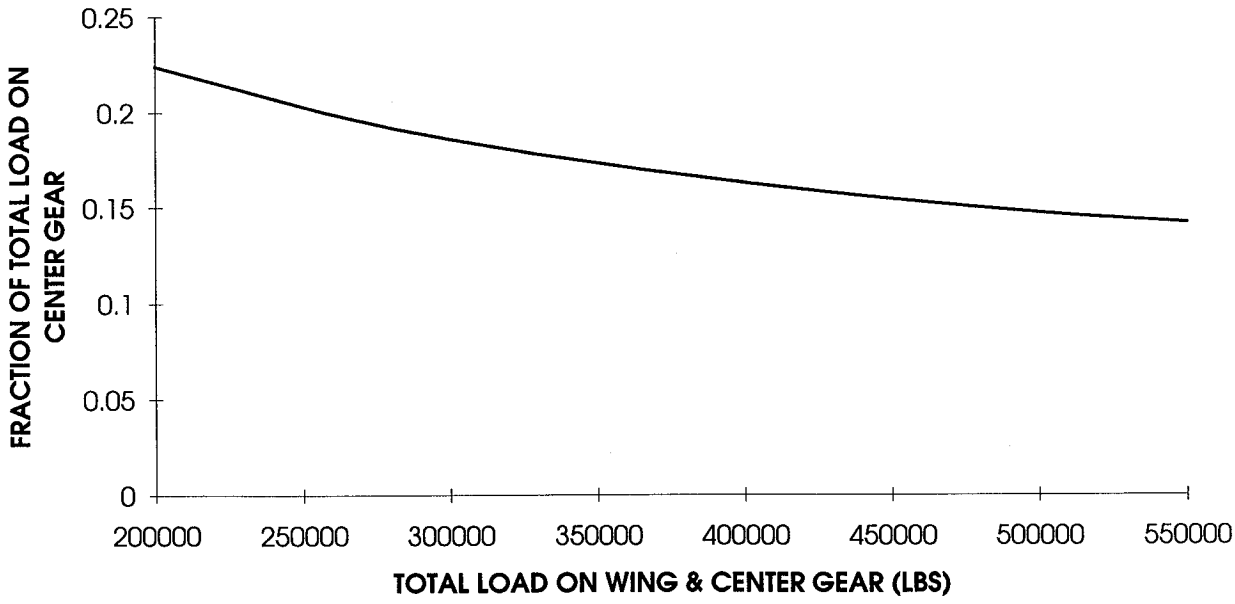

FIGURE 3.17.

NOSEWHEEL STEERING VALVE FLOW COEFFICIENT

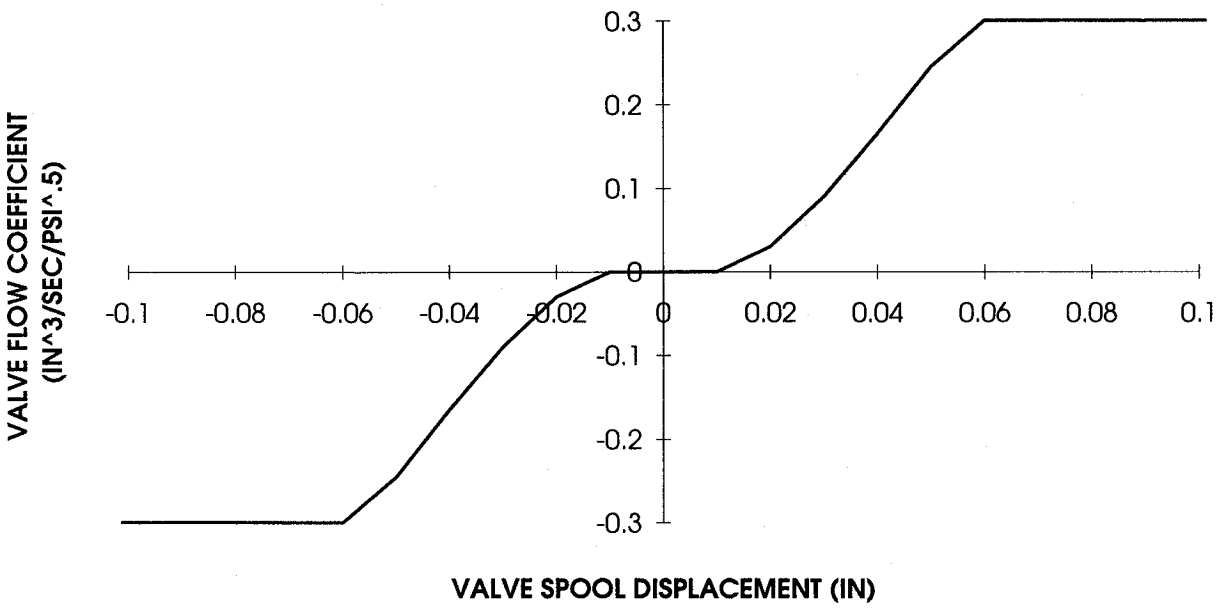

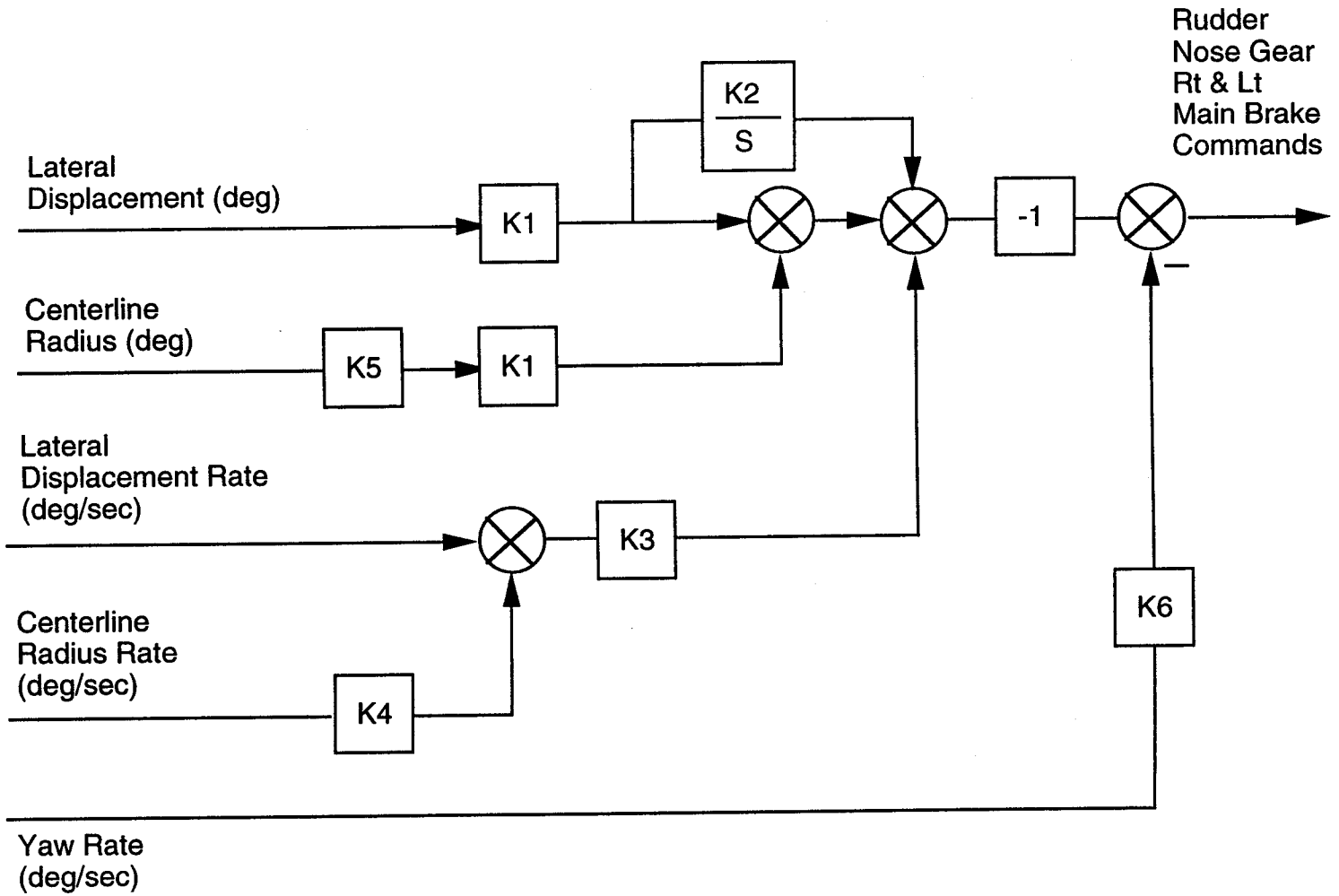

Figure 3.18 ROTO Steering Control Law

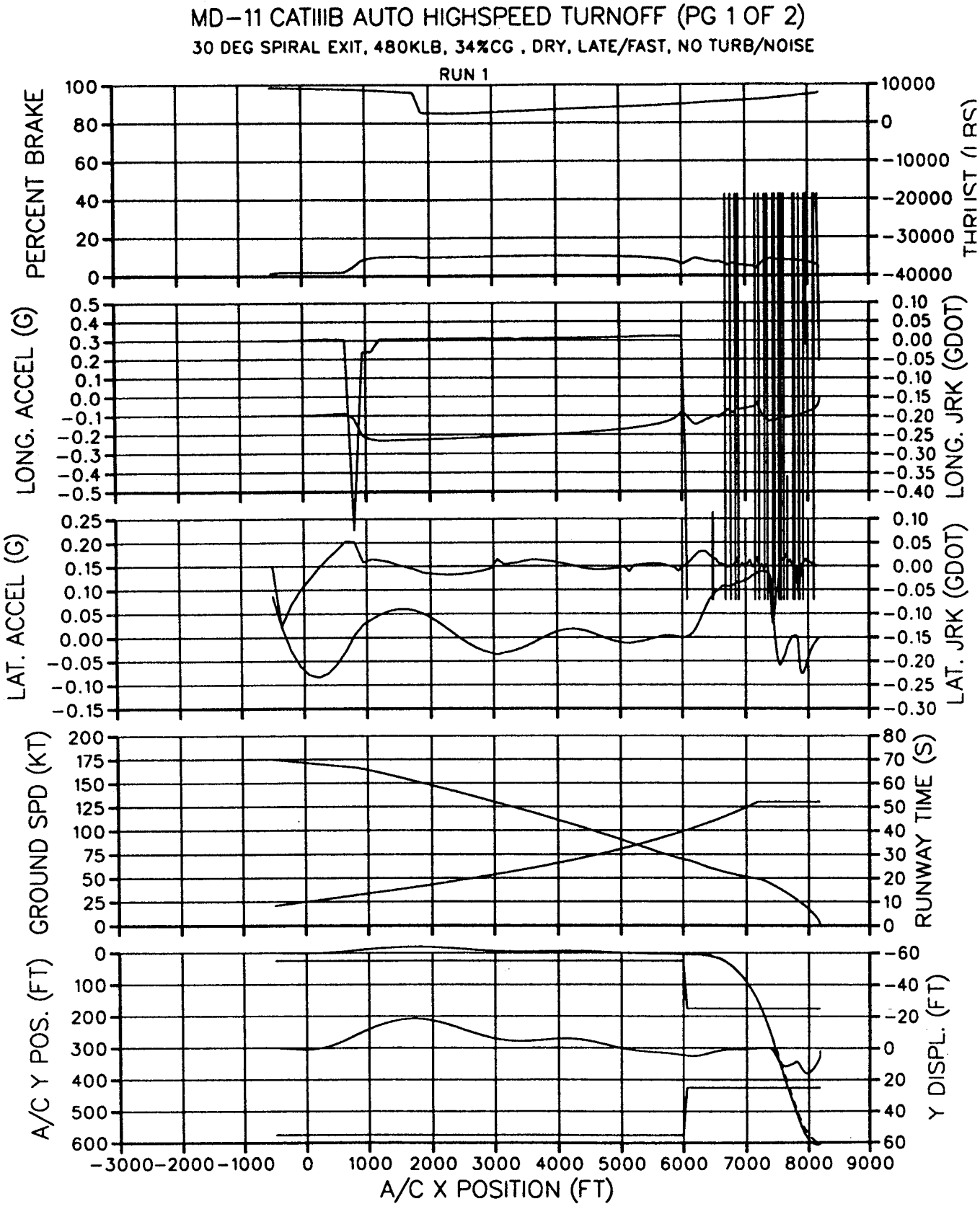
MD-11 CATIIIB AUTO HIGHSPEED TURNOFF (PG 1 OF 2)
30 DEG SPIRAL EXIT, 480KLB, 34%CG , DRY, LATE/FAST, NO TURB/NOISE
RUN 1
PERCENT BRAKE
THRUST (LBS)
LONG. ACCEL (G)
LONG. JRK (GDOT)
LAT. ACCEL (G)
LAT. JRK (GDOT)
GROUND SPD (KT)
RUNWAY TIME (S)
A/C Y POS. (FT)
Y DISPL. (FT)
A/C X POSITION (FT)

Figure 5.1

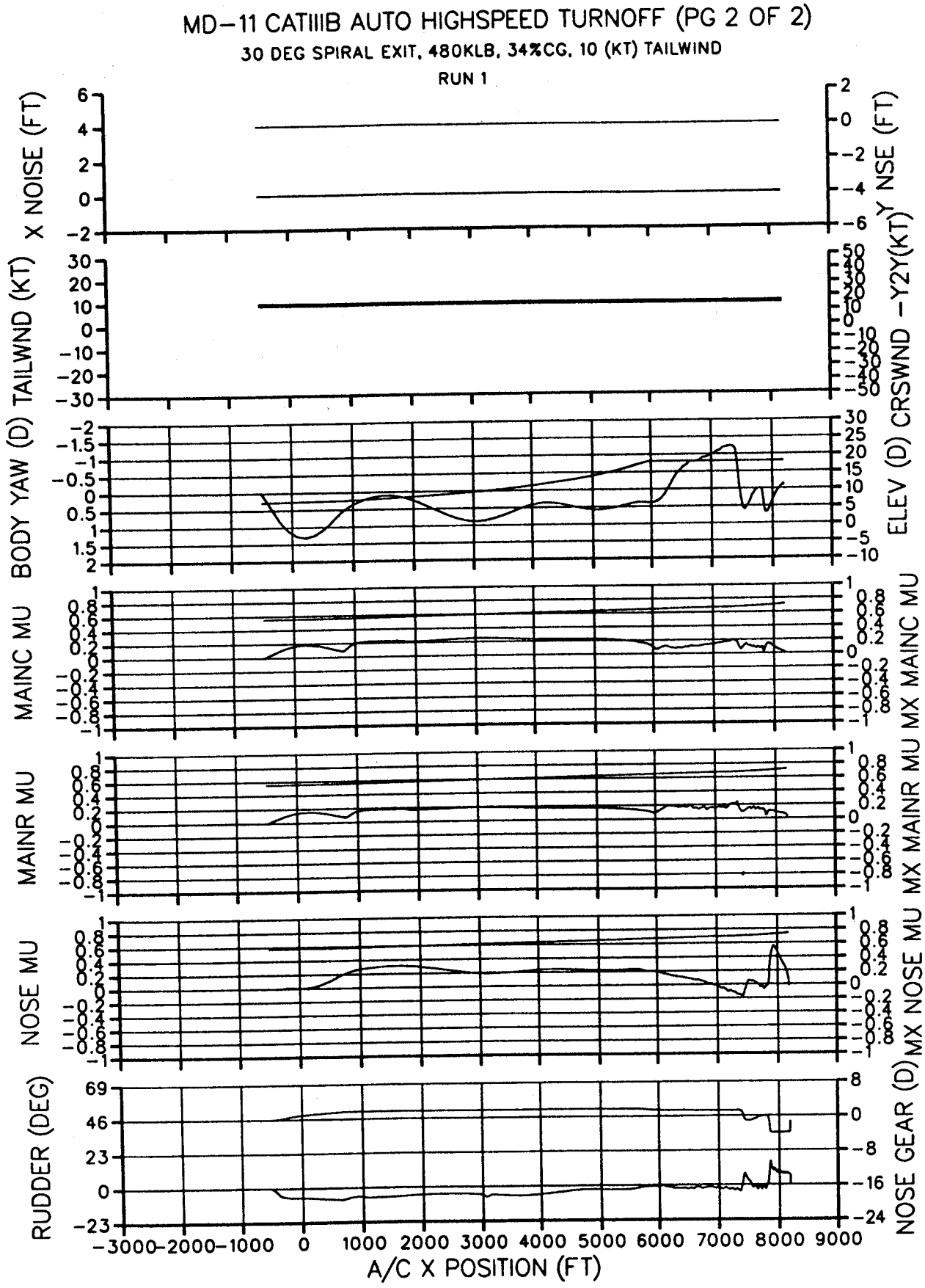
MD–11 CATIIIB AUTO HIGHSPEED TURNOFF (PG 2 OF 2)
30 DEG SPIRAL EXIT, 480KLB, 34%CG, 10 (KT) TAILWIND
RUN 1
X NOISE (FT)
Y NSE (FT)
TAILWND (KT)
CRSWND –Y2Y(KT)
BODY YAW (D)
ELEV (D)
MAINC MU
MX MAINC MU
MAINR MU
MX MAINR MU
NOSE MU
MX NOSE MU
RUDDER (DEG)
NOSE GEAR (D)
A/C X POSITION (FT)

Figure 5.2

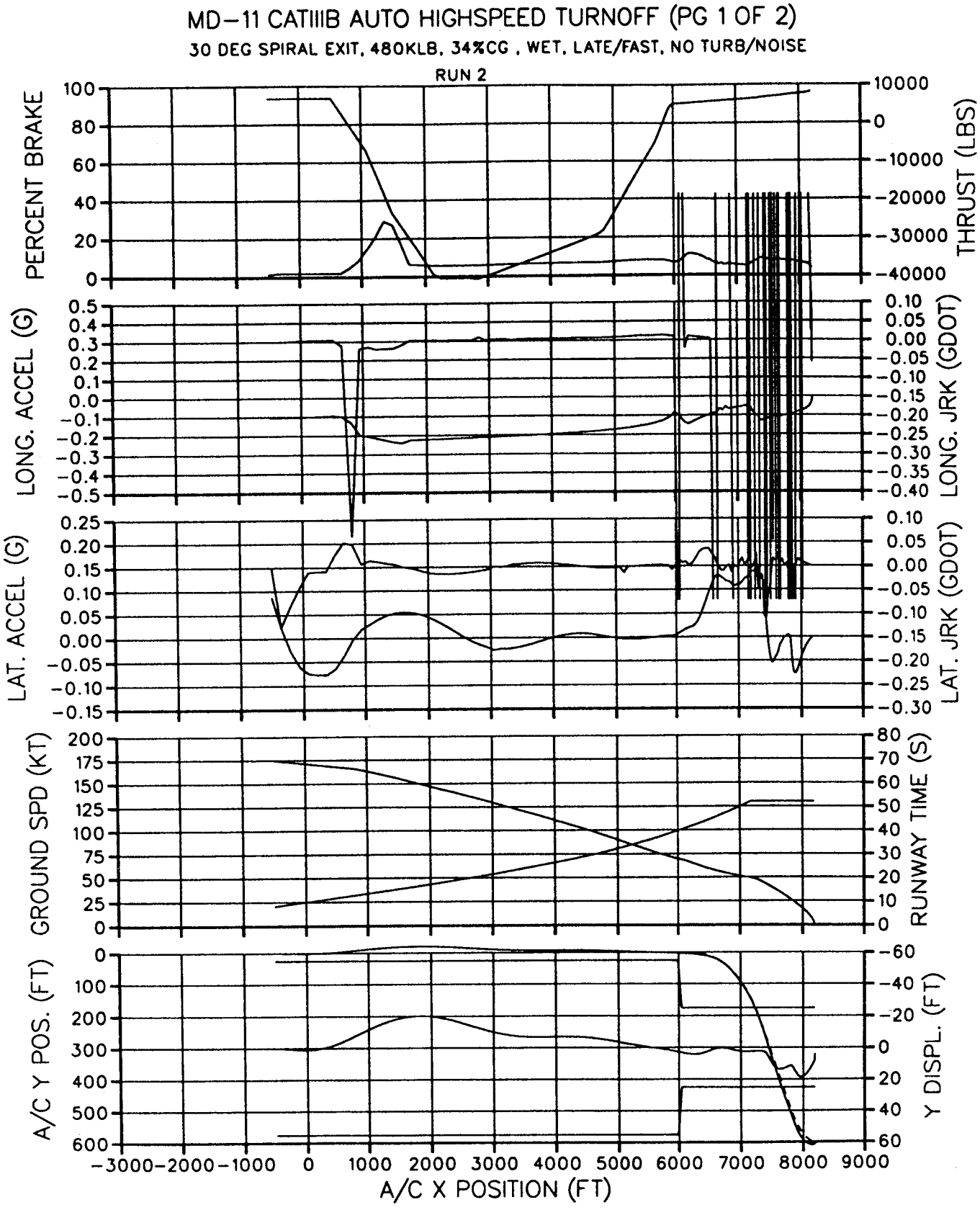
MD-11 CATIIIB AUTO HIGHSPEED TURNOFF (PG 1 OF 2)
30 DEG SPIRAL EXIT, 480KLB, 34%CG , WET, LATE/FAST, NO TURB/NOISE
RUN 2
PERCENT BRAKE
THRUST (LBS)
LONG. ACCEL (G)
LONG. JRK (GDOT)
LAT. ACCEL (G)
LAT. JRK (GDOT)
GROUND SPD (KT)
RUNWAY TIME (S)
A/C Y POS. (FT)
Y DISPL. (FT)
A/C X POSITION (FT)

Figure 5.3

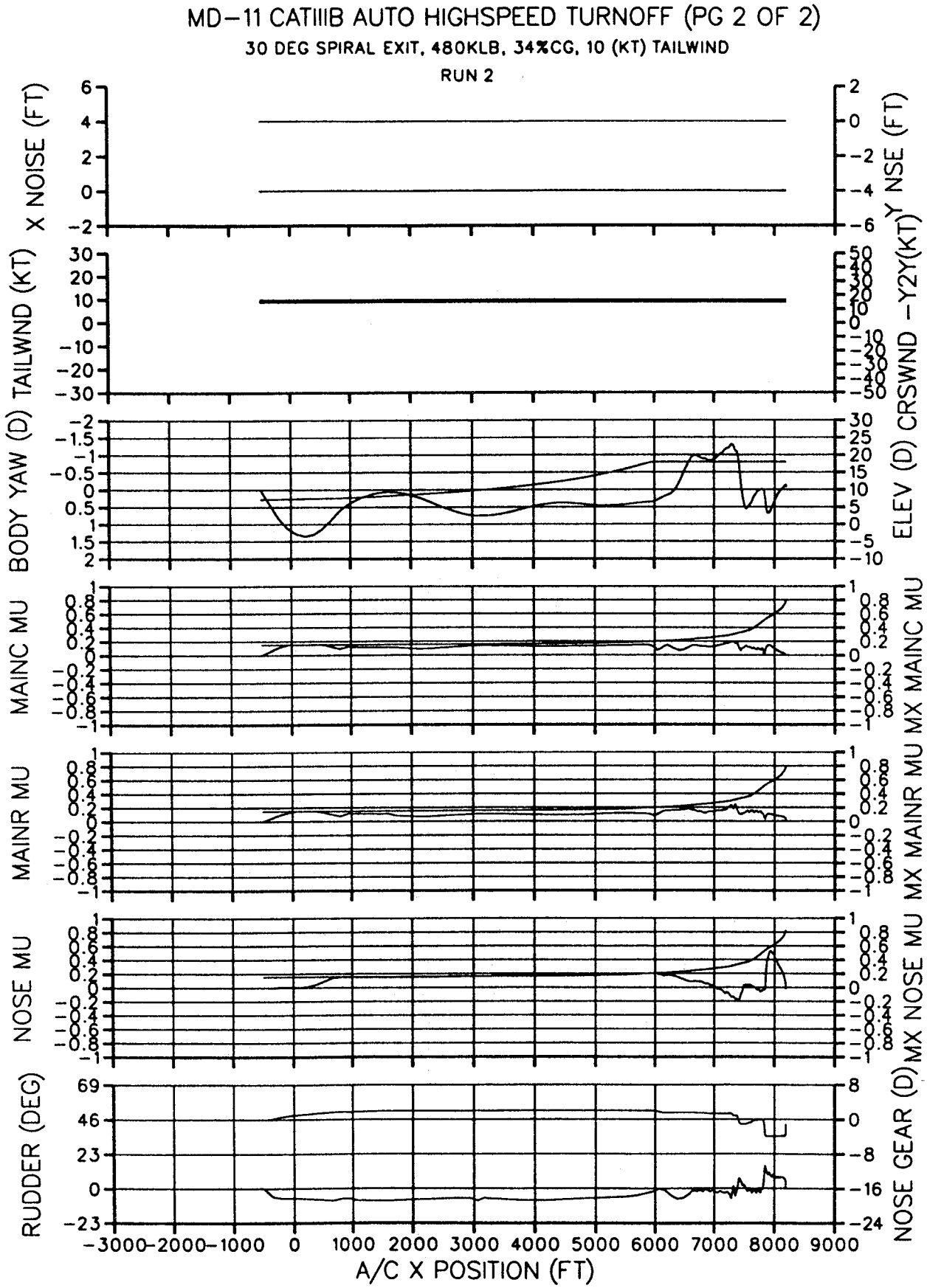
MD-11 CATIIIB AUTO HIGHSPEED TURNOFF (PG 2 OF 2)
30 DEG SPIRAL EXIT, 480KLB, 34%CG, 10 (KT) TAILWIND
RUN 2
X NOISE (FT)
Y NSE (FT)
TAILWND (KT)
CRSWND -Y2Y(KT)
BODY YAW (D)
ELEV (D)
MAINC MU
MX MAINC MU
MAINR MU
MX MAINR MU
NOSE MU
MX NOSE MU
RUDDER (DEG)
NOSE GEAR (D)
A/C X POSITION (FT)

Figure 5.4

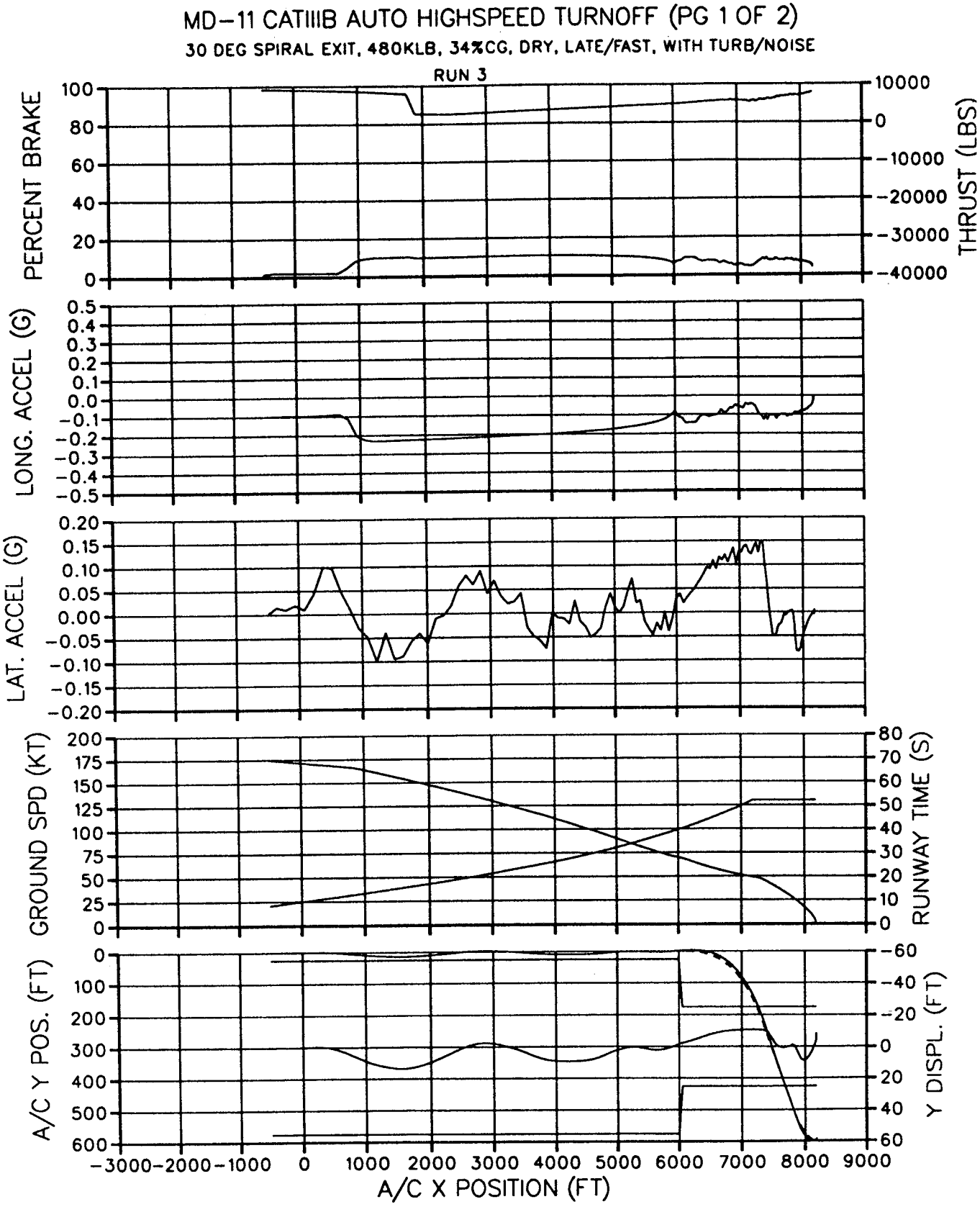
MD-11 CATIIIB AUTO HIGHSPEED TURNOFF (PG 1 OF 2)
30 DEG SPIRAL EXIT, 480KLB, 34%CG, DRY, LATE/FAST, WITH TURB/NOISE
RUN 3
PERCENT BRAKE
THRUST (LBS)
LONG. ACCEL (G)
LAT. ACCEL (G)
GROUND SPD (KT)
RUNWAY TIME (S)
A/C Y POS. (FT)
Y DISPL. (FT)
A/C X POSITION (FT)

Figure 5.5

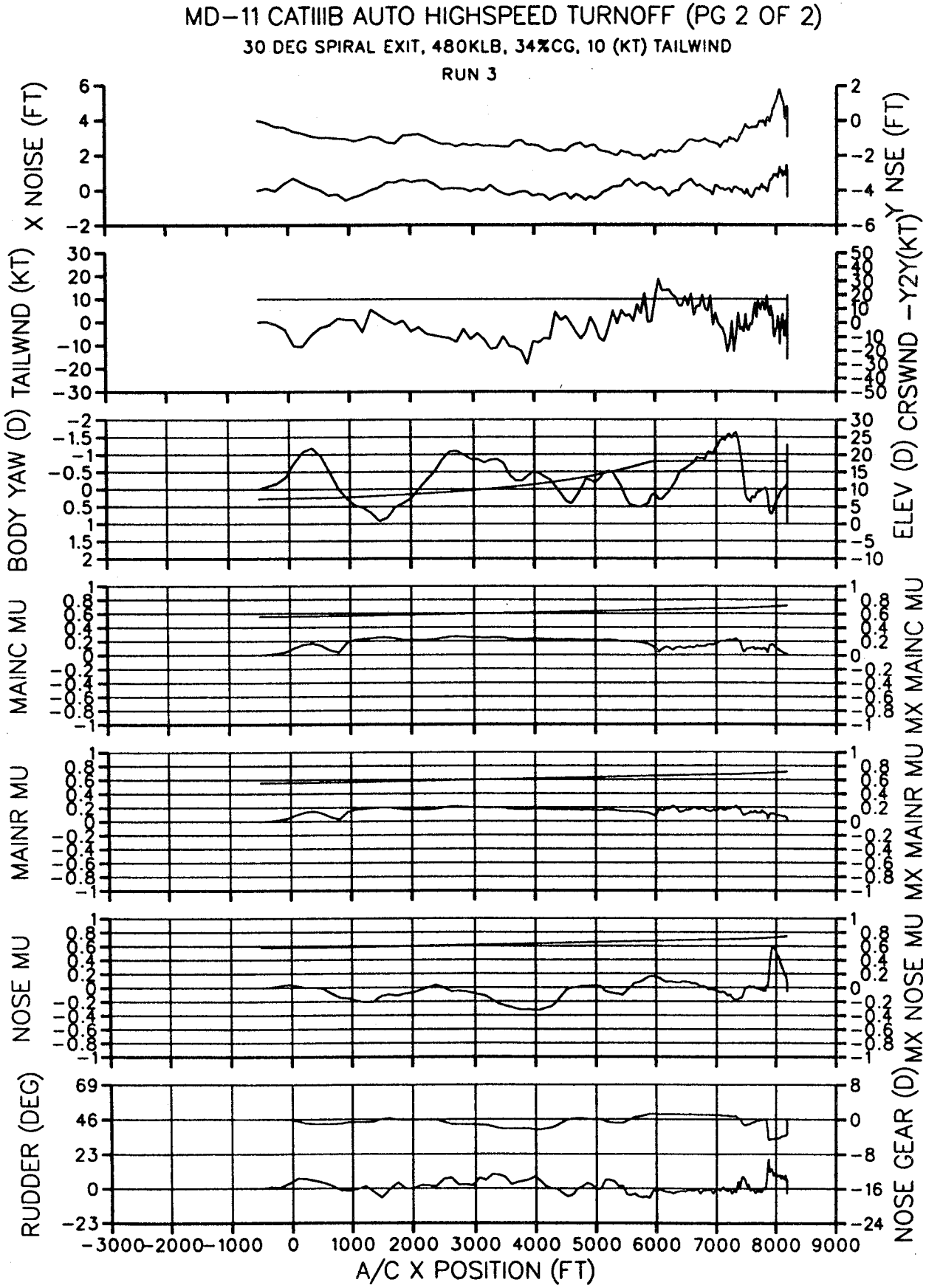
MD-11 CATIIIB AUTO HIGHSPEED TURNOFF (PG 2 OF 2)
30 DEG SPIRAL EXIT, 480KLB, 34%CG, 10 (KT) TAILWIND
RUN 3
X NOISE (FT)
Y NSE (FT)
TAILWND (KT)
CRSWND -Y2Y(KT)
BODY YAW (D)
ELEV (D)
MAINC MU
MX MAINC MU
MAINR MU
MX MAINR MU
NOSE MU
MX NOSE MU
RUDDER (DEG)
NOSE GEAR (D)
A/C X POSITION (FT)

Figure 5.6

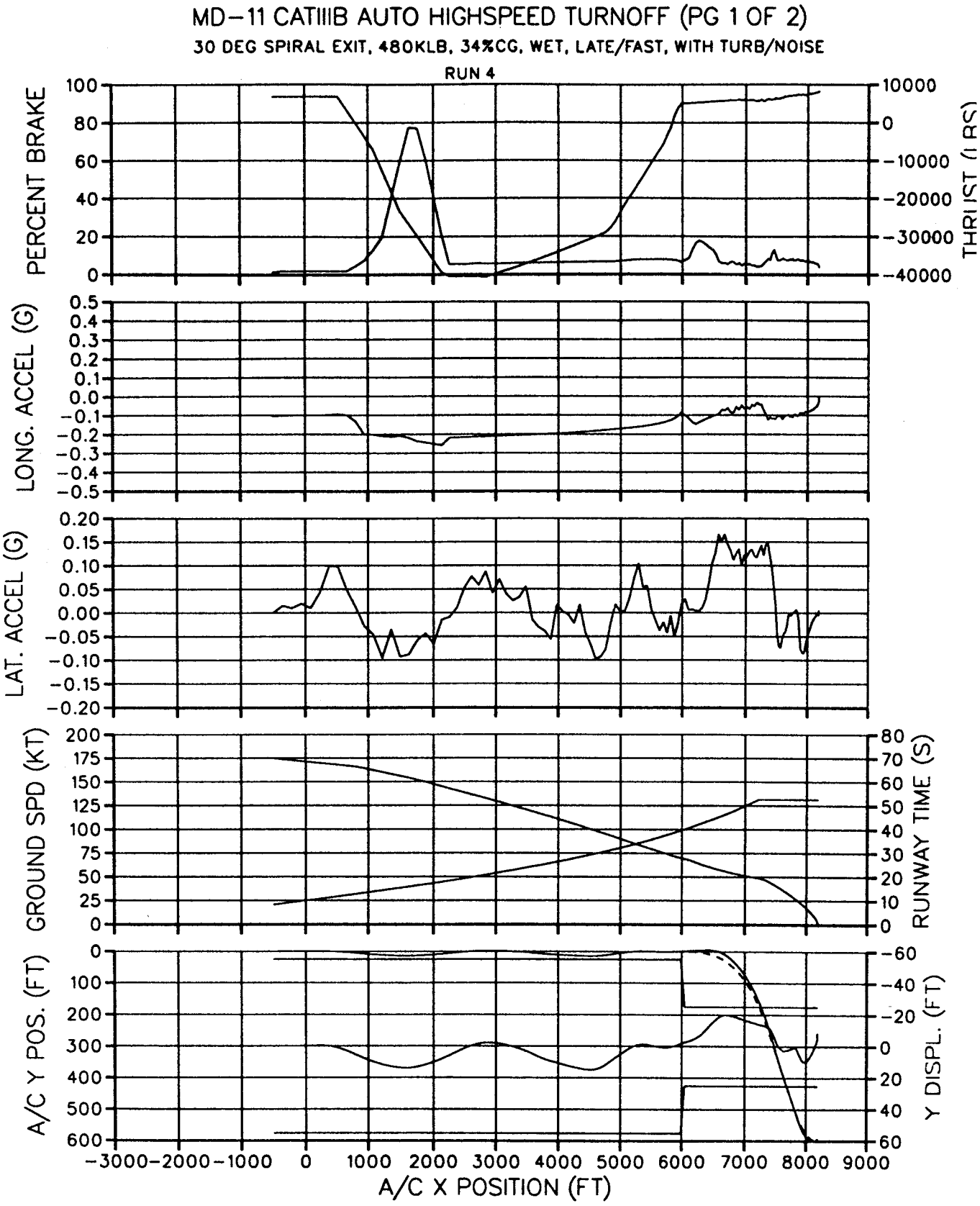
MD-11 CATIIIB AUTO HIGHSPEED TURNOFF (PG 1 OF 2)
30 DEG SPIRAL EXIT, 480KLB, 34%CG, WET, LATE/FAST, WITH TURB/NOISE
RUN 4
PERCENT BRAKE
100
80
60
40
20
0
10000
0
-10000
-20000
-30000
-40000
LONG. ACCEL (G)
0.5
0.4
0.3
0.2
0.1
0.0
-0.1
-0.2
-0.3
-0.4
-0.5
LAT. ACCEL (G)
0.20
0.15
0.10
0.05
0.00
-0.05
-0.10
-0.15
-0.20
GROUND SPD (KT)
200
175
150
125
100
75
50
25
0
RUNWAY TIME (S)
80
70
60
50
40
30
20
10
0
A/C Y POS. (FT)
0
100
200
300
400
500
600
Y DISPL. (FT)
-60
-40
-20
0
20
40
60
-3000 -2000 -1000 0 1000 2000 3000 4000 5000 6000 7000 8000 9000
A/C X POSITION (FT)

Figure 5.7

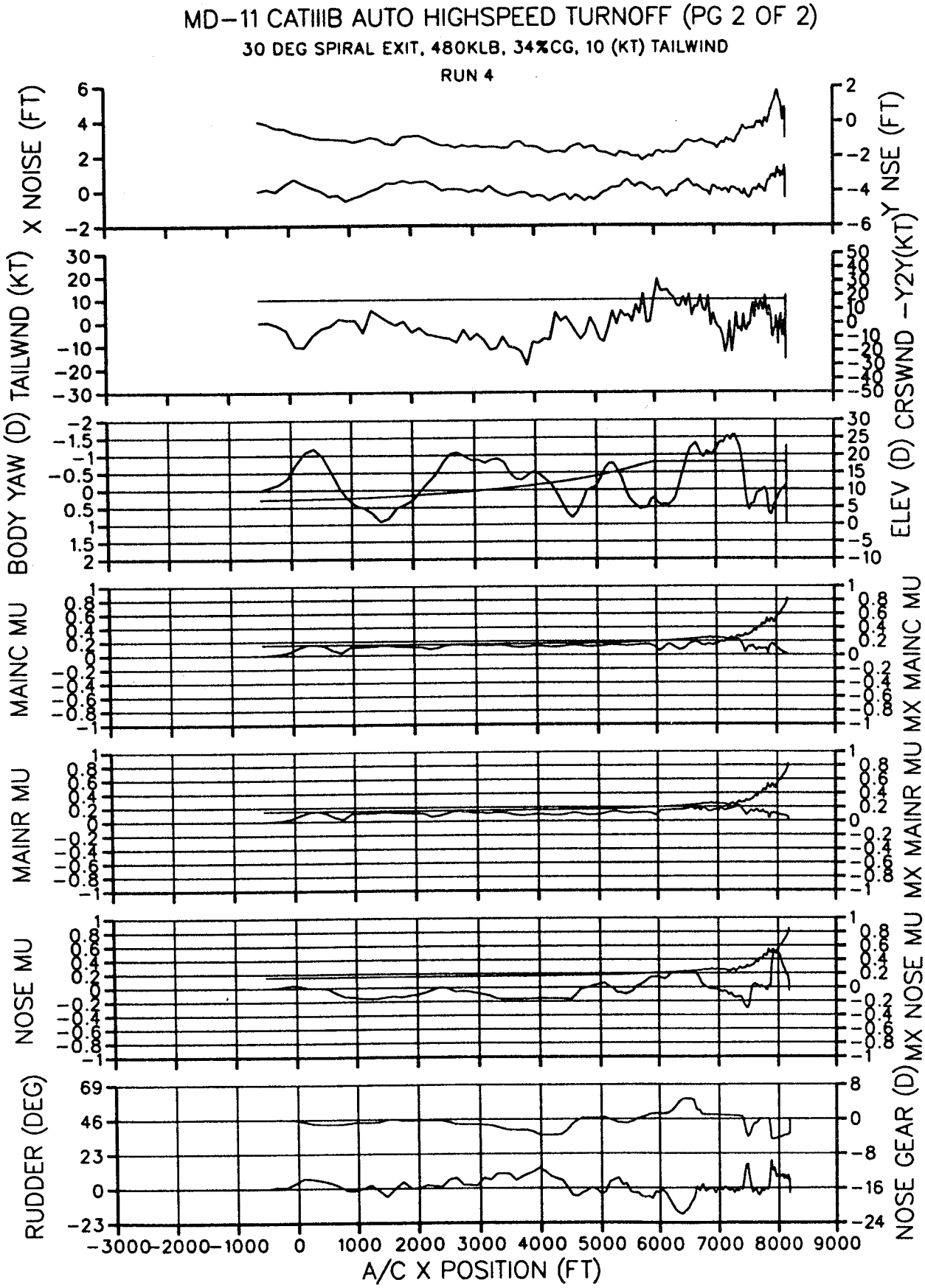
MD-11 CATIIIB AUTO HIGHSPEED TURNOFF (PG 2 OF 2)
30 DEG SPIRAL EXIT, 480KLB, 34%CG, 10 (KT) TAILWIND
RUN 4
X NOISE (FT)
Y NSE (FT)
TAILWND (KT)
CRSWND -Y2Y(KT)
BODY YAW (D)
ELEV (D)
MAINC MU
MX MAINC MU
MAINR MU
MX MAINR MU
NOSE MU
MX NOSE MU
RUDDER (DEG)
NOSE GEAR (D)
A/C X POSITION (FT)

Figure 5.8

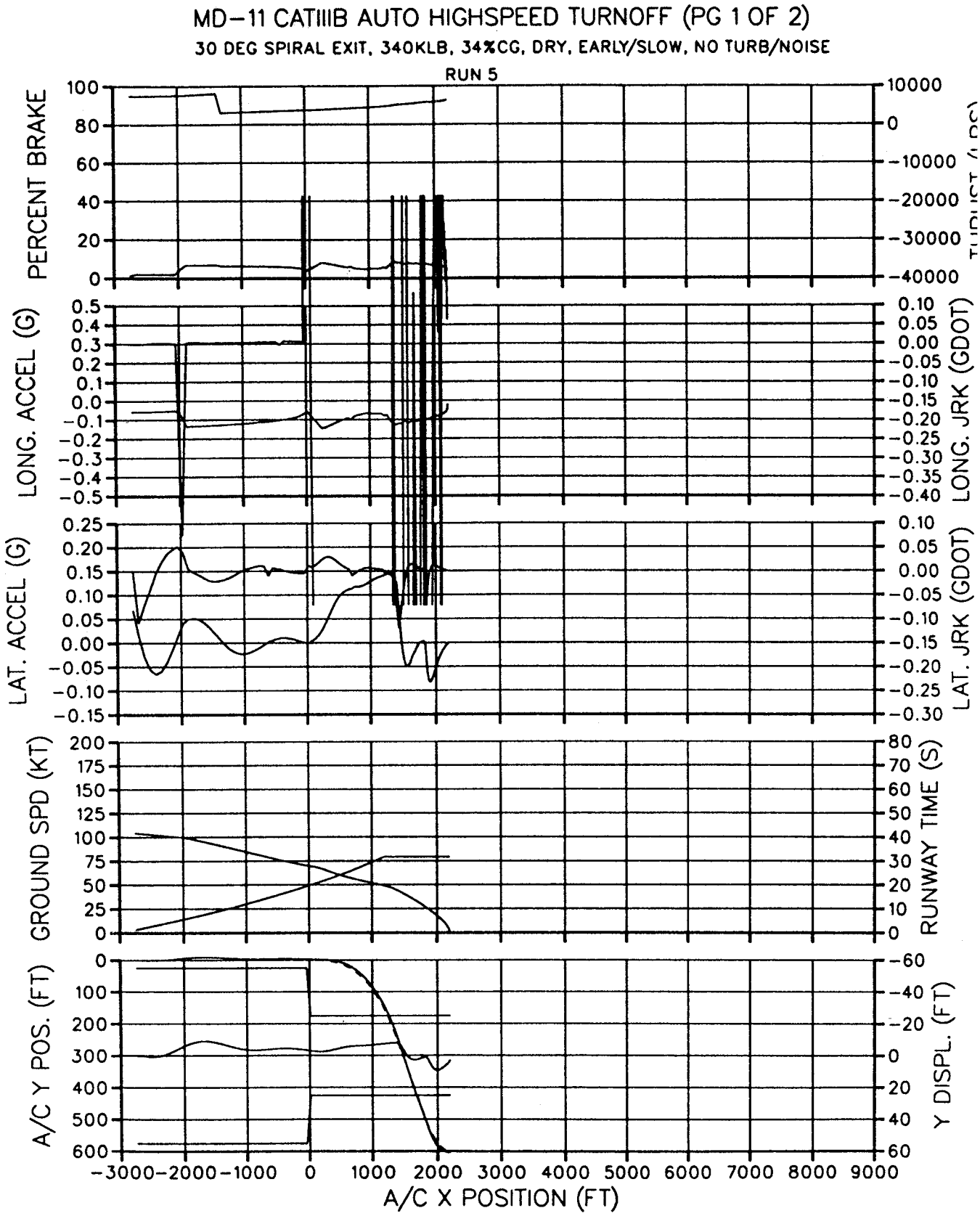
MD-11 CATIIIB AUTO HIGHSPEED TURNOFF (PG 1 OF 2)
30 DEG SPIRAL EXIT, 340KLB, 34%CG, DRY, EARLY/SLOW, NO TURB/NOISE
RUN 5
PERCENT BRAKE
LONG. ACCEL (G)
LONG. JRK (GDOT)
LAT. ACCEL (G)
LAT. JRK (GDOT)
GROUND SPD (KT)
RUNWAY TIME (S)
A/C Y POS. (FT)
Y DISPL. (FT)
A/C X POSITION (FT)

Figure 5.9

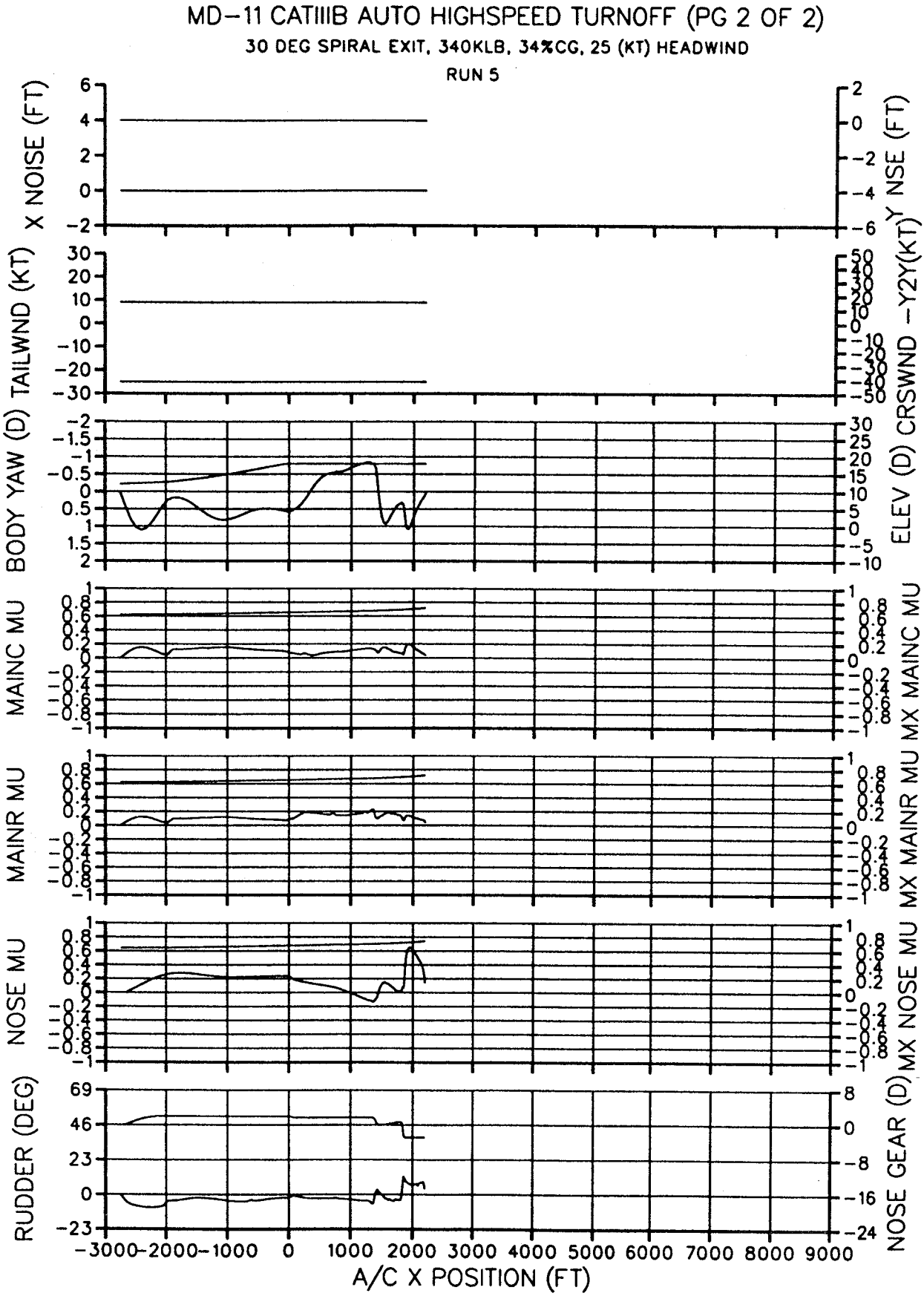
MD-11 CATIIIB AUTO HIGHSPEED TURNOFF (PG 2 OF 2)
30 DEG SPIRAL EXIT, 340KLB, 34%CG, 25 (KT) HEADWIND
RUN 5
X NOISE (FT)
Y NSE (FT)
TAILWND (KT)
CRSWND -Y2Y(KT)
BODY YAW (D)
ELEV (D)
MAINC MU
MX MAINC MU
MAINR MU
MX MAINR MU
NOSE MU
MX NOSE MU
RUDDER (DEG)
NOSE GEAR (D)
A/C X POSITION (FT)

Figure 5.10

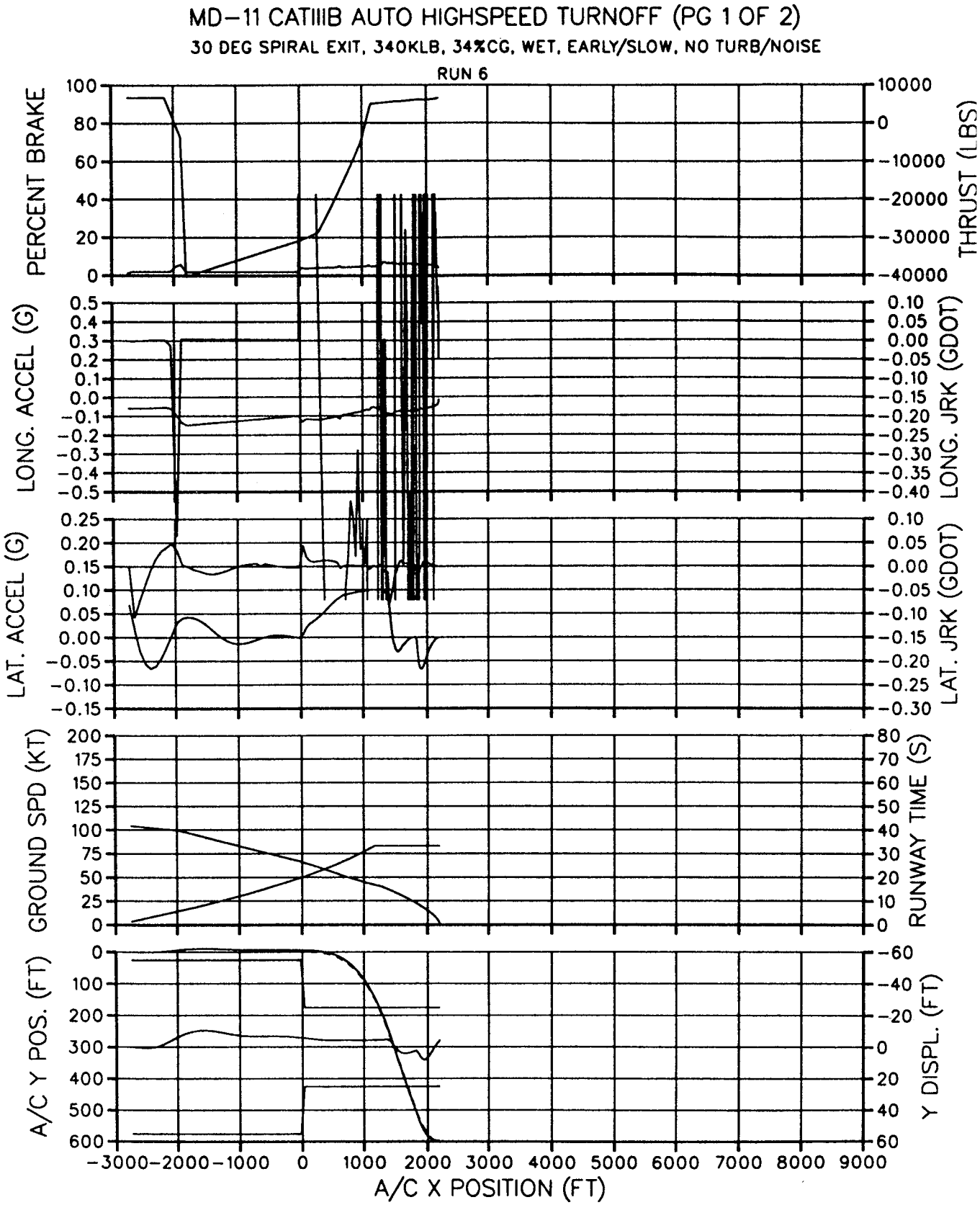
MD–11 CATIIIB AUTO HIGHSPEED TURNOFF (PG 1 OF 2)
30 DEG SPIRAL EXIT, 340KLB, 34%CG, WET, EARLY/SLOW, NO TURB/NOISE
RUN 6
PERCENT BRAKE
THRUST (LBS)
LONG. ACCEL (G)
LONG. JRK (GDOT)
LAT. ACCEL (G)
LAT. JRK (GDOT)
GROUND SPD (KT)
RUNWAY TIME (S)
A/C Y POS. (FT)
Y DISPL. (FT)
A/C X POSITION (FT)

Figure 5.11

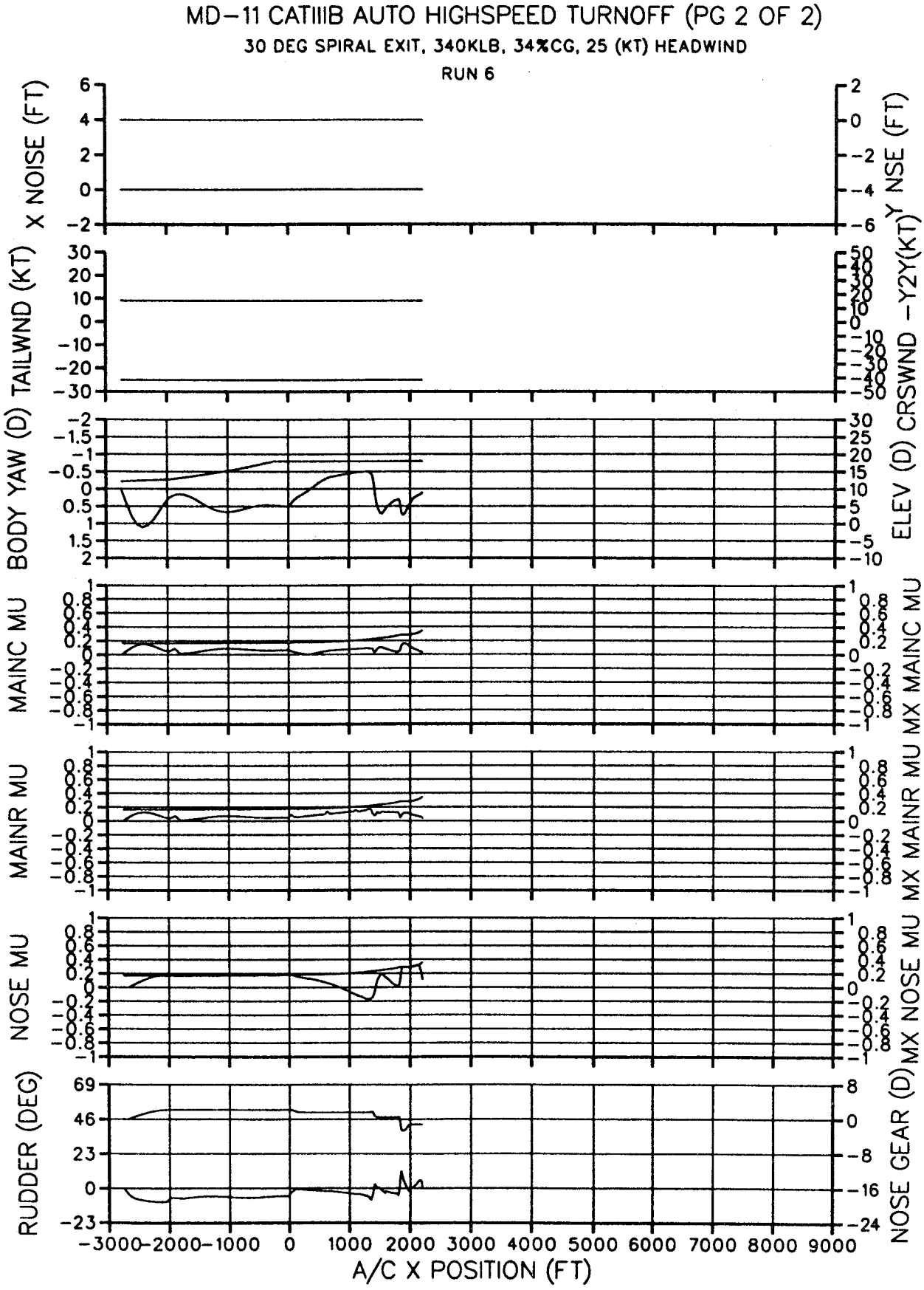
MD-11 CATIIIB AUTO HIGHSPEED TURNOFF (PG 2 OF 2)
30 DEG SPIRAL EXIT, 340KLB, 34%CG, 25 (KT) HEADWIND
RUN 6
X NOISE (FT)
Y NSE (FT)
TAILWND (KT)
-Y2Y(KT)
CRSWND
BODY YAW (D)
ELEV (D)
MAINC MU
MX MAINC MU
MAINR MU
MX MAINR MU
NOSE MU
MX NOSE MU
RUDDER (DEG)
NOSE GEAR (D)
-3000 -2000 -1000 0 1000 2000 3000 4000 5000 6000 7000 8000 9000
A/C X POSITION (FT)

Figure 5.12

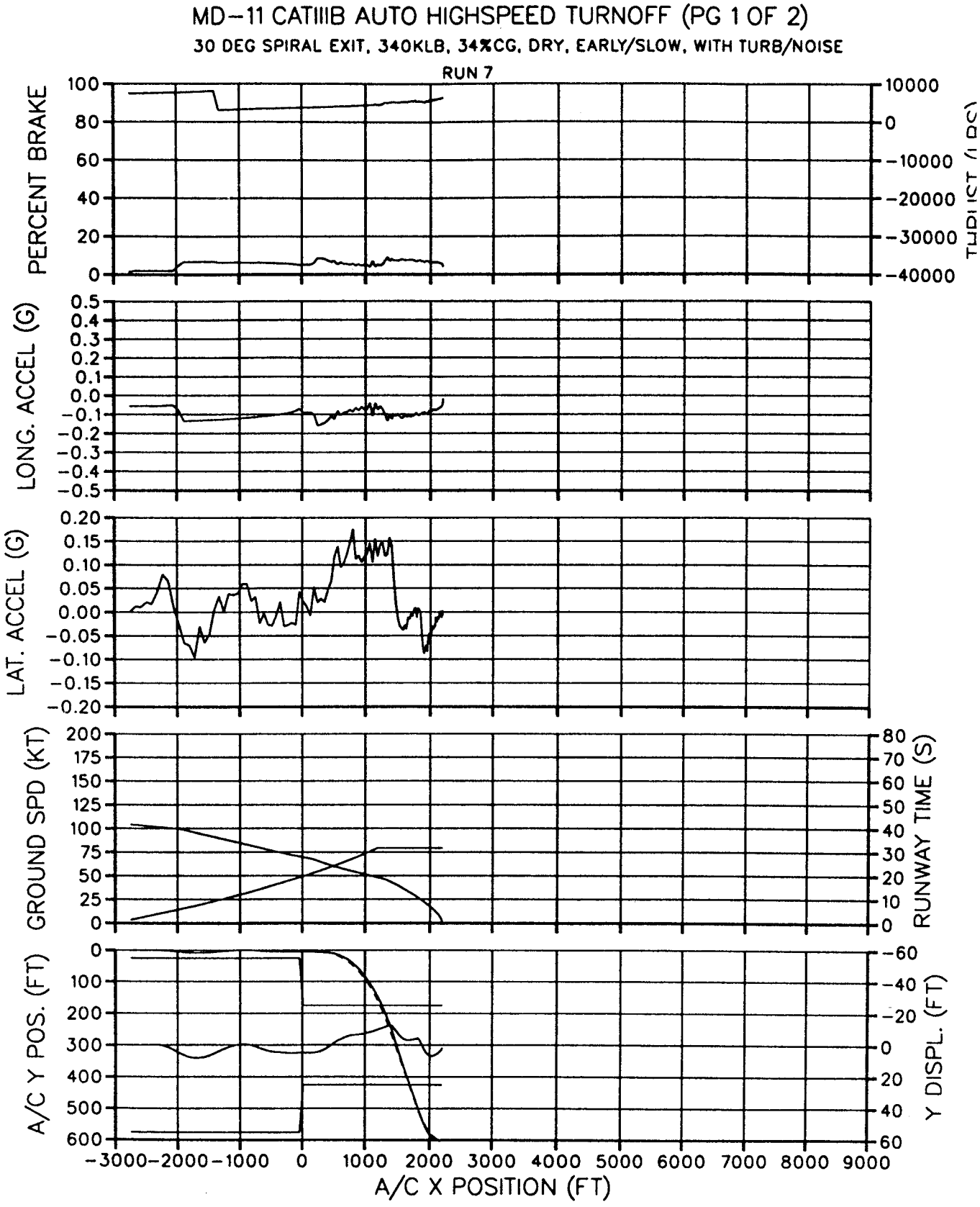
MD-11 CATIIIB AUTO HIGHSPEED TURNOFF (PG 1 OF 2)
30 DEG SPIRAL EXIT, 340KLB, 34%CG, DRY, EARLY/SLOW, WITH TURB/NOISE
RUN 7
PERCENT BRAKE
LONG. ACCEL (G)
LAT. ACCEL (G)
GROUND SPD (KT)
RUNWAY TIME (S)
A/C Y POS. (FT)
Y DISPL. (FT)
A/C X POSITION (FT)

Figure 5.13

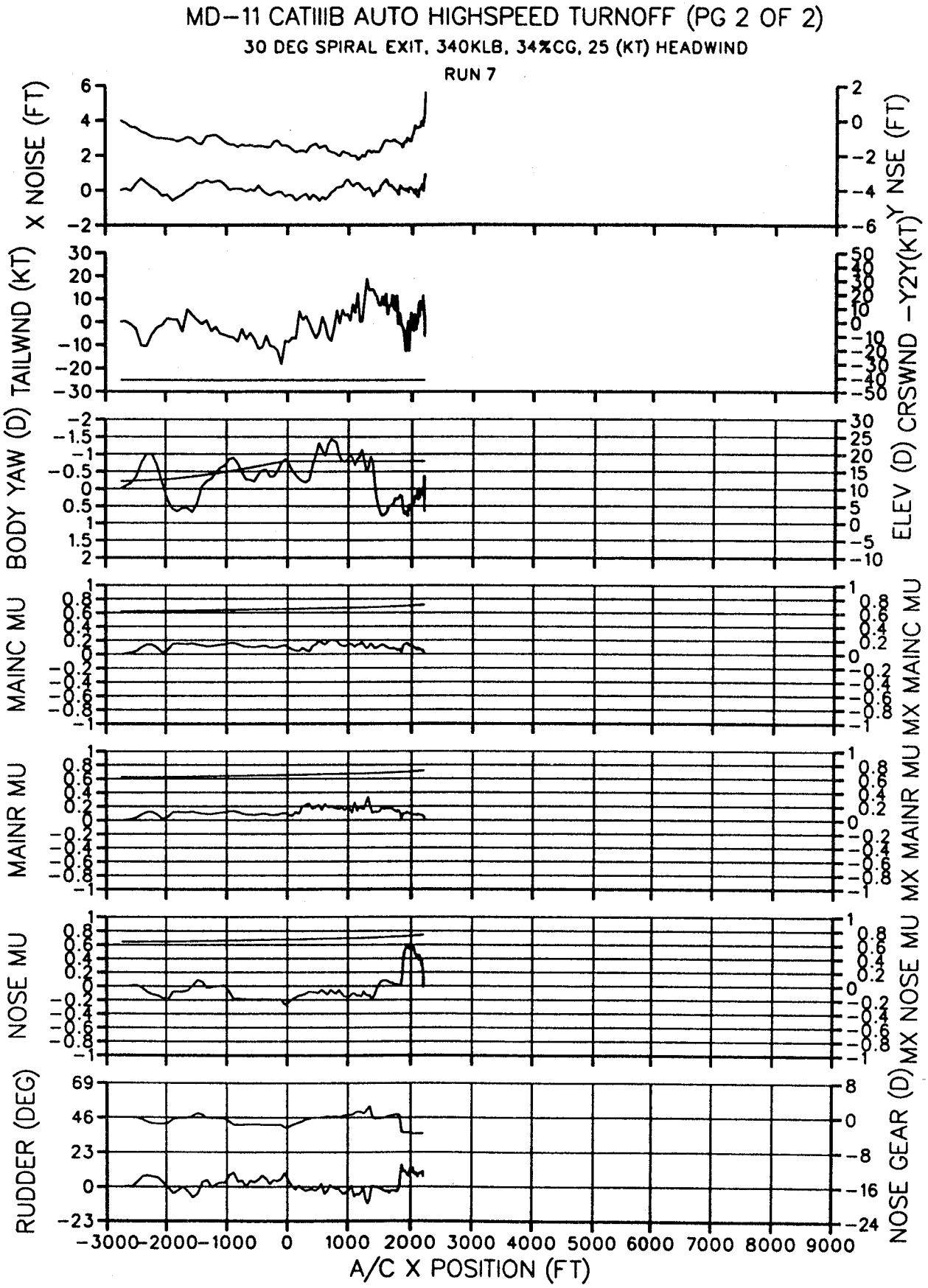
MD-11 CATIIIB AUTO HIGHSPEED TURNOFF (PG 2 OF 2)
30 DEG SPIRAL EXIT, 340KLB, 34%CG, 25 (KT) HEADWIND
RUN 7
X NOISE (FT)
Y NSE (FT)
BODY YAW (D)
TAILWND (KT)
CRSWND -Y2Y(KT)
ELEV (D)
MAINC MU
MX MAINC MU
MAINR MU
MX MAINR MU
NOSE MU
MX NOSE MU
RUDDER (DEG)
NOSE GEAR (D)
A/C X POSITION (FT)

Figure 5.14

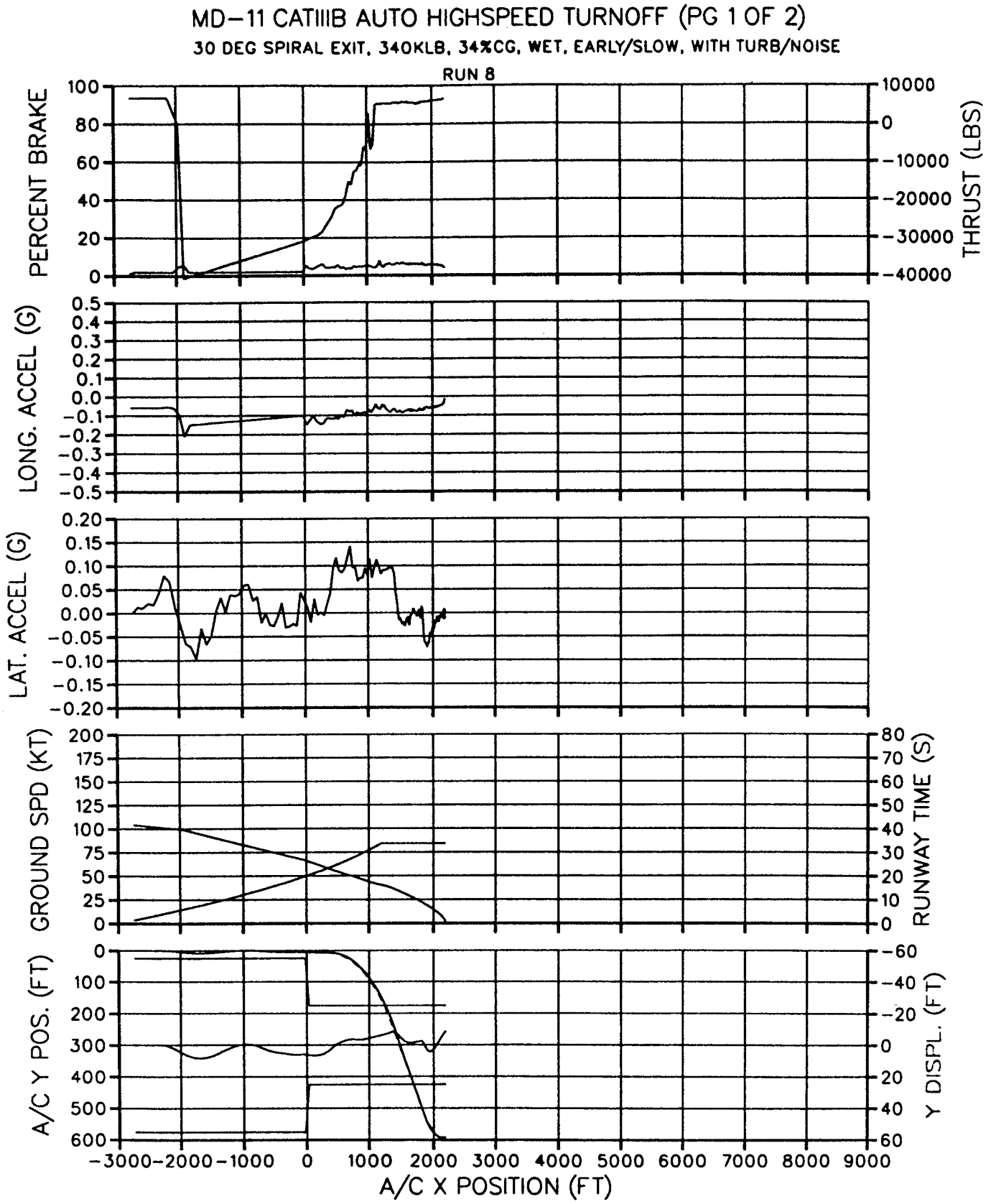
MD-11 CATIIIB AUTO HIGHSPEED TURNOFF (PG 1 OF 2)
30 DEG SPIRAL EXIT, 340KLB, 34%CG, WET, EARLY/SLOW, WITH TURB/NOISE
RUN 8
PERCENT BRAKE
THRUST (LBS)
LONG. ACCEL (G)
LAT. ACCEL (G)
GROUND SPD (KT)
RUNWAY TIME (S)
A/C Y POS. (FT)
Y DISPL. (FT)
A/C X POSITION (FT)

Figure 5.15

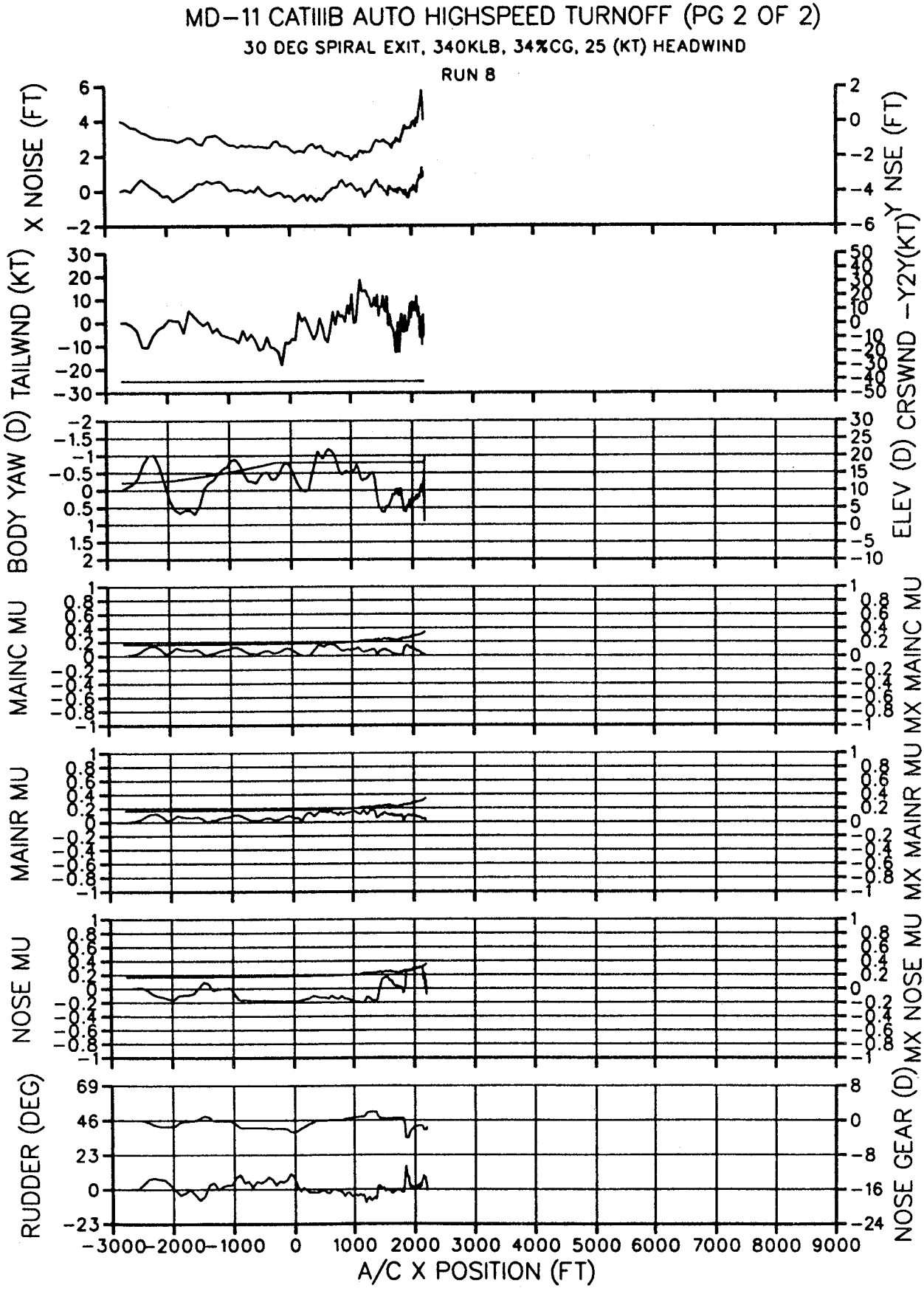
MD-11 CATIIIB AUTO HIGHSPEED TURNOFF (PG 2 OF 2)
30 DEG SPIRAL EXIT, 340KLB, 34%CG, 25 (KT) HEADWIND
RUN 8
X NOISE (FT)
Y NSE (FT)
TAILWND (KT)
CRSWND -Y2Y(KT)
BODY YAW (D)
ELEV (D)
MAINC MU
MX MAINC MU
MAINR MU
MX MAINR MU
NOSE MU
MX NOSE MU
RUDDER (DEG)
NOSE GEAR (D)
-3000 -2000 -1000 0 1000 2000 3000 4000 5000 6000 7000 8000 9000
A/C X POSITION (FT)

Figure 5.16

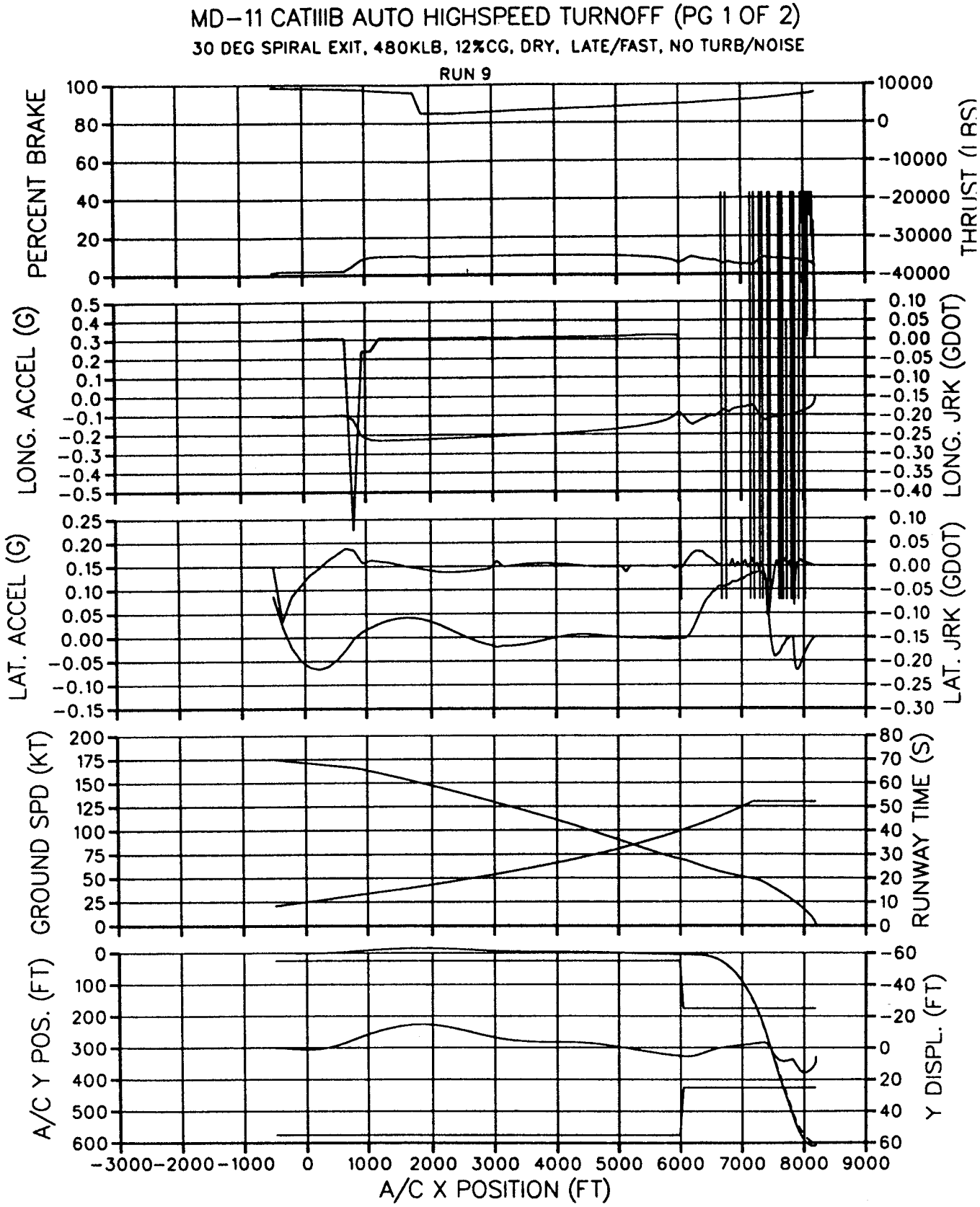
MD-11 CATIIIB AUTO HIGHSPEED TURNOFF (PG 1 OF 2)
30 DEG SPIRAL EXIT, 480KLB, 12%CG, DRY, LATE/FAST, NO TURB/NOISE
RUN 9
PERCENT BRAKE
THRUST (I RS)
LONG. ACCEL (G)
LONG. JRK (GDOT)
LAT. ACCEL (G)
LAT. JRK (GDOT)
GROUND SPD (KT)
RUNWAY TIME (S)
A/C Y POS. (FT)
Y DISPL. (FT)
A/C X POSITION (FT)

Figure 5.17

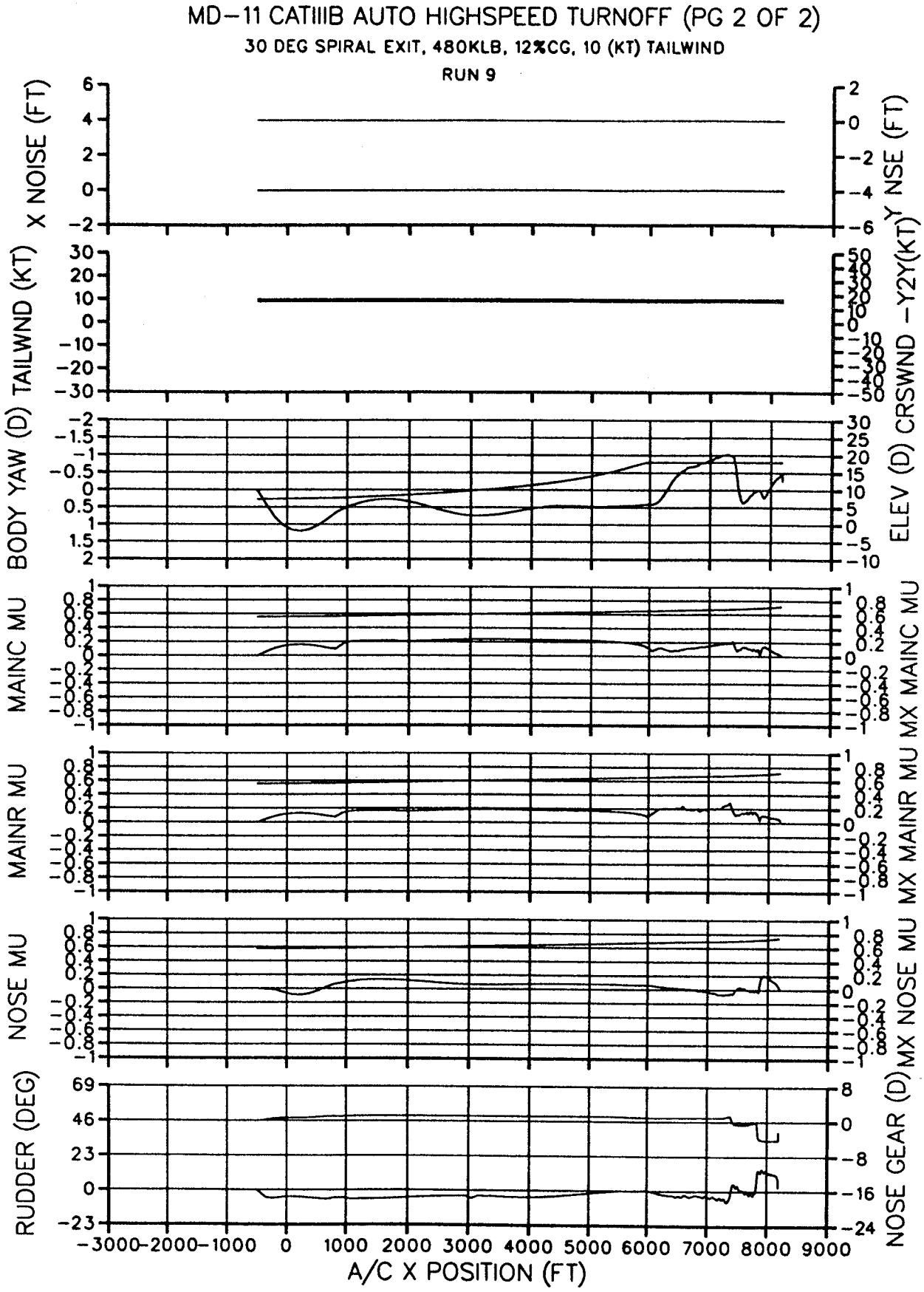
MD–11 CATIIIB AUTO HIGHSPEED TURNOFF (PG 2 OF 2)
30 DEG SPIRAL EXIT, 480KLB, 12%CG, 10 (KT) TAILWIND
RUN 9
X NOISE (FT)
Y NSE (FT)
TAILWND (KT)
CRSWND –Y2Y(KT)
BODY YAW (D)
ELEV (D)
MAINC MU
MX MAINC MU
MAINR MU
MX MAINR MU
NOSE MU
MX NOSE MU
RUDDER (DEG)
NOSE GEAR (D)
A/C X POSITION (FT)

Figure 5.18

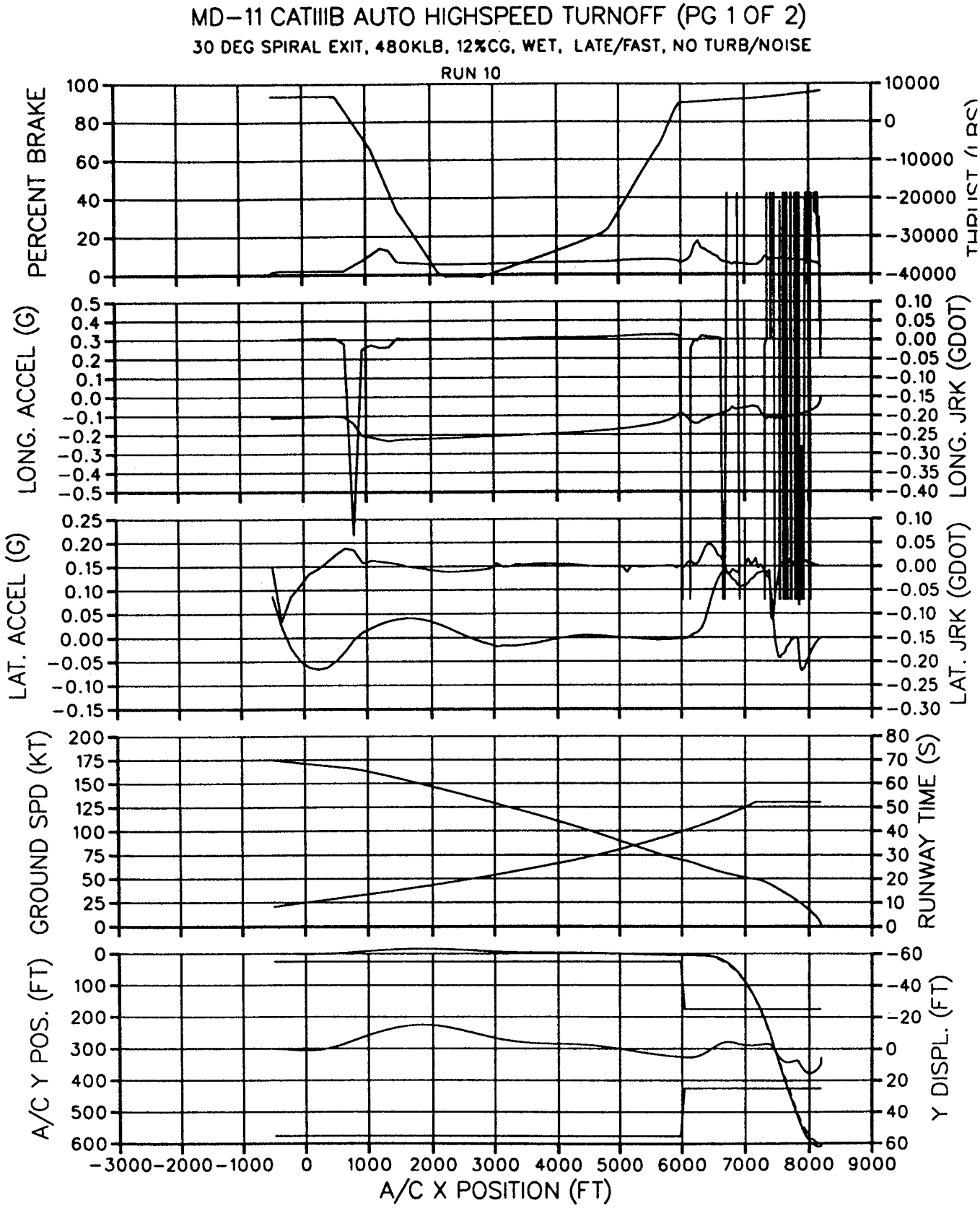
MD-11 CATIIIB AUTO HIGHSPEED TURNOFF (PG 1 OF 2)
30 DEG SPIRAL EXIT, 480KLB, 12%CG, WET, LATE/FAST, NO TURB/NOISE
RUN 10
PERCENT BRAKE
LONG. ACCEL (G)
LONG. JRK (GDOT)
LAT. ACCEL (G)
LAT. JRK (GDOT)
GROUND SPD (KT)
RUNWAY TIME (S)
A/C Y POS. (FT)
Y DISPL. (FT)
A/C X POSITION (FT)

Figure 5.19

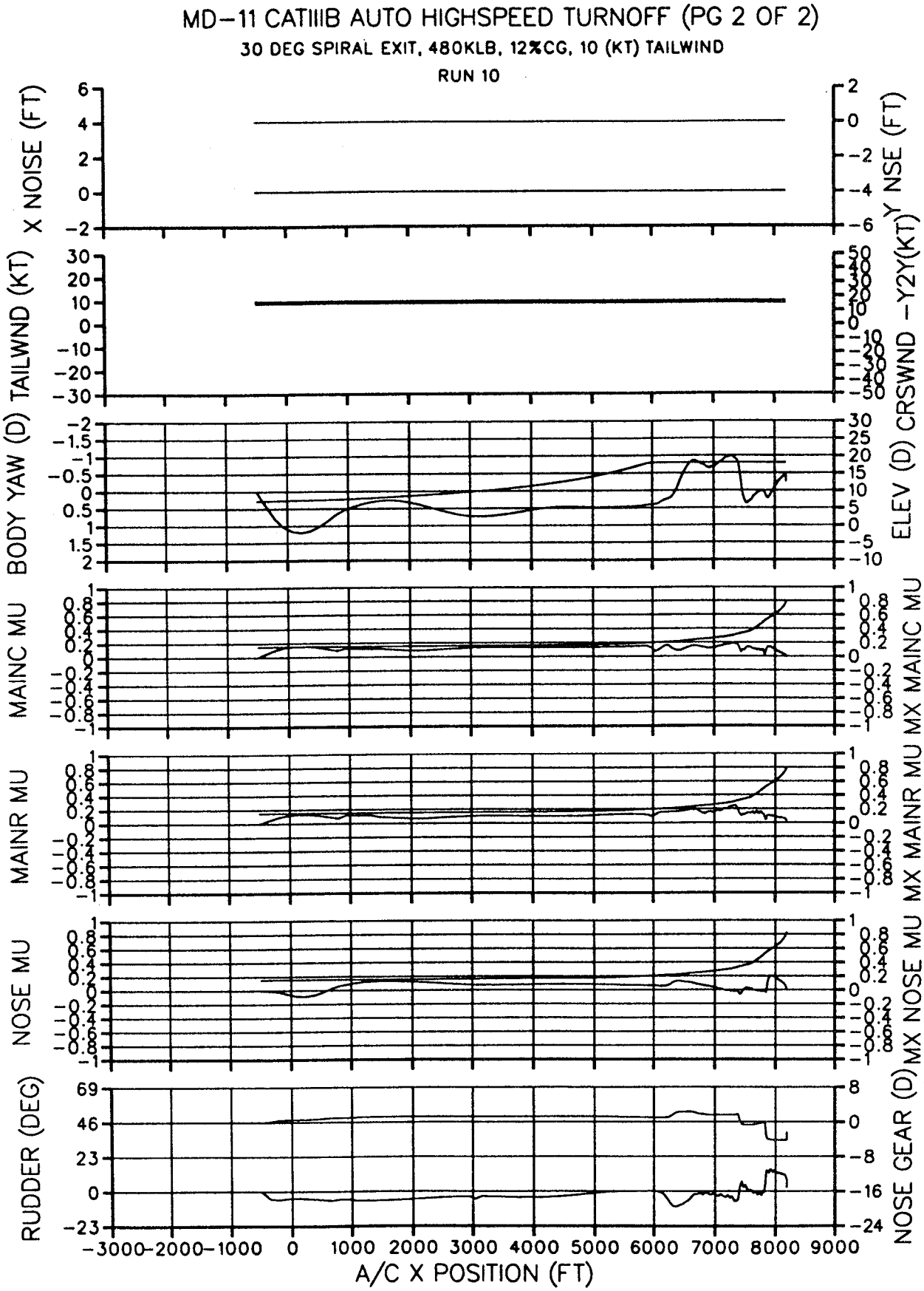
MD-11 CATIIIB AUTO HIGHSPEED TURNOFF (PG 2 OF 2)
30 DEG SPIRAL EXIT, 480KLB, 12%CG, 10 (KT) TAILWIND
RUN 10
X NOISE (FT)
Y NSE (FT)
TAILWND (KT)
CRSWND -Y2Y(KT)
BODY YAW (D)
ELEV (D)
MAINC MU
MX MAINC MU
MAINR MU
MX MAINR MU
NOSE MU
MX NOSE MU
RUDDER (DEG)
NOSE GEAR (D)
-3000 -2000 -1000 0 1000 2000 3000 4000 5000 6000 7000 8000 9000
A/C X POSITION (FT)

Figure 5.20

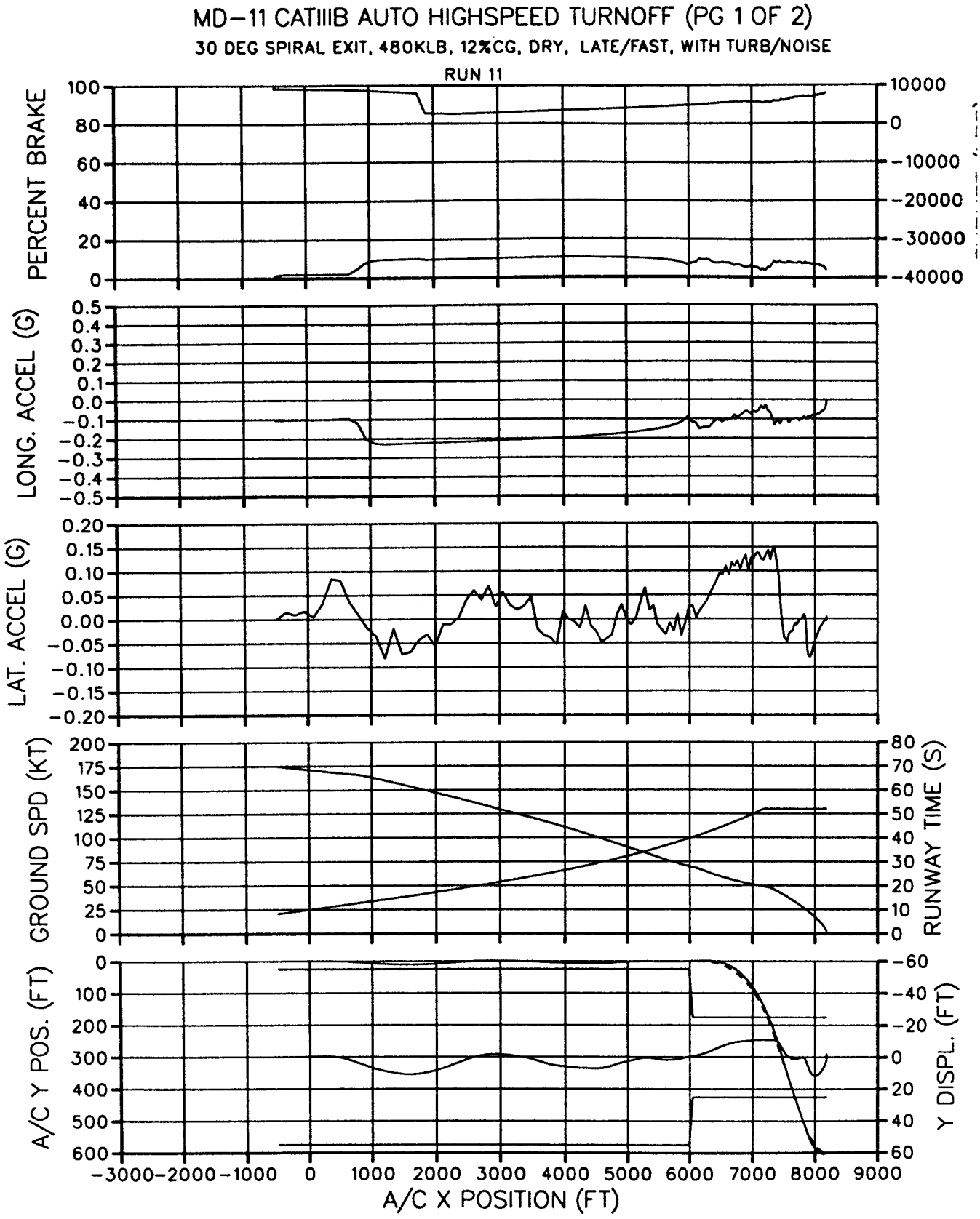
MD–11 CATIIIB AUTO HIGHSPEED TURNOFF (PG 1 OF 2)
30 DEG SPIRAL EXIT, 480KLB, 12%CG, DRY, LATE/FAST, WITH TURB/NOISE
RUN 11
PERCENT BRAKE
LONG. ACCEL (G)
LAT. ACCEL (G)
GROUND SPD (KT)
RUNWAY TIME (S)
A/C Y POS. (FT)
Y DISPL. (FT)
A/C X POSITION (FT)

Figure 5.21

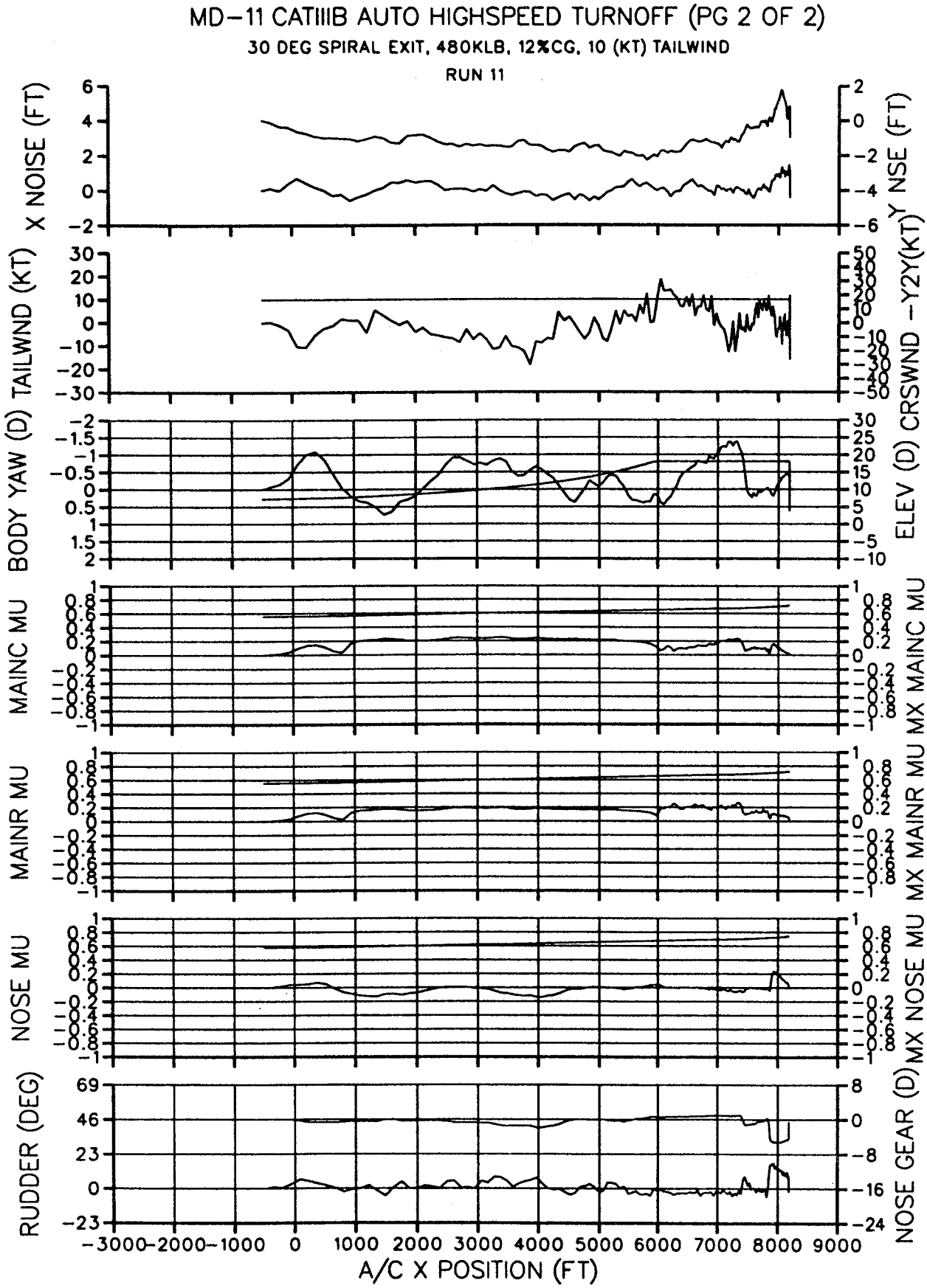
MD-11 CATIIIB AUTO HIGHSPEED TURNOFF (PG 2 OF 2)
30 DEG SPIRAL EXIT, 480KLB, 12%CG, 10 (KT) TAILWIND
RUN 11
X NOISE (FT)
Y NSE (FT)
TAILWND (KT)
CRSWND -Y2Y(KT)
BODY YAW (D)
ELEV (D)
MAINC MU
MX MAINC MU
MAINR MU
MX MAINR MU
NOSE MU
MX NOSE MU
RUDDER (DEG)
NOSE GEAR (D)
-3000 -2000 -1000 0 1000 2000 3000 4000 5000 6000 7000 8000 9000
A/C X POSITION (FT)

Figure 5.22

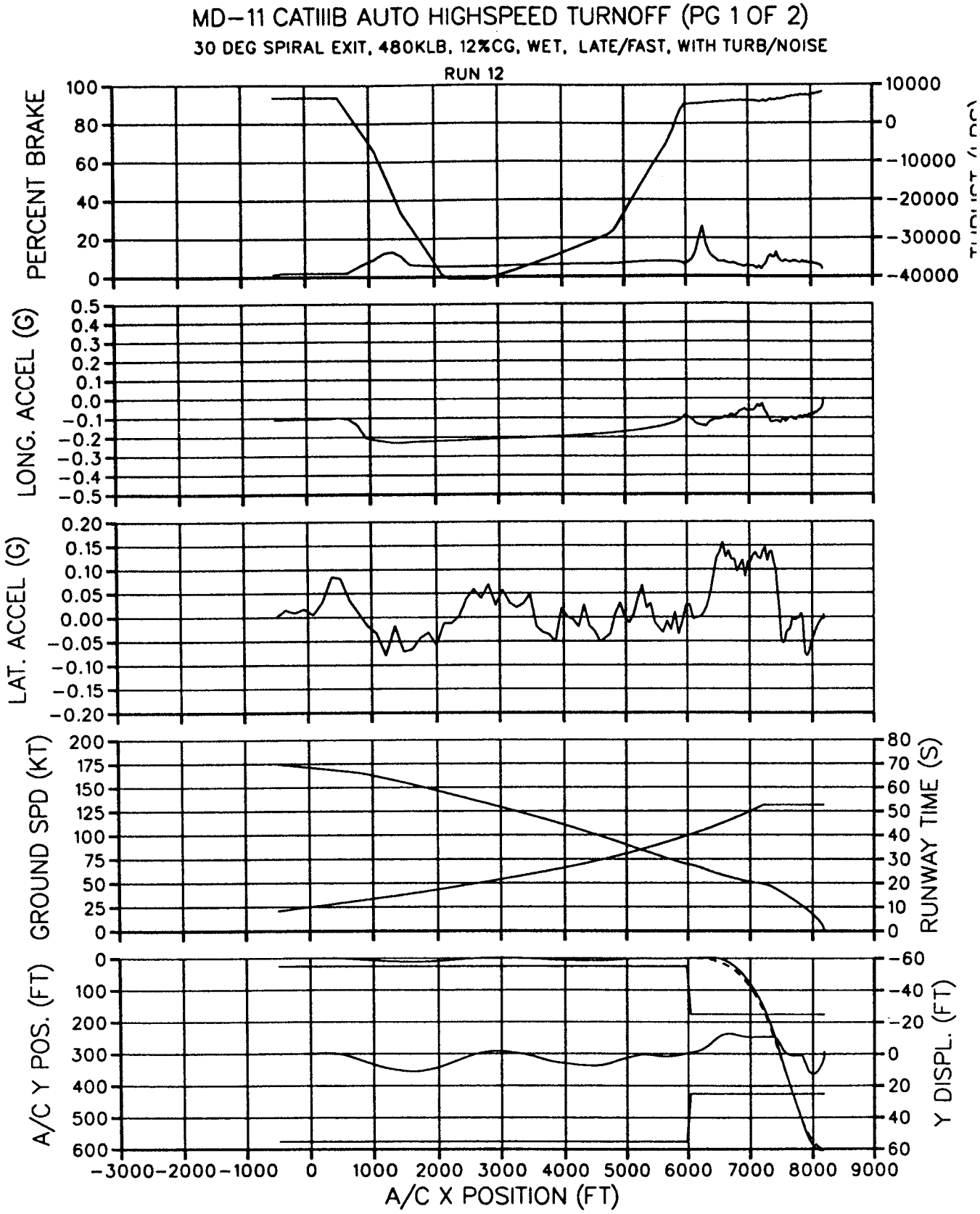
MD-11 CATIIIB AUTO HIGHSPEED TURNOFF (PG 1 OF 2)
30 DEG SPIRAL EXIT, 480KLB, 12%CG, WET, LATE/FAST, WITH TURB/NOISE
RUN 12
PERCENT BRAKE
LONG. ACCEL (G)
LAT. ACCEL (G)
GROUND SPD (KT)
RUNWAY TIME (S)
A/C Y POS. (FT)
Y DISPL. (FT)
A/C X POSITION (FT)

Figure 5.23

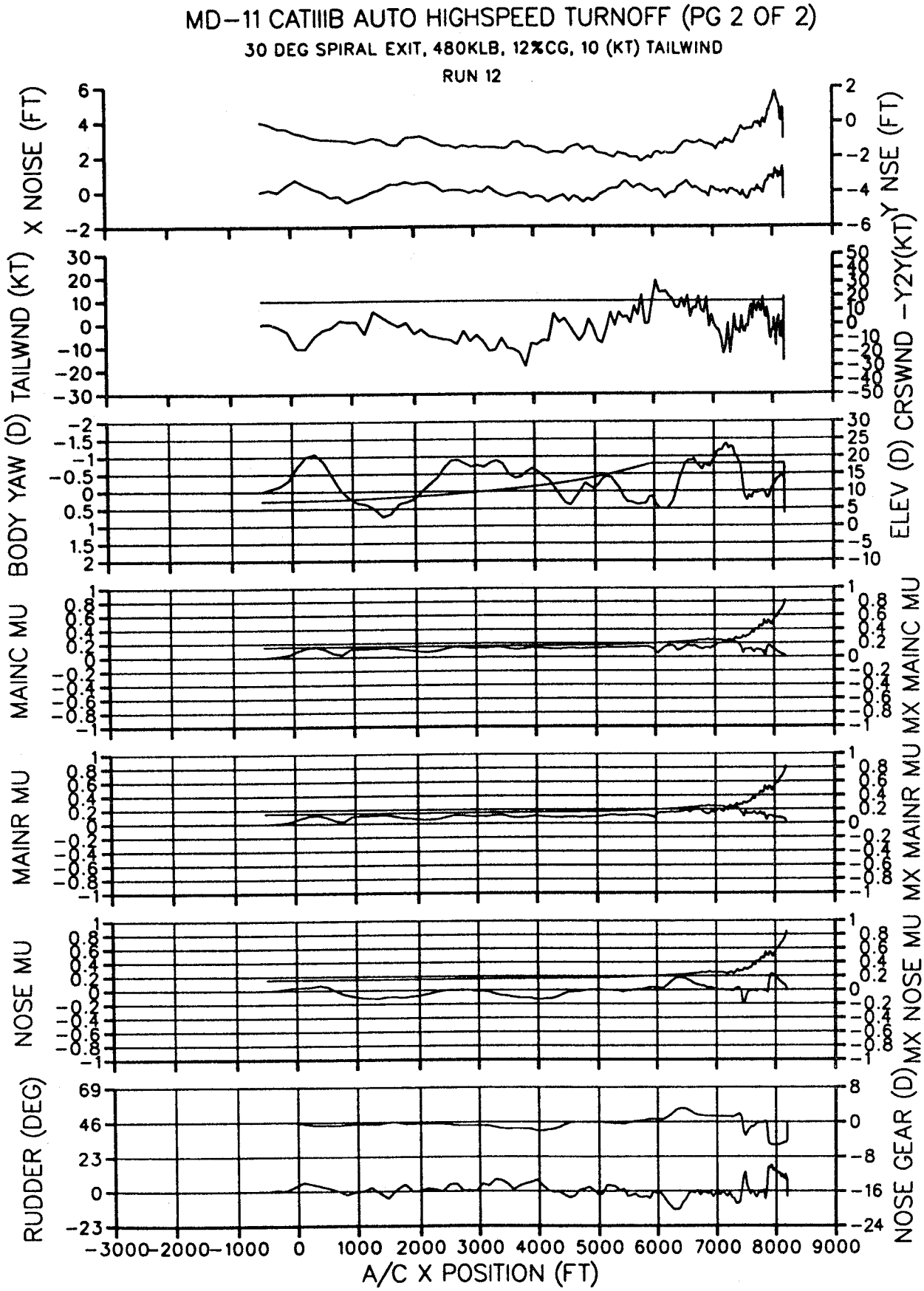
MD-11 CATIIIB AUTO HIGHSPEED TURNOFF (PG 2 OF 2)
30 DEG SPIRAL EXIT, 480KLB, 12%CG, 10 (KT) TAILWIND
RUN 12
X NOISE (FT)
Y NSE (FT)
TAILWND (KT)
CRSWND -Y2Y(KT)
BODY YAW (D)
ELEV (D)
MAINC MU
MX MAINC MU
MAINR MU
MX MAINR MU
NOSE MU
MX NOSE MU
RUDDER (DEG)
NOSE GEAR (D)
A/C X POSITION (FT)

Figure 5.24

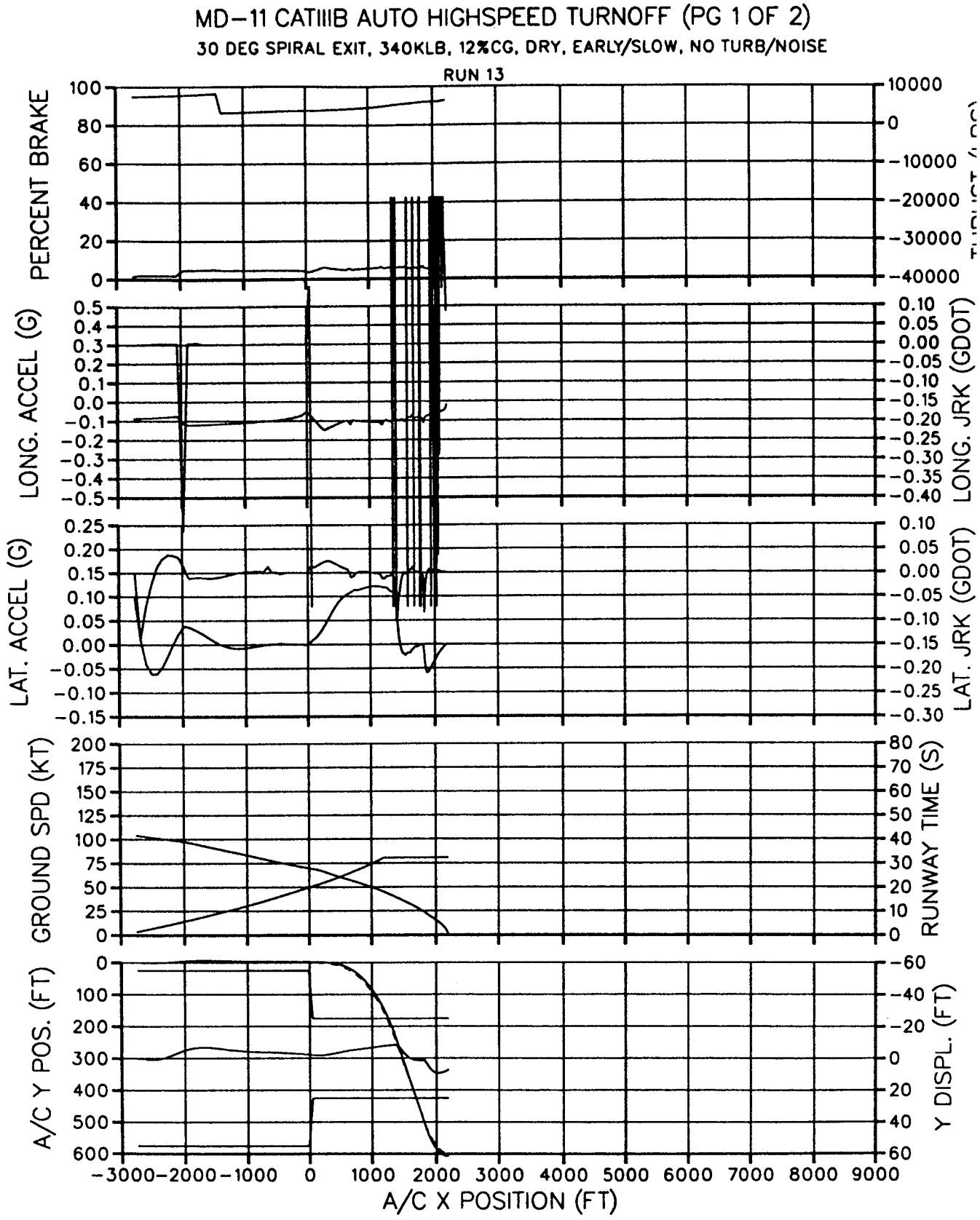
MD-11 CATIIIB AUTO HIGHSPEED TURNOFF (PG 1 OF 2)
30 DEG SPIRAL EXIT, 340KLB, 12%CG, DRY, EARLY/SLOW, NO TURB/NOISE
RUN 13
PERCENT BRAKE
LONG. ACCEL (G)
LONG. JRK (GDOT)
LAT. ACCEL (G)
LAT. JRK (GDOT)
GROUND SPD (KT)
RUNWAY TIME (S)
A/C Y POS. (FT)
Y DISPL. (FT)
A/C X POSITION (FT)

Figure 5.25

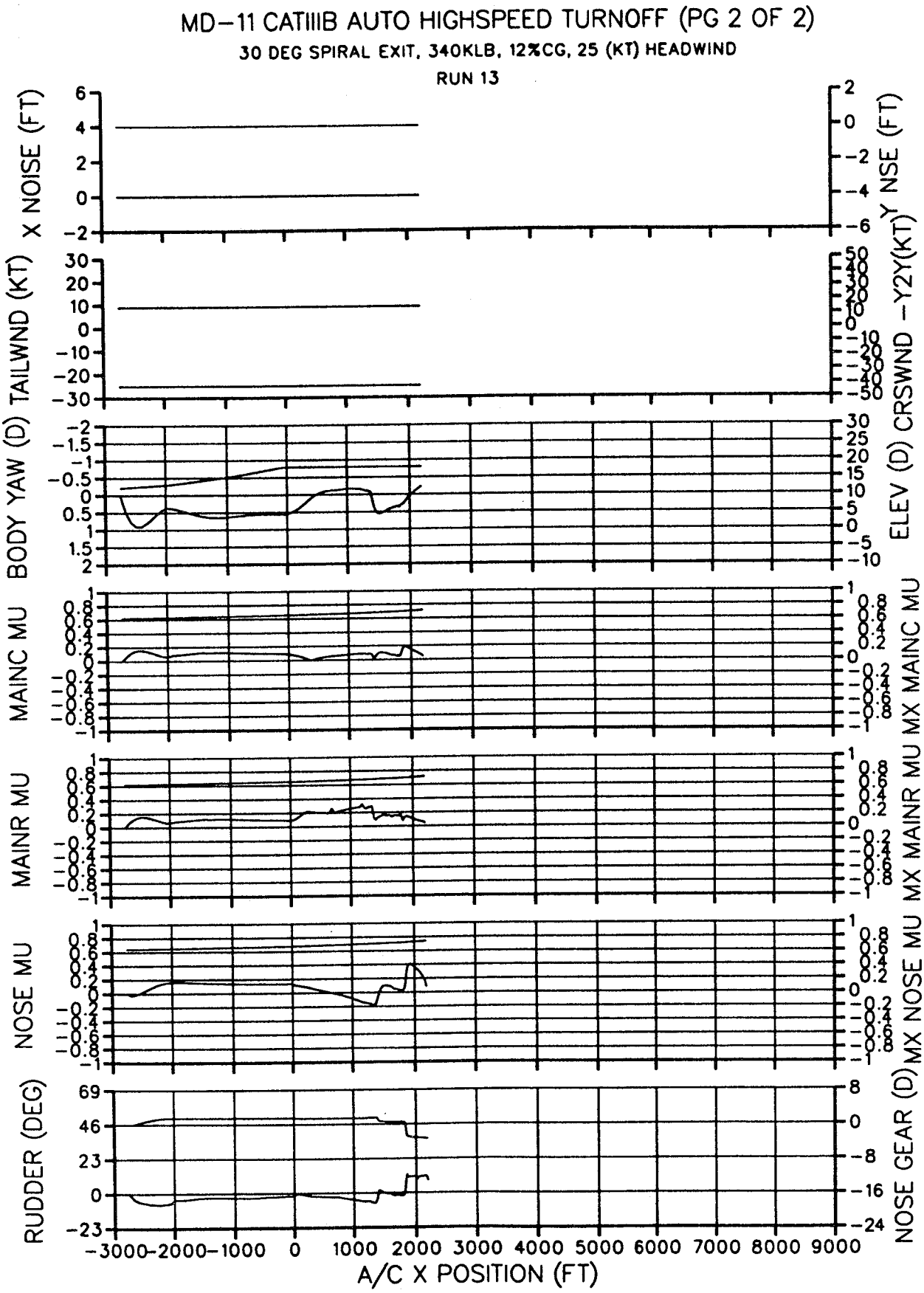
MD-11 CATIIIB AUTO HIGHSPEED TURNOFF (PG 2 OF 2)
30 DEG SPIRAL EXIT, 340KLB, 12%CG, 25 (KT) HEADWIND
RUN 13
X NOISE (FT)
Y NSE (FT)
TAILWND (KT)
CRSWND -Y2Y(KT)
BODY YAW (D)
ELEV (D)
MAINC MU
MX MAINC MU
MAINR MU
MX MAINR MU
NOSE MU
MX NOSE MU
RUDDER (DEG)
NOSE GEAR (D)
-3000 -2000 -1000 0 1000 2000 3000 4000 5000 6000 7000 8000 9000
A/C X POSITION (FT)

Figure 5.26

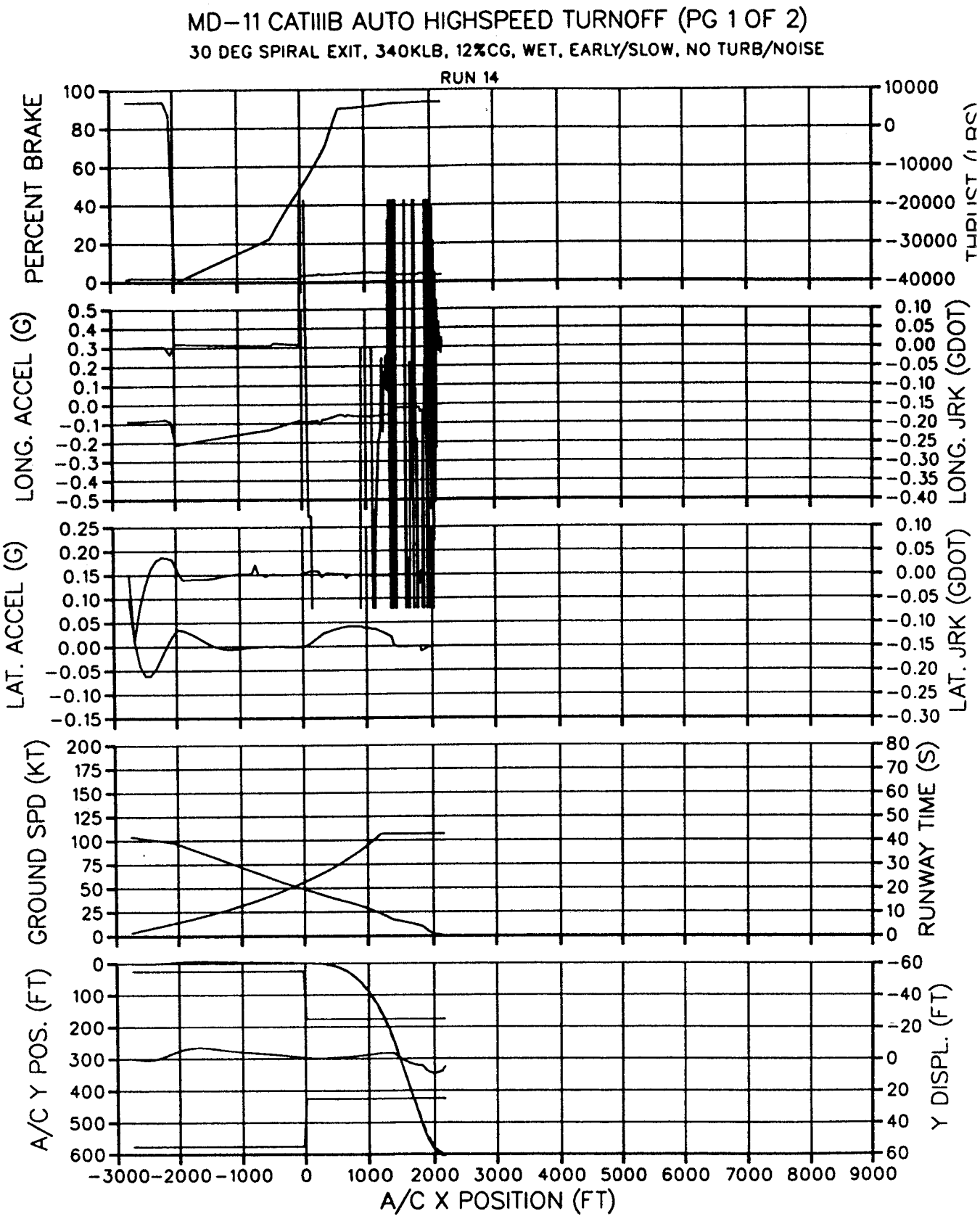
MD-11 CATIIIB AUTO HIGHSPEED TURNOFF (PG 1 OF 2)
30 DEG SPIRAL EXIT, 340KLB, 12%CG, WET, EARLY/SLOW, NO TURB/NOISE
RUN 14
PERCENT BRAKE
LONG. ACCEL (G)
LONG. JRK (GDOT)
LAT. ACCEL (G)
LAT. JRK (GDOT)
GROUND SPD (KT)
RUNWAY TIME (S)
A/C Y POS. (FT)
Y DISPL. (FT)
A/C X POSITION (FT)

Figure 5.27

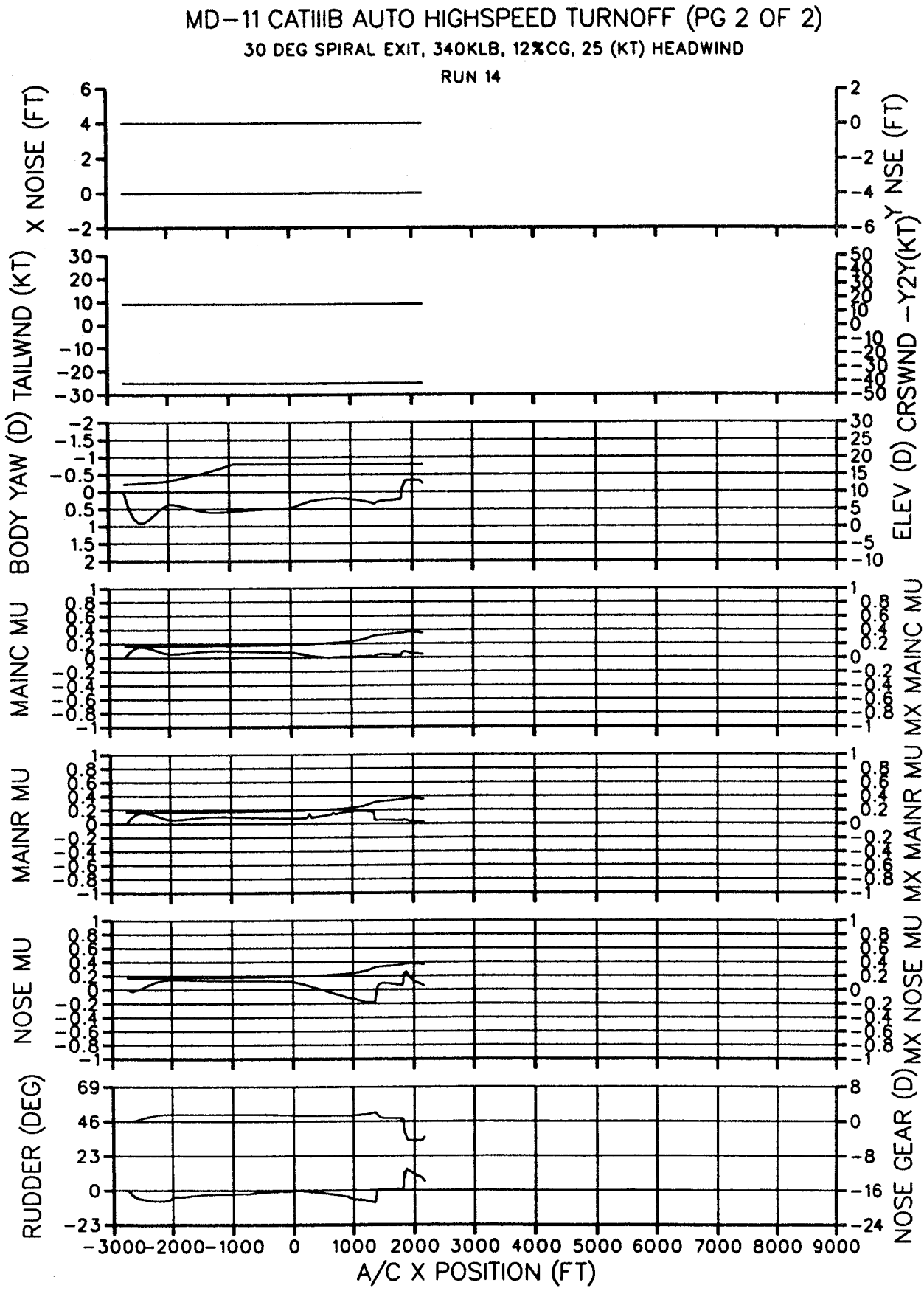
MD-11 CATIIIB AUTO HIGHSPEED TURNOFF (PG 2 OF 2)
30 DEG SPIRAL EXIT, 340KLB, 12%CG, 25 (KT) HEADWIND
RUN 14
X NOISE (FT)
Y NSE (FT)
TAILWND (KT)
Y2Y(KT) CRSWND
BODY YAW (D)
ELEV (D)
MAINC MU
MX MAINC MU
MAINR MU
MX MAINR MU
NOSE MU
MX NOSE MU
RUDDER (DEG)
NOSE GEAR (D)
A/C X POSITION (FT)

Figure 5.28

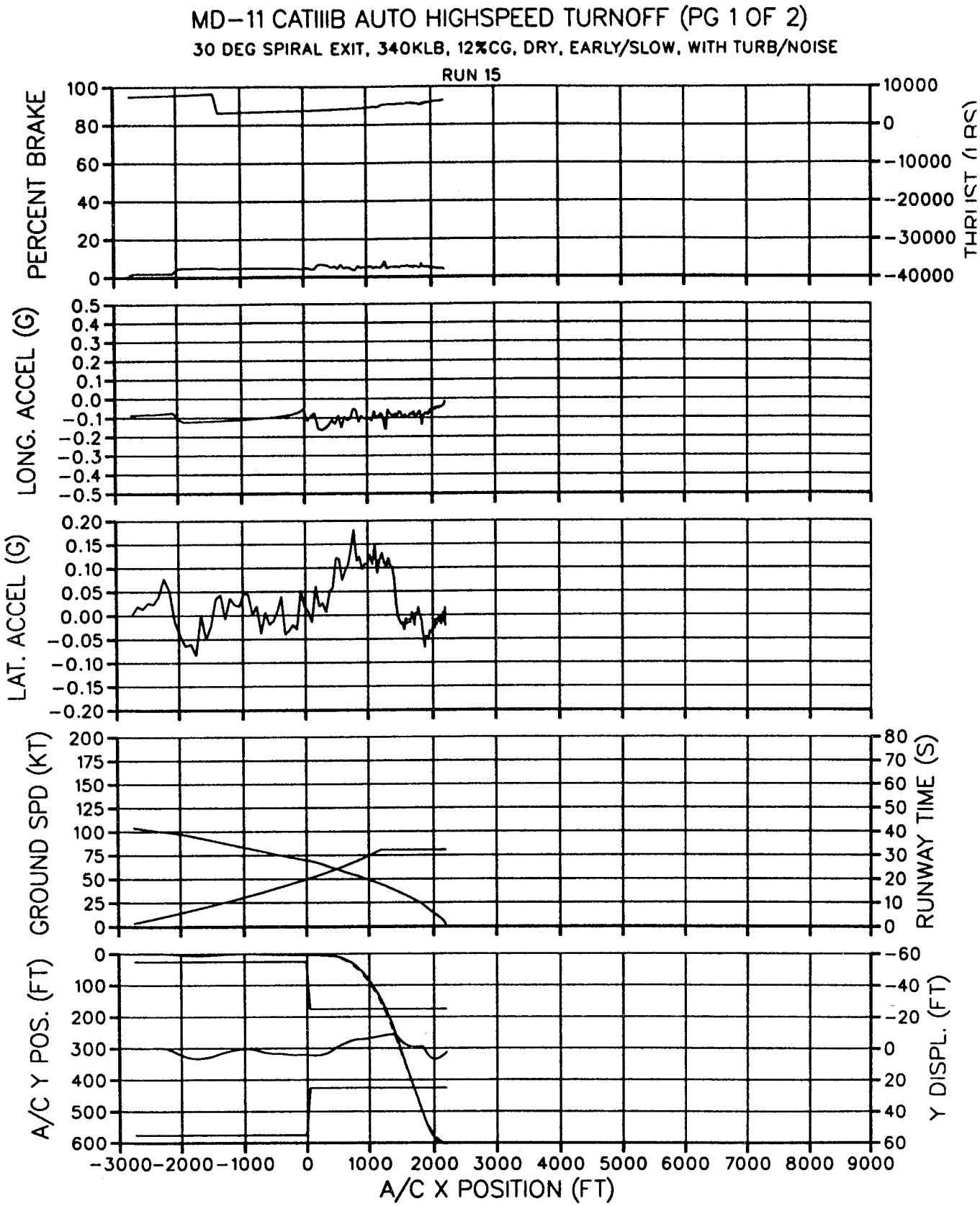
MD-11 CATIIIB AUTO HIGHSPEED TURNOFF (PG 1 OF 2)
30 DEG SPIRAL EXIT, 340KLB, 12%CG, DRY, EARLY/SLOW, WITH TURB/NOISE
RUN 15
PERCENT BRAKE
100
80
60
40
20
0
10000
0
-10000
-20000
-30000
-40000
LONG. ACCEL (G)
0.5
0.4
0.3
0.2
0.1
0.0
-0.1
-0.2
-0.3
-0.4
-0.5
LAT. ACCEL (G)
0.20
0.15
0.10
0.05
0.00
-0.05
-0.10
-0.15
-0.20
GROUND SPD (KT)
200
175
150
125
100
75
50
25
0
RUNWAY TIME (S)
80
70
60
50
40
30
20
10
0
A/C Y POS. (FT)
0
100
200
300
400
500
600
Y DISPL. (FT)
-60
-40
-20
0
20
40
60
-3000 -2000 -1000 0 1000 2000 3000 4000 5000 6000 7000 8000 9000
A/C X POSITION (FT)

Figure 5.29

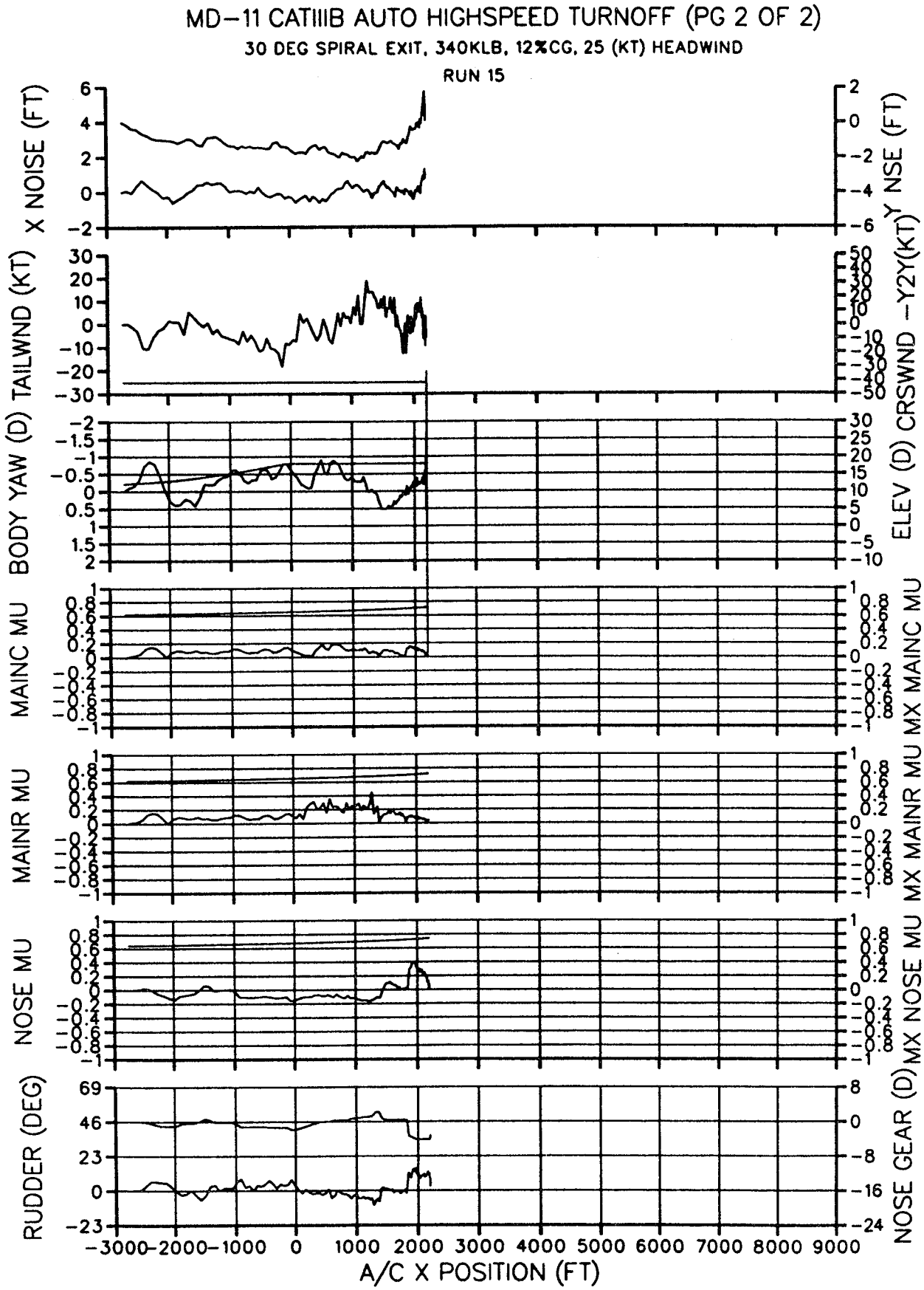
MD-11 CATIIIB AUTO HIGHSPEED TURNOFF (PG 2 OF 2)
30 DEG SPIRAL EXIT, 340KLB, 12%CG, 25 (KT) HEADWIND
RUN 15
X NOISE (FT)
Y NSE (FT)
TAILWND (KT)
-Y2Y(KT)
BODY YAW (D)
CRSWND
ELEV (D)
MAINC MU
MX MAINC MU
MAINR MU
MX MAINR MU
NOSE MU
MX NOSE MU
RUDDER (DEG)
NOSE GEAR (D)
-3000 -2000 -1000 0 1000 2000 3000 4000 5000 6000 7000 8000 9000
A/C X POSITION (FT)

Figure 5.30

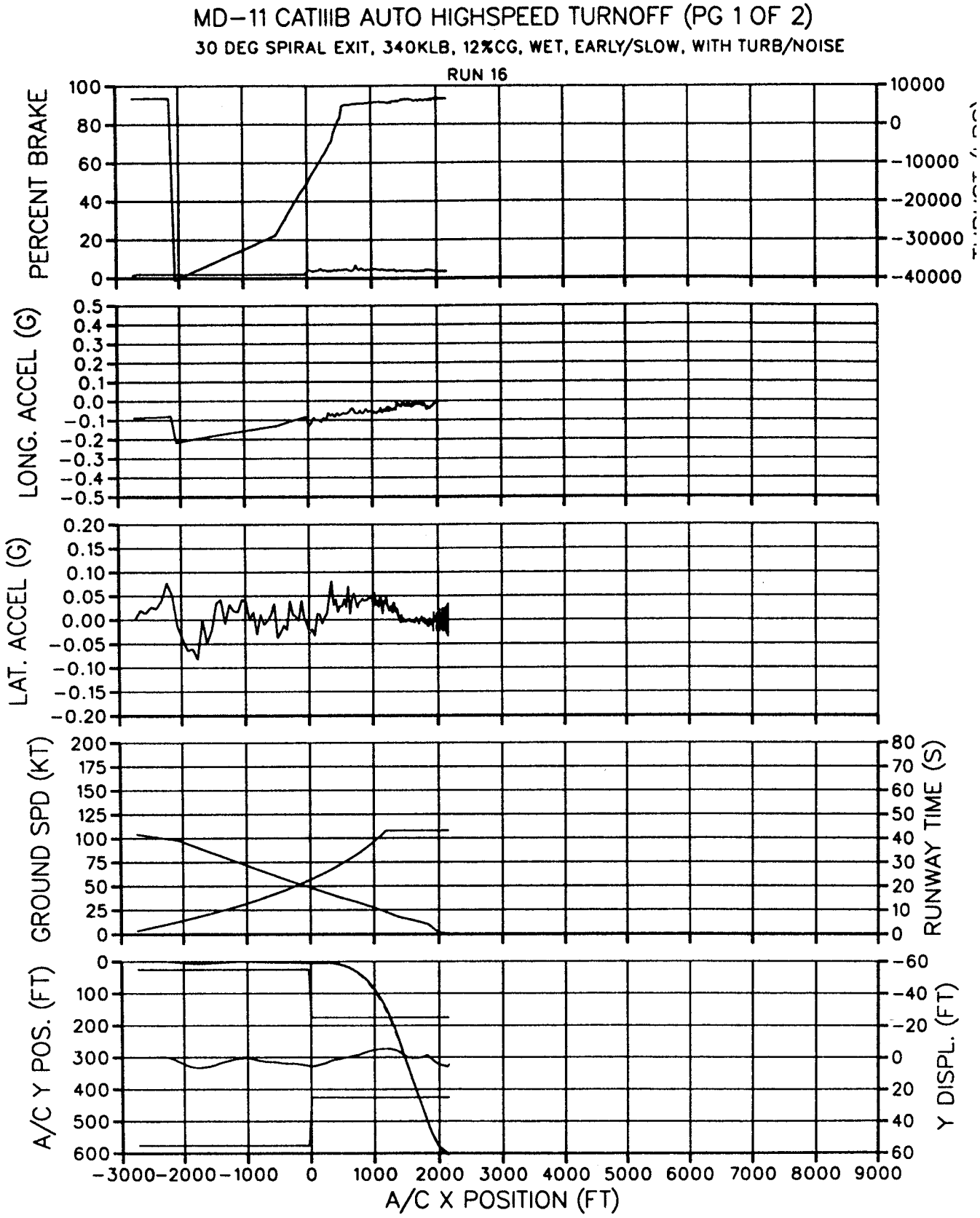
MD–11 CATIIIB AUTO HIGHSPEED TURNOFF (PG 1 OF 2)
30 DEG SPIRAL EXIT, 340KLB, 12%CG, WET, EARLY/SLOW, WITH TURB/NOISE
RUN 16
PERCENT BRAKE
LONG. ACCEL (G)
LAT. ACCEL (G)
GROUND SPD (KT)
RUNWAY TIME (S)
A/C Y POS. (FT)
Y DISPL. (FT)
A/C X POSITION (FT)

Figure 5.31

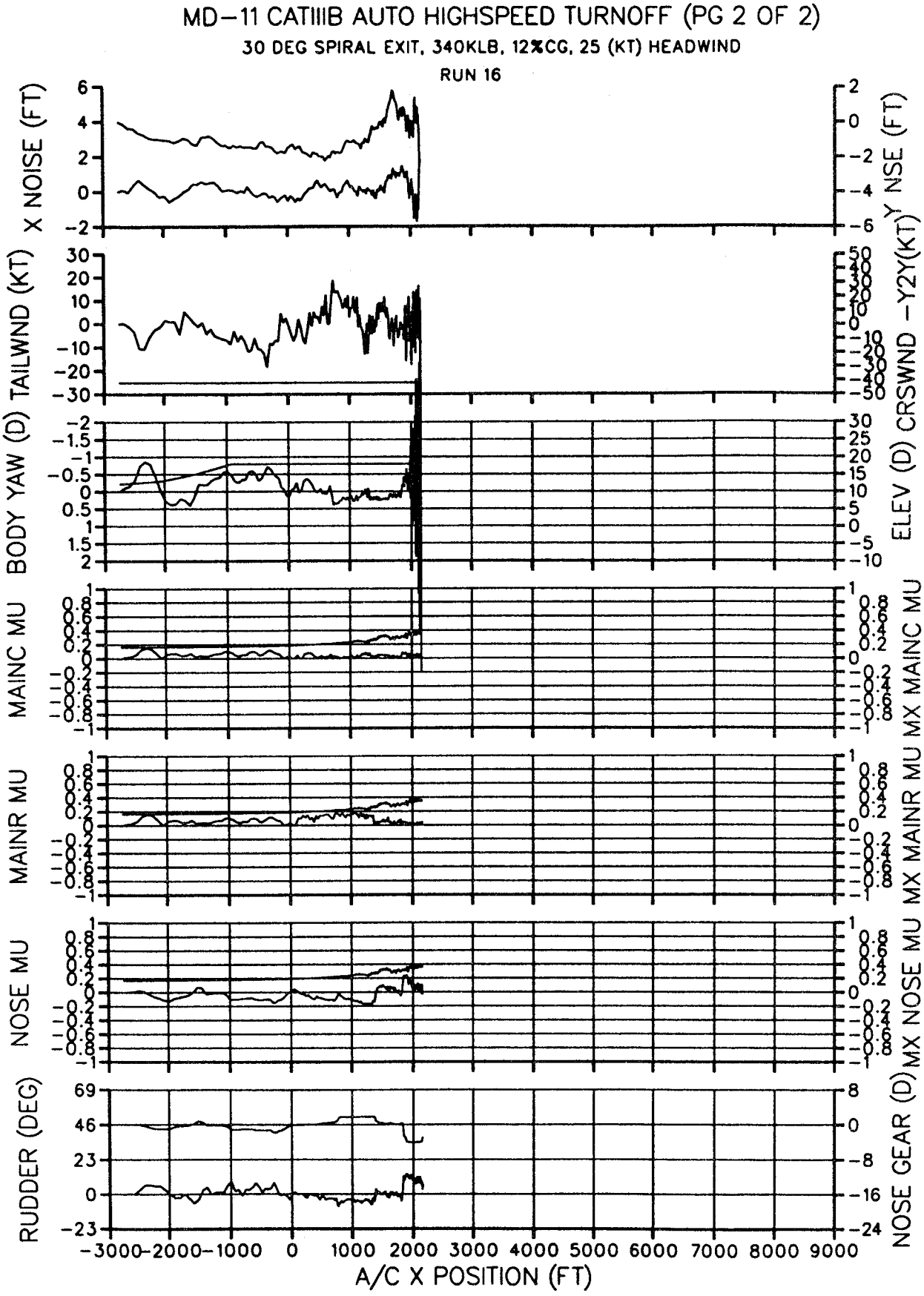
MD–11 CATIIIB AUTO HIGHSPEED TURNOFF (PG 2 OF 2)
30 DEG SPIRAL EXIT, 340KLB, 12%CG, 25 (KT) HEADWIND
RUN 16
X NOISE (FT)
Y NSE (FT)
TAILWND (KT)
CRSWND –Y2Y(KT)
BODY YAW (D)
ELEV (D)
MAINC MU
MX MAINC MU
MAINR MU
MX MAINR MU
NOSE MU
MX NOSE MU
RUDDER (DEG)
NOSE GEAR (D)
A/C X POSITION (FT)

Figure 5.32

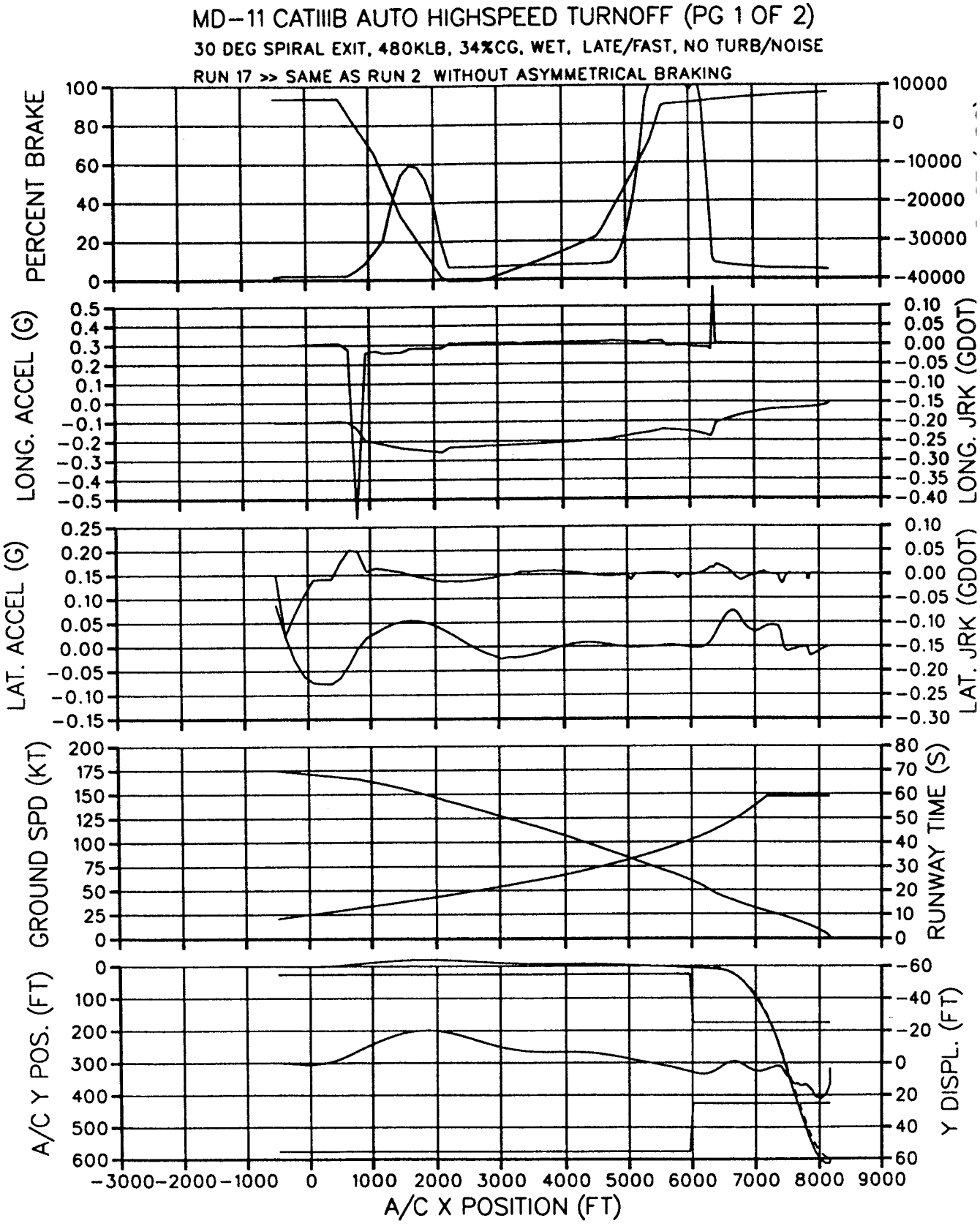
MD-11 CATIIIB AUTO HIGHSPEED TURNOFF (PG 1 OF 2)
30 DEG SPIRAL EXIT, 480KLB, 34%CG, WET, LATE/FAST, NO TURB/NOISE
RUN 17 >> SAME AS RUN 2 WITHOUT ASYMMETRICAL BRAKING
PERCENT BRAKE
LONG. ACCEL (G)
LONG. JRK (GDOT)
LAT. ACCEL (G)
LAT. JRK (GDOT)
GROUND SPD (KT)
RUNWAY TIME (S)
A/C Y POS. (FT)
Y DISPL. (FT)
A/C X POSITION (FT)

Figure 5.33

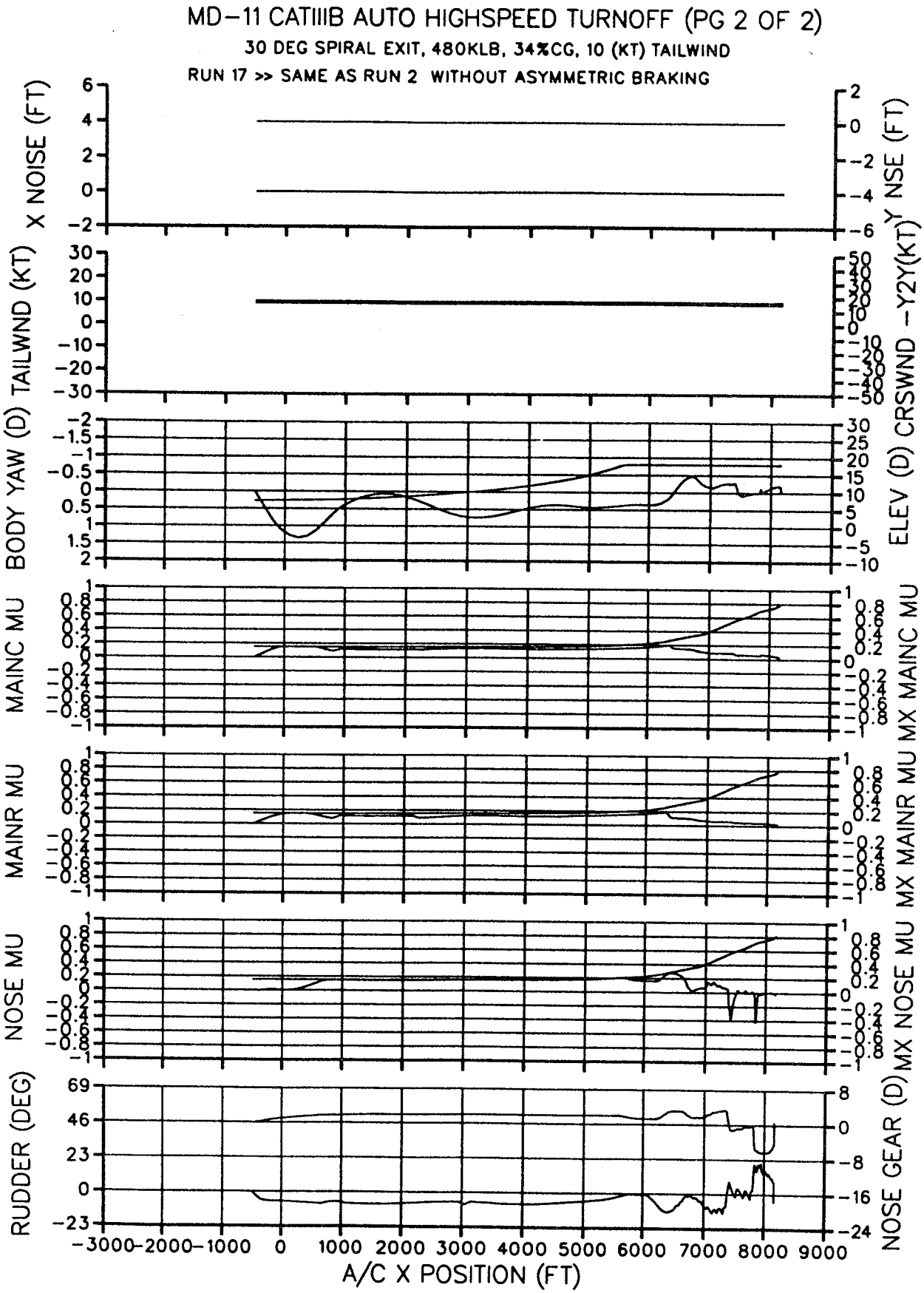
MD-11 CATIIIB AUTO HIGHSPEED TURNOFF (PG 2 OF 2)
30 DEG SPIRAL EXIT, 480KLB, 34%CG, 10 (KT) TAILWIND
RUN 17 >> SAME AS RUN 2 WITHOUT ASYMMETRIC BRAKING
X NOISE (FT)
Y NSE (FT)
TAILWND (KT)
CRSWND -Y2Y(KT)
BODY YAW (D)
ELEV (D)
MAINC MU
MX MAINC MU
MAINR MU
MX MAINR MU
NOSE MU
MX NOSE MU
RUDDER (DEG)
NOSE GEAR (D)
-3000 -2000 -1000 0 1000 2000 3000 4000 5000 6000 7000 8000 9000
A/C X POSITION (FT)

Figure 5.34

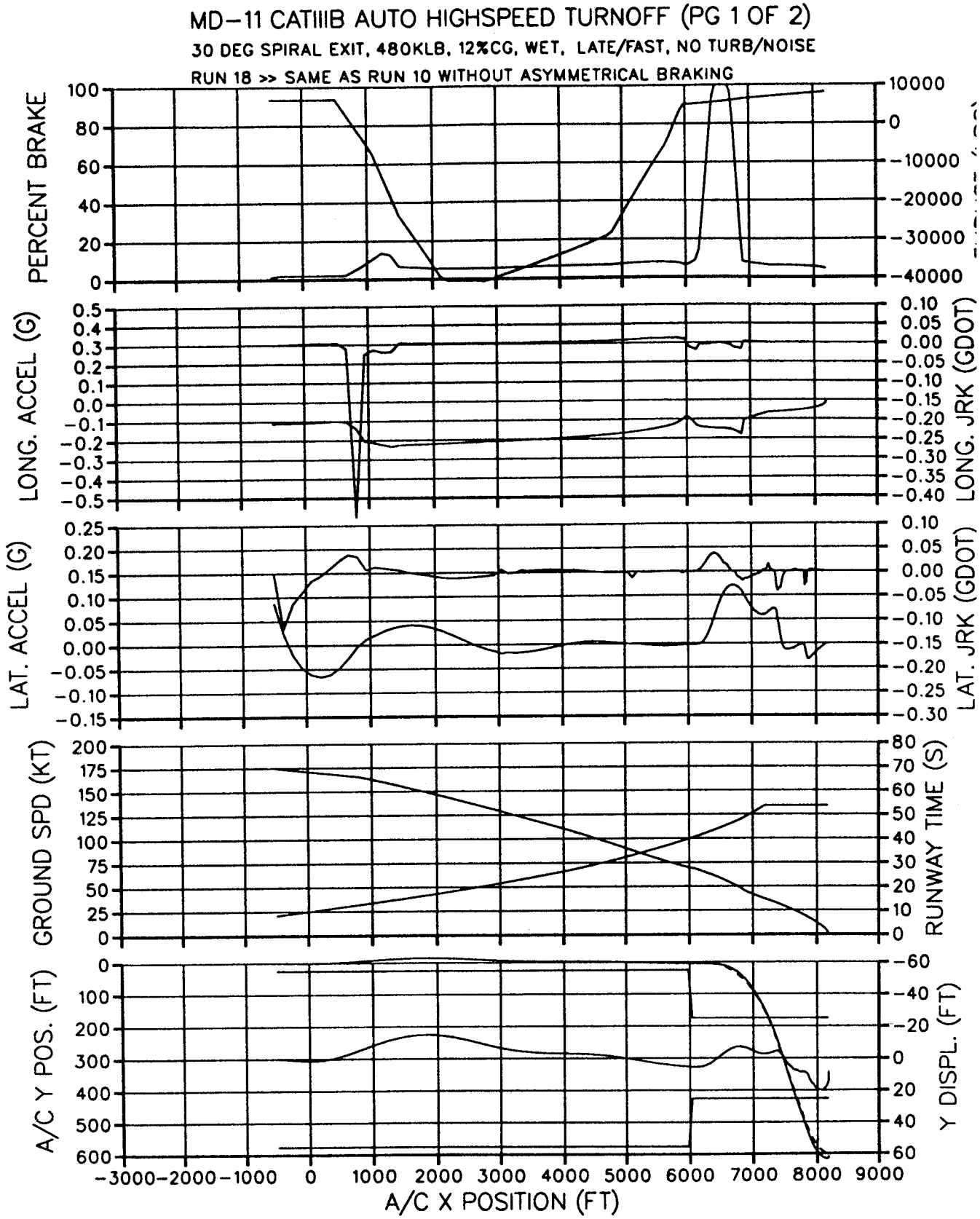
MD-11 CATIIIB AUTO HIGHSPEED TURNOFF (PG 1 OF 2)
30 DEG SPIRAL EXIT, 480KLB, 12%CG, WET, LATE/FAST, NO TURB/NOISE
RUN 18 >> SAME AS RUN 10 WITHOUT ASYMMETRICAL BRAKING
PERCENT BRAKE
LONG. ACCEL (G)
LONG. JRK (GDOT)
LAT. ACCEL (G)
LAT. JRK (GDOT)
GROUND SPD (KT)
RUNWAY TIME (S)
A/C Y POS. (FT)
Y DISPL. (FT)
A/C X POSITION (FT)

Figure 5.35

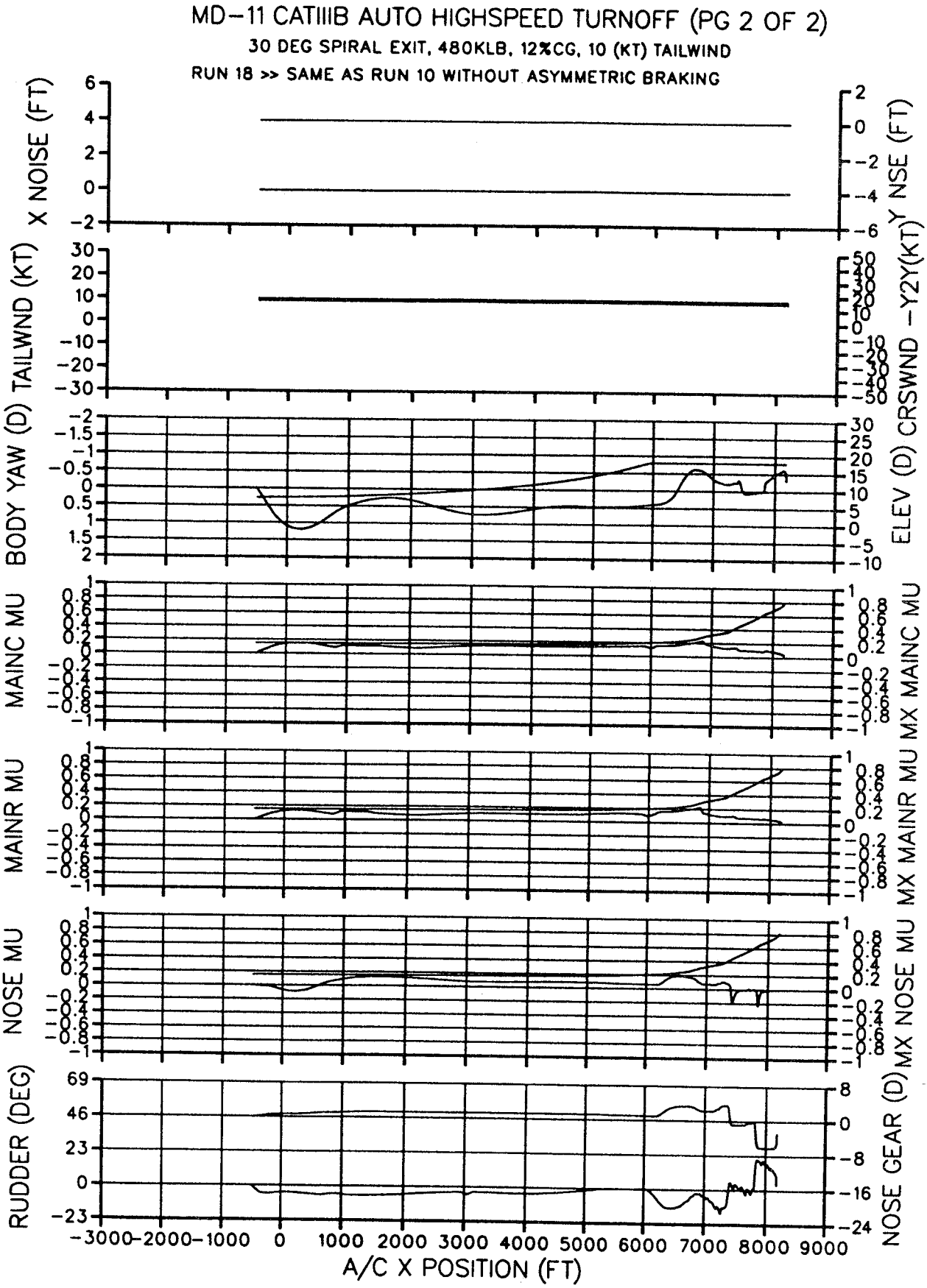
MD-11 CATIIIB AUTO HIGHSPEED TURNOFF (PG 2 OF 2)
30 DEG SPIRAL EXIT, 480KLB, 12%CG, 10 (KT) TAILWIND
RUN 18 >> SAME AS RUN 10 WITHOUT ASYMMETRIC BRAKING
X NOISE (FT)
Y NSE (FT)
TAILWND (KT)
CRSWND -Y2Y(KT)
BODY YAW (D)
ELEV (D)
MAINC MU
MX MAINC MU
MAINR MU
MX MAINR MU
NOSE MU
MX NOSE MU
RUDDER (DEG)
NOSE GEAR (D)
A/C X POSITION (FT)

Figure 5.36

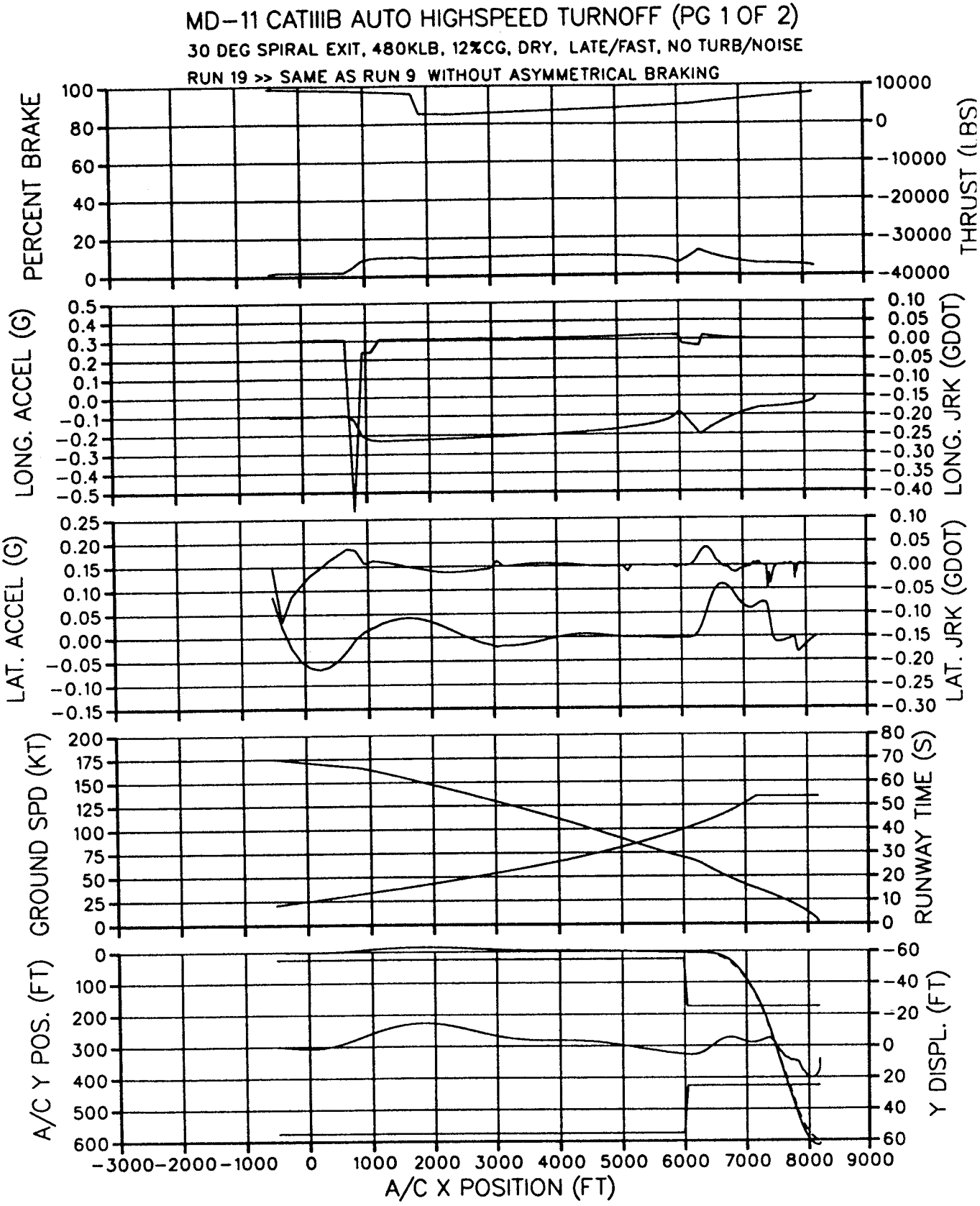
MD-11 CATIIIB AUTO HIGHSPEED TURNOFF (PG 1 OF 2)
30 DEG SPIRAL EXIT, 480KLB, 12%CG, DRY, LATE/FAST, NO TURB/NOISE
RUN 19 >> SAME AS RUN 9 WITHOUT ASYMMETRICAL BRAKING
PERCENT BRAKE
THRUST (LBS)
LONG. ACCEL (G)
LONG. JRK (GDOT)
LAT. ACCEL (G)
LAT. JRK (GDOT)
GROUND SPD (KT)
RUNWAY TIME (S)
A/C Y POS. (FT)
Y DISPL. (FT)
A/C X POSITION (FT)

Figure 5.37

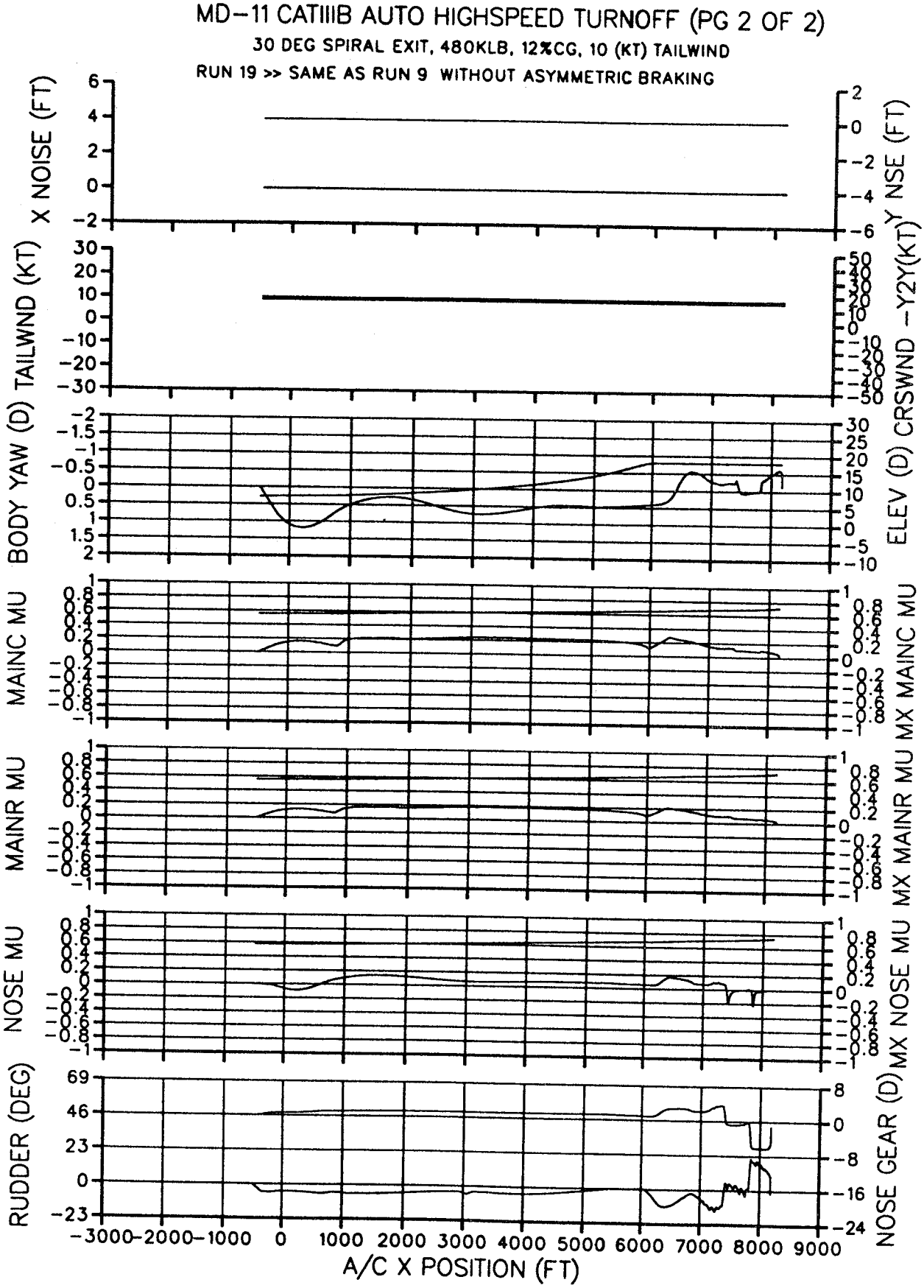
MD-11 CATIIIB AUTO HIGHSPEED TURNOFF (PG 2 OF 2)
30 DEG SPIRAL EXIT, 480KLB, 12%CG, 10 (KT) TAILWIND
RUN 19 >> SAME AS RUN 9 WITHOUT ASYMMETRIC BRAKING
X NOISE (FT)
Y NSE (FT)
TAILWND (KT)
-Y2Y(KT) CRSWND
BODY YAW (D)
ELEV (D)
MAINC MU
MX MAINC MU
MAINR MU
MX MAINR MU
NOSE MU
MX NOSE MU
RUDDER (DEG)
NOSE GEAR (D)
A/C X POSITION (FT)

Figure 5.38

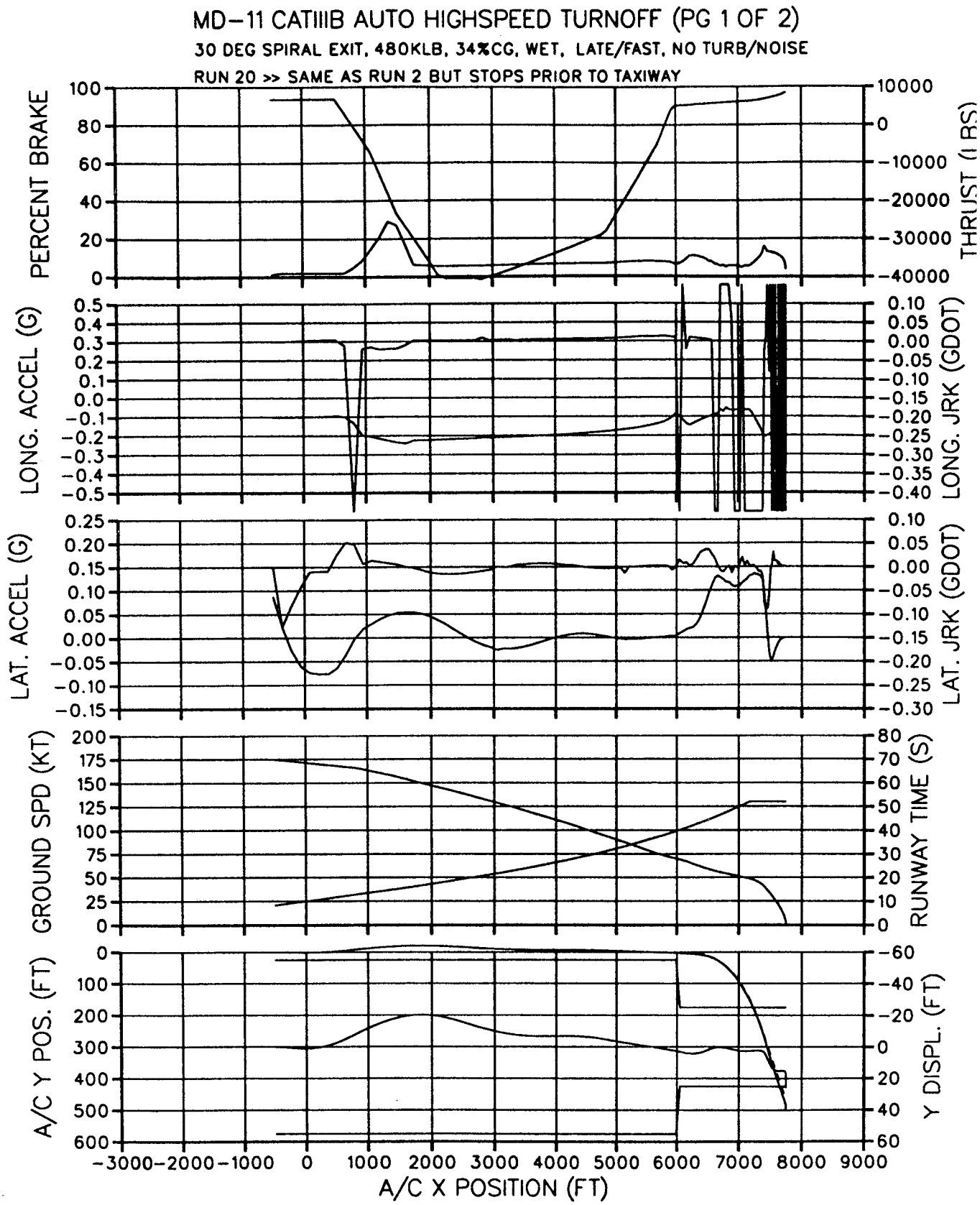
MD-11 CATIIIB AUTO HIGHSPEED TURNOFF (PG 1 OF 2)
30 DEG SPIRAL EXIT, 480KLB, 34%CG, WET, LATE/FAST, NO TURB/NOISE
RUN 20 >> SAME AS RUN 2 BUT STOPS PRIOR TO TAXIWAY
PERCENT BRAKE
THRUST (LBS)
LONG. ACCEL (G)
LONG. JRK (GDOT)
LAT. ACCEL (G)
LAT. JRK (GDOT)
GROUND SPD (KT)
RUNWAY TIME (S)
A/C Y POS. (FT)
Y DISPL. (FT)
A/C X POSITION (FT)

Figure 5.39

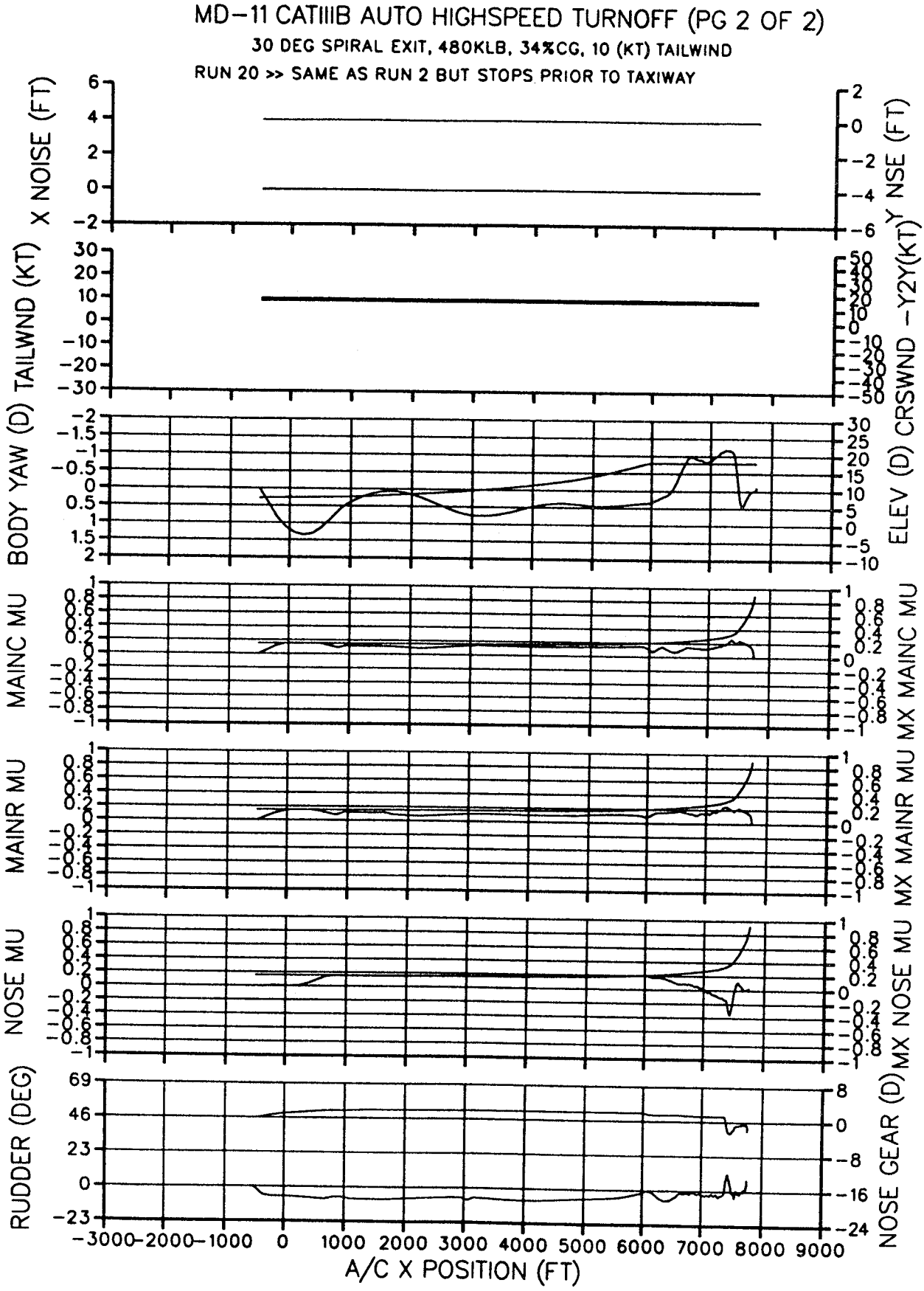
MD-11 CATIIIB AUTO HIGHSPEED TURNOFF (PG 2 OF 2)
30 DEG SPIRAL EXIT, 480KLB, 34%CG, 10 (KT) TAILWIND
RUN 20 >> SAME AS RUN 2 BUT STOPS PRIOR TO TAXIWAY
X NOISE (FT)
Y NSE (FT)
TAILWND (KT)
CRSWND -Y2Y(KT)
BODY YAW (D)
ELEV (D)
MAINC MU
MX MAINC MU
MAINR MU
MX MAINR MU
NOSE MU
MX NOSE MU
RUDDER (DEG)
NOSE GEAR (D)
A/C X POSITION (FT)

Figure 5.40

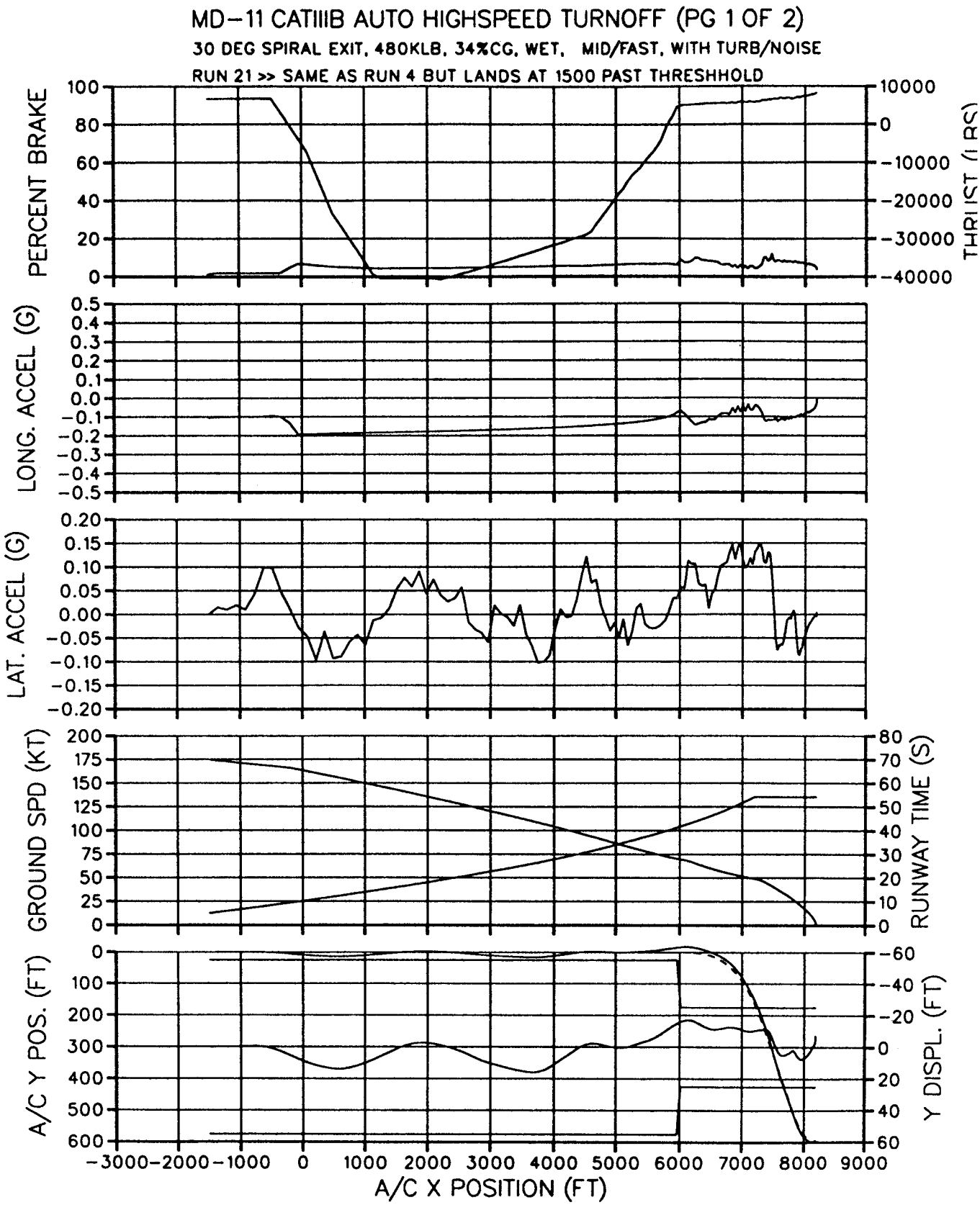
MD-11 CATIIIB AUTO HIGHSPEED TURNOFF (PG 1 OF 2)
30 DEG SPIRAL EXIT, 480KLB, 34%CG, WET, MID/FAST, WITH TURB/NOISE
RUN 21 >> SAME AS RUN 4 BUT LANDS AT 1500 PAST THRESHHOLD
PERCENT BRAKE
THRUST (LBS)
LONG. ACCEL (G)
LAT. ACCEL (G)
GROUND SPD (KT)
RUNWAY TIME (S)
A/C Y POS. (FT)
Y DISPL. (FT)
A/C X POSITION (FT)

Figure 5.41

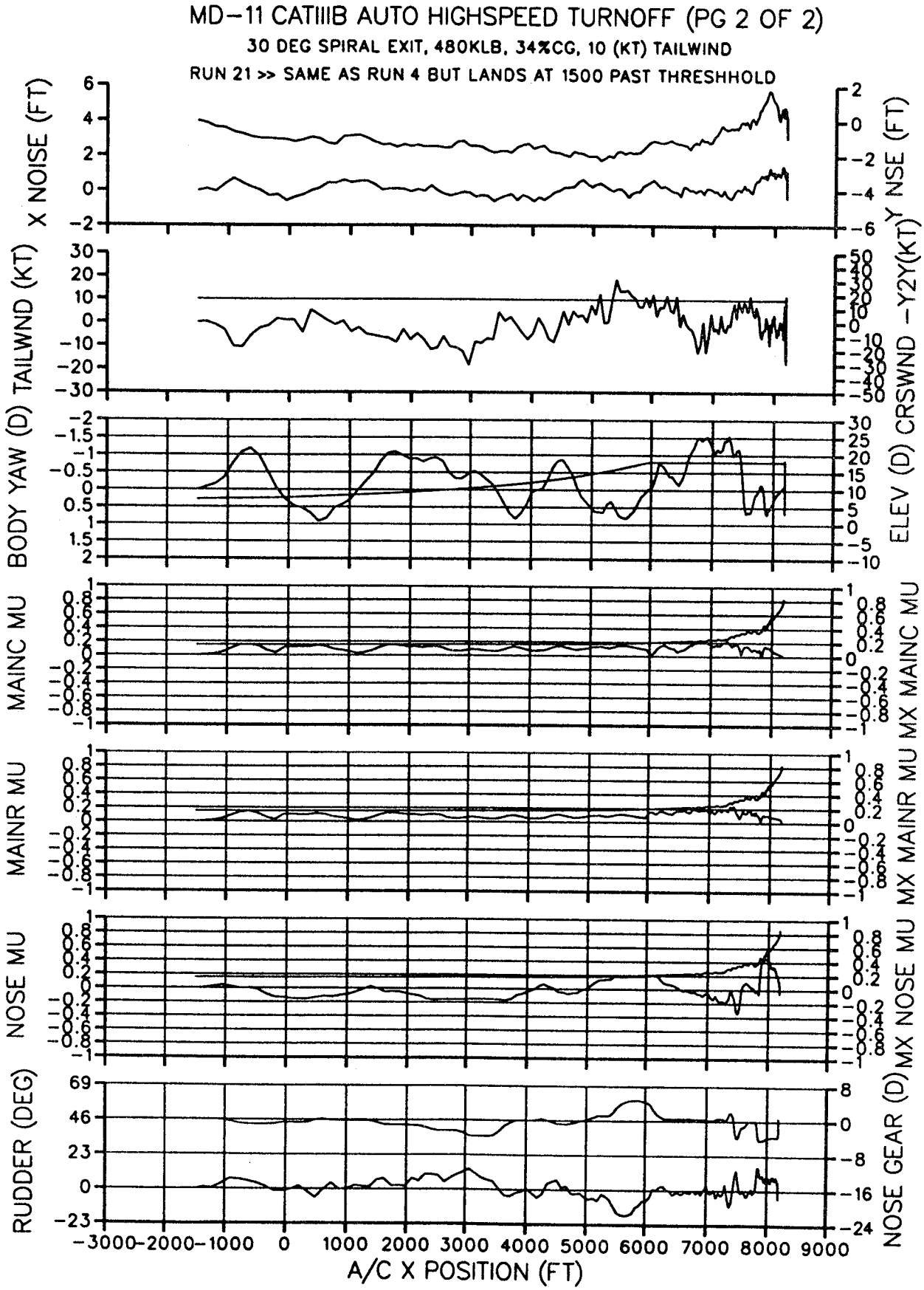
MD-11 CATIIIB AUTO HIGHSPEED TURNOFF (PG 2 OF 2)
30 DEG SPIRAL EXIT, 480KLB, 34%CG, 10 (KT) TAILWIND
RUN 21 >> SAME AS RUN 4 BUT LANDS AT 1500 PAST THRESHHOLD
X NOISE (FT)
Y NSE (FT)
TAILWND (KT)
Y2Y(KT)
CRSWND -
BODY YAW (D)
ELEV (D)
MAINC MU
MX MAINC MU
MAINR MU
MX MAINR MU
NOSE MU
MX NOSE MU
RUDDER (DEG)
NOSE GEAR (D)
A/C X POSITION (FT)

Figure 5.42

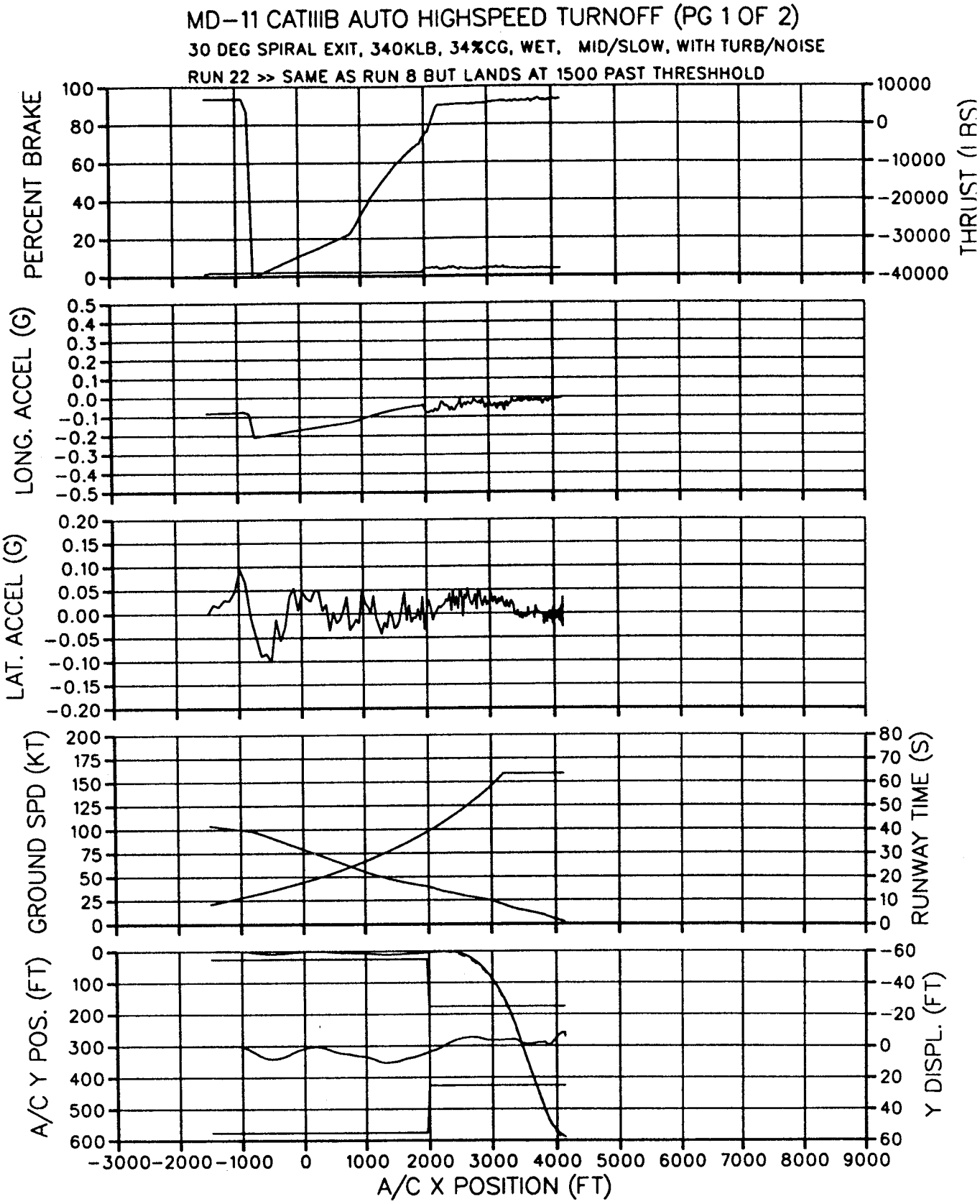
MD-11 CATIIIB AUTO HIGHSPEED TURNOFF (PG 1 OF 2)
30 DEG SPIRAL EXIT, 340KLB, 34%CG, WET, MID/SLOW, WITH TURB/NOISE
RUN 22 >> SAME AS RUN 8 BUT LANDS AT 1500 PAST THRESHHOLD
PERCENT BRAKE
THRUST (LBS)
LONG. ACCEL (G)
LAT. ACCEL (G)
GROUND SPD (KT)
RUNWAY TIME (S)
A/C Y POS. (FT)
Y DISPL. (FT)
A/C X POSITION (FT)

Figure 5.43

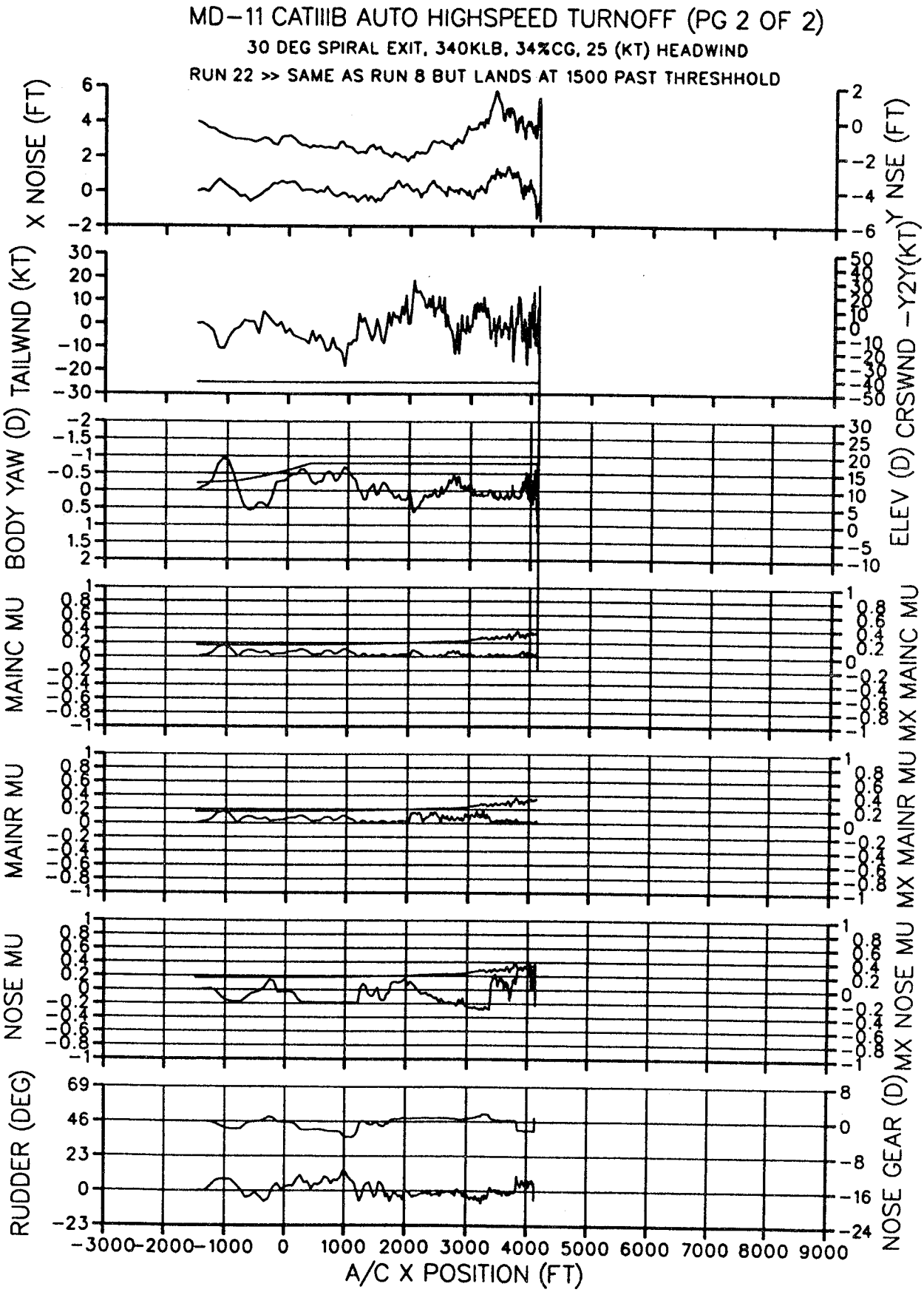

Figure 5.44

C-2

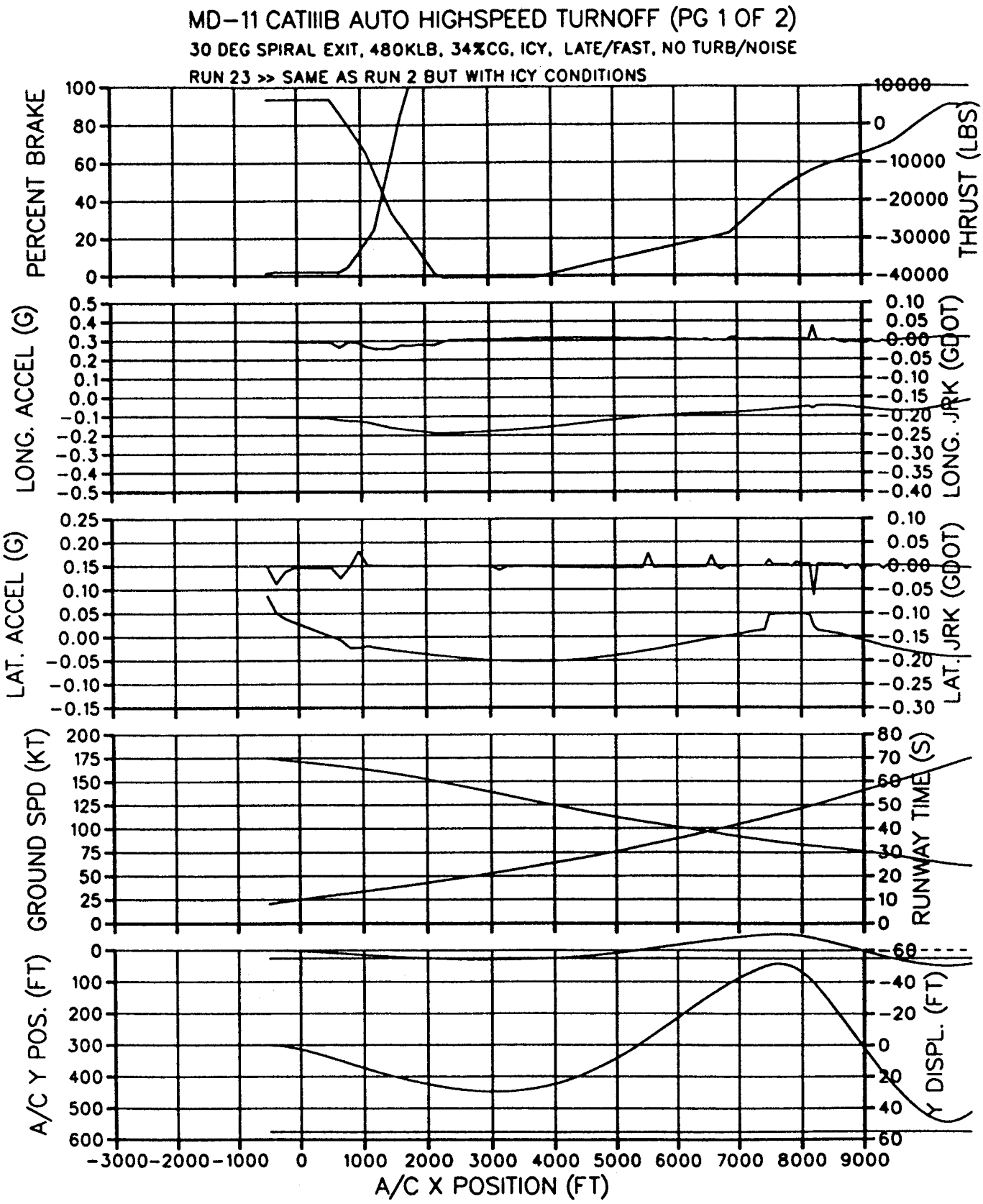
MD-11 CATIIIB AUTO HIGHSPEED TURNOFF (PG 1 OF 2)
30 DEG SPIRAL EXIT, 480KLB, 34%CG, ICY, LATE/FAST, NO TURB/NOISE
RUN 23 >> SAME AS RUN 2 BUT WITH ICY CONDITIONS
PERCENT BRAKE
THRUST (LBS)
LONG. ACCEL (G)
LONG. JRK (GDOT)
LAT. ACCEL (G)
LAT. JRK (GDOT)
GROUND SPD (KT)
RUNWAY TIME (S)
A/C Y POS. (FT)
Y DISPL. (FT)
A/C X POSITION (FT)

Figure 5.45

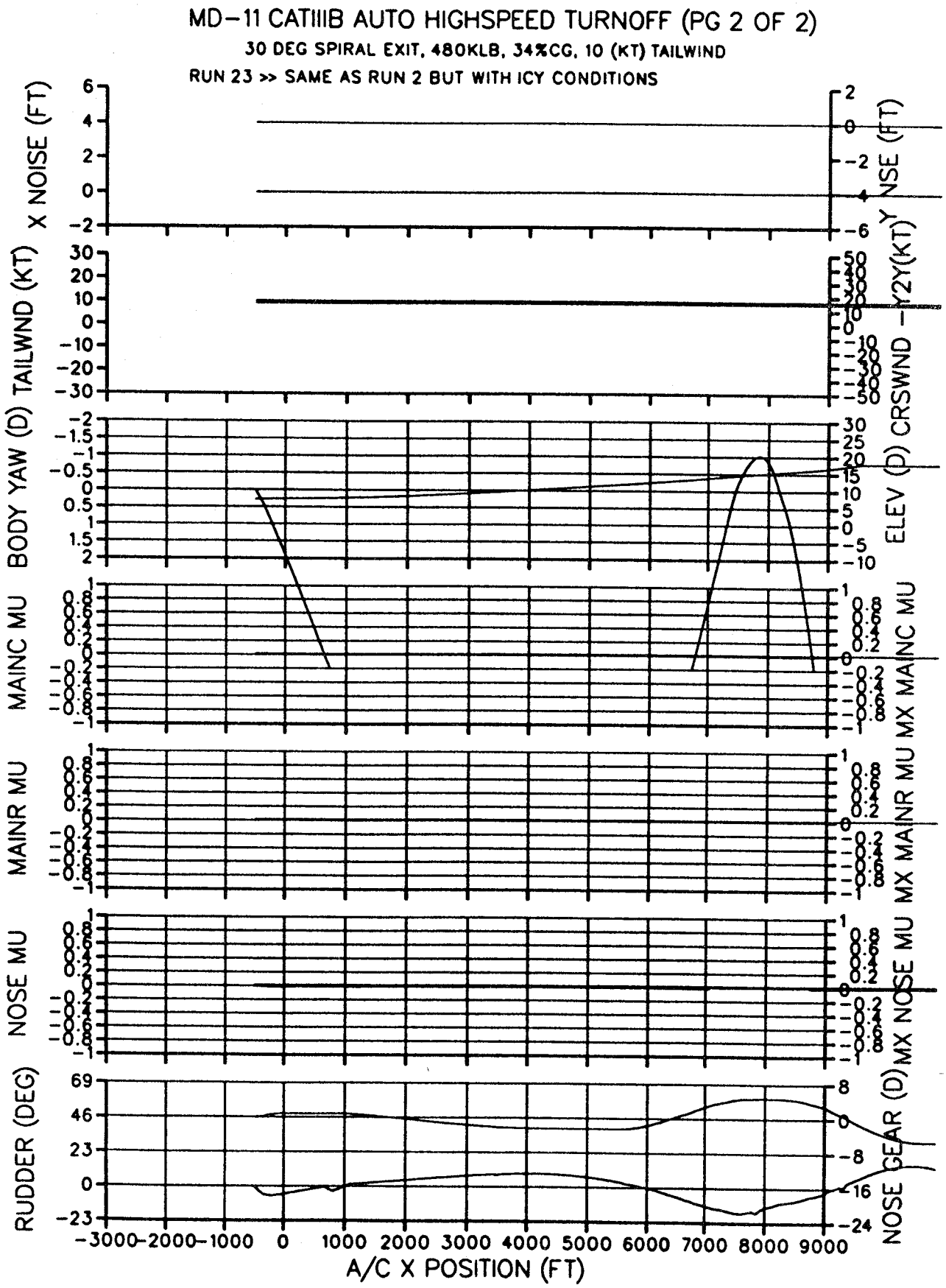
MD-11 CATIIIB AUTO HIGHSPEED TURNOFF (PG 2 OF 2)
30 DEG SPIRAL EXIT, 480KLB, 34%CG, 10 (KT) TAILWIND
RUN 23 >> SAME AS RUN 2 BUT WITH ICY CONDITIONS
X NOISE (FT)
Y NSE (FT)
TAILWND (KT)
CRSWND -Y2Y(KT)
BODY YAW (D)
ELEV (D)
MAINC MU
MX MAINC MU
MAINR MU
MX MAINR MU
NOSE MU
MX NOSE MU
RUDDER (DEG)
NOSE GEAR (D)
-3000 -2000 -1000 0 1000 2000 3000 4000 5000 6000 7000 8000 9000
A/C X POSITION (FT)

Figure 5.46

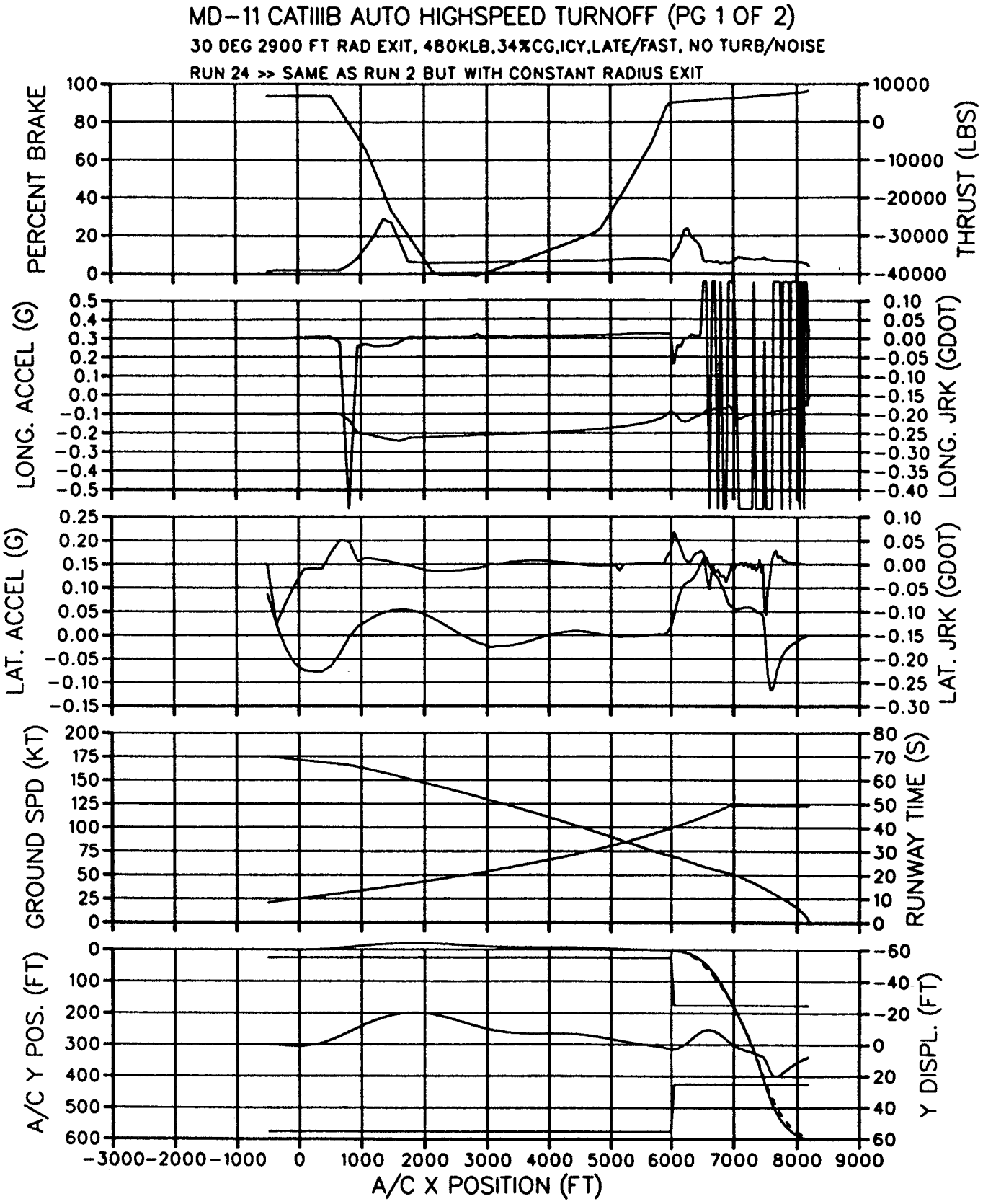
MD-11 CATIIIB AUTO HIGHSPEED TURNOFF (PG 1 OF 2)
30 DEG 2900 FT RAD EXIT, 480KLB,34%CG,ICY,LATE/FAST, NO TURB/NOISE
RUN 24 >> SAME AS RUN 2 BUT WITH CONSTANT RADIUS EXIT
PERCENT BRAKE
THRUST (LBS)
LONG. ACCEL (G)
LONG. JRK (GDOT)
LAT. ACCEL (G)
LAT. JRK (GDOT)
GROUND SPD (KT)
RUNWAY TIME (S)
A/C Y POS. (FT)
Y DISPL. (FT)
A/C X POSITION (FT)

Figure 5.47

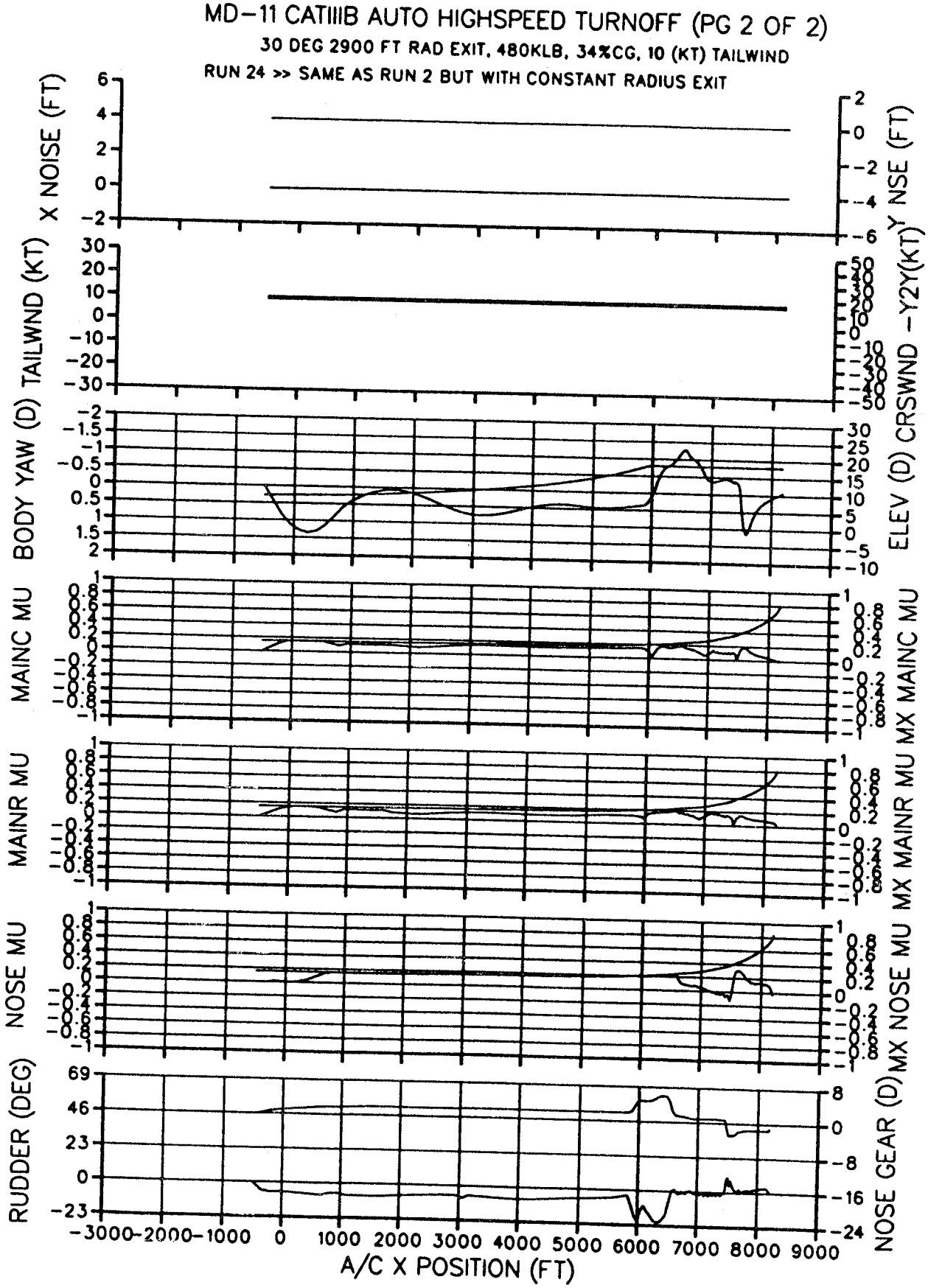
MD-11 CATIIIB AUTO HIGHSPEED TURNOFF (PG 2 OF 2)
30 DEG 2900 FT RAD EXIT, 480KLB, 34%CG, 10 (KT) TAILWIND
RUN 24 >> SAME AS RUN 2 BUT WITH CONSTANT RADIUS EXIT
X NOISE (FT)
Y NSE (FT)
TAILWND (KT)
-Y2Y(KT)
BODY YAW (D)
ELEV (D)
CRSWND
MAINC MU
MX MAINC MU
MAINR MU
MX MAINR MU
NOSE MU
MX NOSE MU
RUDDER (DEG)
NOSE GEAR (D)
A/C X POSITION (FT)

Figure 5.48

APPENDIX A

SURVEY OF RUNWAY COEFFICIENT OF FRICTION MEASUREMENT

INTRODUCTION

OVERVIEW

As a part of the overall objective for Task 3, "The ROTO guidance and control requirements developed in this task shall satisfy and/or accommodate certain factors and/or restrictions or they must include statements as to why certain factors or restrictions cannot be met."

To accomplish the high speed roll-out and turn-off control of the aircraft on the ground is of utmost importance. Since propulsion control provisions of an aircraft are not yet available, the tire-pavement interface friction enables the aircraft components to development loads for guidance, braking and turning of the aircraft on the ground. Accomplishing this maneuver in ceiling and visibility unlimited (CAVU) conditions is critical and even more critical under Category III B conditions for which this study is to address.

Background

Extensive work has been done on the measurement of runway friction with friction measuring carts and vehicles and correlation of the measured friction with that experienced by an aircraft. This work dates back, at least, to the early 1960's; however, congressional emphasis was placed on the problem after two aircraft accidents involving contaminated runways occurred early in 1983. After these, The U. S. Congress passed a bill directing that "the FAA, in conjunction with NASA, study the correlation between aircraft stopping performance and runway friction measurement on wet and contaminated surfaces... ." Since that time much work has been done by the FAA and NASA on the testing of several friction measuring vehicles and obtaining correlation of the measured friction values with those which were obtained with aircraft. The most significant and comprehensive reporting of this work is given by a compendium, Reference A5.

Work has been done relative to runway occupancy, turn-off and attendant problems as shown in references given in this Appendix. However, a cursory review of some of these indicates that the consideration of runway friction coefficient has not been addressed. Therefore, the study of runway friction relative to accomplishing high speed turn-off will be greatly beneficial.

The scope of this study encompasses the review of pertinent references as they apply to the following specific items for consideration:

> Assess the state-of-the-art in measurement of runway coefficient of friction for various runway conditions - dry, wet, icy, snow-packed and slush.

Identify operational limits and concerns in achieving the runway coefficient of friction measurement.

Perform literature search to determine the practicality of providing a sufficiently accurate coefficient of friction measurement for the ROTO braking function.

DISCUSSION

STATE-OF-THE-ART

Each of the considerations listed above will be addressed separately. The first of these is: "Assess the state-of-the-art in measurement of runway coefficient of friction for various runway conditions - dry, wet, icy, snow-packed and slush."

Current and Recent Work

The latest work with runway friction and measuring vehicles is reported by the Summary and Proceedings of the First Annual Tire/Runway Friction Workshop held at NASA Wallops Flight Facility, May 1994 (Reference A6). This was an international workshop with people from Canada, England, France, Hong Kong, Japan, Norway, Scotland, Sweden, United States, and The Netherlands giving reports on tests on thirteen friction measuring vehicles and seven texture measuring devices. Copies of only ten of the sixteen reports were disseminated with the proceedings, and of those published, additional study of the data obtained will be necessary before their full significance can be determined. The Proceedings and the attendance illustrate the interest of the international community and the progress that may be expected in the near future.

Qualification of Runway Friction Equipment

The Office of Airport Safety and Standards, Federal Aviation Administration has qualified several runway friction measuring devices. Correlation and Performance Reliability of Several Types of Friction Measuring Devices is recorded by Reference (A7), unpublished, to Reference (A9). Reference (A9) reports on the reliability and performance of friction measuring tires and equipment correlation.

This program was initiated in September 1978 with the objectives to: (1) update, expand and disseminate improved guidance material contained in Advisor Circular AC 150/5320/12 ...; (2) provide airport managers with timely input from the friction and pavement condition surveys ...; (3) increase the effectiveness of the 1982 Airport and Airway Improvement Program ...; (4) enhance safety at airports by reducing the hydroplaning potential and improving runway pavement surface friction characteristics ... . The purpose of the test program was twofold: to establish the reliability, performance and consistency of tires' quality used on friction measuring devices and to select the best performing tire(s) for use on the friction equipment.

Initially it was found that the mu number indicating the coefficient could vary by as much as 10 between tire batches because of the poor quality control. This was considered a major finding. Several parameters were used for obtaining correlation between the tires, friction

measuring equipment and the pavement. The Standard Error of Estimate (SEE) related to the mu numbers. If this value exceeded +/-3.5, the tires' rating was degraded.

The program consisted of some 1650 tests conducted on five types of surfaces with three different brands of tires and four different types of friction measuring devices. The runway surfaces were made wet with the self-wetting equipment on the devices.

The McCreary tire was found the perform best on the Runway Friction Tester (RFT), Saab Friction Tester (SFT) and the Skiddometer (SKD). The Dico tire performed best on the Mu Meter (MUM).

The report concluded the McCreary tire performed within the performance criteria established and is qualified for use on the friction devices mentioned above. The Dico tire is qualified for use on the MuMeter alone.

Description of Friction Equipment

As mentioned above the friction measuring devices were the Mu Meter (MUM), Runway Friction Tester (RFT), Saab Friction Tester (SFT) and the Skiddometer (SKD). The following descriptions are taken from Reference (A9):

Mu Meter Trailer.

The Mark 4 Mu meter is a side force friction measuring device, pulled by a tow vehicle. The trailer weighs approximately 540 lbs (240 kg) and uses a vertical load of 171 lbs (78)kg) over each of the two friction measuring tires. The friction measuring wheels were position at 7.5 degrees yaw in the test mode and produce an apparent wheel slip ratio of 13.5 percent. This test mode resulted in an included yaw angle of 15 degrees with respect to the direction of the test run. The rear wheel measures the distance traveled and provides trailer stability. Figure A1 illustrates the Mu Meter.

Saab Friction Tester Automobile

The Mark 2 Saab Friction Tester is a Saab sedan vehicle equipped with front wheel drive and an hydraulically retractable friction measuring wheel installed behind the read axle. The measuring wheel is positioned at zero degree yaw angle with respect to the orientation of the rear vehicle wheels. The friction measuring wheel arm has a chain drive connection with the vehicles rear axle and contains the torque gauge used to determine the braking friction values. The measuring wheel turns at a slower speed than the vehicle and depending on tire configuration, at a fixed slip ratio of 10 to 12 percent. A vertical load of 310 pounds (140 kg) is applied on the friction measuring wheel. Figure A4 shows an overview of the Mark 2 Saab Friction Tester Automobile.

Runway Friction Tester Minivan

The M 6800 RFT is a front wheel drive minivan with a friction measuring wheel connected to the rear axle by a gear drive producing a 13 percent fixed slip ratio. The measuring wheel

is positioned at zero degree yaw angle with respect to the orientation of the rear vehicle wheels. The friction measuring tire has a vertical load of 300 lbs (136 kg). Figure A2 show an over view of the M 6800 Runway Friction Tester Minivan.

Skiddometer Trailer

The BV-11 Skiddometer trailer is equipped with a friction measuring wheel designed to operate at a fixed slip ration of 15 to 17 percent. The measuring wheel is positioned at zero degree yaw angle with respect to the orientation of the wheels mounted on the trailer. The trailer weighs about 795 lbs (3660 kg) and consists of a welded steel frame supported by three in-line wheels, of which two operate independently of the friction measuring wheel. A vertical load of 220 lbs (100 kg) is applied to the friction measuring wheel. Figure A3 shows an overview of the BV-11 Skiddometer Trailer.

CORRELATION OF AIRCRAFT AND TEST VEHICLE FRICTION.

Scope of Testing

The most significant and comprehensive reporting of work done with runway friction measuring devices and their correlation with the friction of the aircraft friction is given by Reference (A5). This work was done with the cooperation of FAA and NASA on six different test sites during a 5-year program, and 12 grooved and ungrooved concrete and asphalt runway surfaces. Performance data for evaluation was obtained from dry, truck-wet and rain-wet, and snow-, slush-, and ice-cover conditions. Over 1100 runs were made with six different ground test vehicles -- the four mentioned above together with the Diagonal-Braked vehicle, and the runway condition reading vehicle. These vehicles are described by Figures (A7) and (A8).

Aircraft testing was also performed to obtain friction data from the aircraft for comparison with the friction data obtain with the devices. Over 200 runs were conducted with two specially instrumented aircraft, a NASA Boeing 737 and an FAA Boeing 727.

Major Findings and Conclusions

There are several factors that affect the overall friction comparison of the devices and the aircraft. These major considerations are: speed, water depth, surface type and texture, tire tread design, inflation pressure, depth of snow, and solar heating on packed snow and ice. Accounting for several of these affects can be done for specific equipment and specific runways for operation. Considering there are many nuances, as well may be expected, selected findings and conclusions are quoted from Reference (A5).

- "For wet-runway conditions, the estimated aircraft braking performance from the ground-vehicle friction measurement was within +/-0.1 friction-coefficient value of the measured values, except for some rain-wet data.

- For snow- and ice-covered runway conditions, the estimated aircraft braking performance from the ground-vehicle friction measurements was within +/-0.1 friction-coefficient value of the measured values.

- A reasonable method of estimating aircraft tire wet, snow-covered, and ice-covered runway braking performance from different ground-vehicle friction measurements has been established, and available data show good agreement.

- Tire friction measurements should be obtained for a range of rainfall rates on a given runway to identify the influence of surface water depth.

- The range of friction values measured by the different ground vehicles under compacted snow and ice-covered runway conditions could reasonably be divided into four distinct levels of braking action -- excellent, good, marginal, and poor.

- Aircraft and ground-vehicle friction measurements showed little influence of speed and type of surface for dry-runway condition."

Figures (A5) and (A6) illustrate the +/-0.1 friction coefficient conformance.

OPERATIONAL LIMITS and CONCERNS

The second of the Runway Coefficient of Friction items is to "identify operational limits and concerns in achieving the runway coefficient of friction measurement."

Operational Considerations

The objective of the high speed rollout and turnoff operation is to reduce runway occupancy time (ROT). An initial goal is to reduce ROT enough to allow two nautical mile separation for landing aircraft during peak landing periods. To achieve this goal, the ROTO operation will need a good estimate of the runway friction. Presently, the only way to measure runway friction is drive or pull a device down the runway which would require shutting down the runway to traffic. How often this would have to be down and how quickly such a measurement could be down is not known. Of course, any closure of the runway during landing operations would subtract from the capacity increase gained by ROTO operations. Thus, in order to take full advantage of ROTO operations, some non-intrusive method of measuring runway friction is desired.

If parallel runways are used one would be designated the landing runway and the other the take off runway; consequently, the friction of the landing runway, even though dry, will tend to deteriorate rapidly from mechanical wear and polishing due to tire rolling, braking and the accumulation of contaminates such as rubber and grease. Other contaminates such as water, snow, ice and slush, all cause a drastic friction loss of the pavement in a short period of time. Reference (A10) gives frequencies which friction surveys should be conducted with continuous friction measuring equipment (CFME). The recommendation is made that when 20 percent of the operation is with wide-body aircraft and the daily frequency is equal to or greater than 210, the survey should be done weekly at the end of each runway. With airports having the high-speed ROTO capability, the frequency could be considerably greater and surveys would need to be conducted even more frequently.

The ends of the runways do represent critical friction areas because of the accumulation of rubber from the spin-up of wheels, but for the high speed ROTO operation, the portions of the runway where the turn-off is performed are the most critical. If the side load imparted to the tire during turning of the airplane exceeds the available friction only for only a fraction of a second, there is a high probability control of the airplane will be lost with a resulting ground-loop! In such an accident, the damage could be considerable.

During inclement weather, the runway may be affected by water or ice contamination for only small portions or its full length. Also, the time for the contaminate to become severe can be very short. A rain squall can move across a portion of the runway or the whole runway such that a pilot landing before a squall may report braking, "excellent", and the following pilot, just a few minutes later, will report braking, "poor", because the runway had become flooded. Such conditions can be acceptable for a straight-landing braked roll-out, but when a high speed turn-off maneuver is started, the coefficient of friction must be sufficiently high to

prevent the airplane from sliding laterally. If water is present and the temperature of the runway surface is near freezing, the coefficient of friction is minimum.

Runway Surface Condition Sensor.

For the ROTO function, it is essential that the condition of the runway prior to and during the actual turn off be continuously monitored for both "dry" and potentially contaminated conditions to ensure the turn-off can be accomplished with a sufficiently high friction coefficient to support the turn.

Continuous monitoring may be accomplished with a runway surface condition sensor which meets the requirements of Reference (A2). A company, Surface Systems, Inc. (SSI), 11612 LilburnPark Road, St. Louis, MO 63146, provides a system, SCAN, which appears to fill this need. A Product Availability Search was made to find other organizations which manufactured such equipment; however, none were found during the weeks which the search was conducted.

Reference (A1) defines the conditions and limitations for Category III B operations for a straight braked-rollout. The procedures defined by this reference and the recommended usage of continuous friction measuring equipment (CFME) appear to be satisfactory for this operation. For the ROTO function, the runway surface condition sensor can alert airport operational personnel of the climatic conditions and the impending problems with water or water related contaminate in the area of turn-off. Additionally, at appropriately frequent times the area of turn off should be inspected with CFME texture measuring devices to ensure that the area is free from rubber build-up, grease of other similar contaminate that will minimize the coefficient of friction when moisture or other forms of water are present.

PRACTICALITY OF FRICTION MEASUREMENT FOR THE ROTO FUNCTION

The third of the Runway Coefficient of Friction items is for a Literature search to determine the practicality of providing a sufficiently accurate coefficient of friction measurement for the ROTO function.

For a number of years countries, other than the U. S., have used friction measuring devices to determine the quality of braking. Sufficient margin is used with the measured friction values that overrun occurrences have not been a problem. The work in the United States has been to establish precise correlation between the friction measuring device and the friction experienced by an airplane to enable slippery runway stopping distance regulatory accountability to be established. Some other countries have developed operational procedures with data obtained. The following paragraphs briefly describe the operation in Sweden and Japan.

Scandinavian Airway Systems

SAS has been working on runway friction friction measuring devices since 1948. Their first effort was merely a heavily loaded truck. This was unwieldy and inconvenient; so, a Tapely meter was placed in a vehicle from which some values of friction could be read. This approach gave only spot reading. The BV-11 Skiddometer Trailer, Figure (A3) was subsequently developed for providing continuous reading. Figure (A4) shows a modified Saab automobile (Surface Friction Tester (SFT)) to incorporate a friction measuring fifth wheel. These two devices are similar in principle since the sensing wheel has approximately 12% slip, thereby giving virtually the same reading. Reference (A6) is a paper presentation given at the recent NASA Work Shop giving some of their experience and recent developments. Figure (A9) is a copy of a chart from this paper indicating over 15 years of operational experience of reasonably reliable friction measurement.

DC-9 Scandinavian Winter Service Braking Tests

Reference (A14) documents a research program conducted by the Aeronautical Research Institute of Sweden (FAA) and Scandinavian Airlines Systems. A DC-9 aircraft was used and Douglas Aircraft Company supported the program by supplying the aircraft instrumentation and two engineers to assist in data collection and analysis.

The program consisted of 51 landings made on runways covered with snow, slush, ice, and/or water. Landing were made throughout Scandinavia. Figure (A10) is a map of the airports where landings and takeoffs were made. The runways were constructed of concrete or asphalt and friction measurements were made on each with either a BV-11 of a Tapley meter.

Figure (A11) shows the stopping distance ratio (SDR) vs the measured runway friction of the different measuring devices. The SDR is based on the values obtained on clean dry surfaces

with each device then compared with those obtained during test. The solid-line is a least square fit of all the data points friction values lower than 0.4. The standard deviation of the data is 9.1%. These results were obtained, notwithstanding the test parameters evaluated the braking efficiency of the Hydro-Aire Mark III and the Mark IIIA antiskid system, the effect of pilots' braking technique and over speed touchdown.

Stopping performance correlated well with ice and snow, but not as good with water and slush. This is to be expected because of the big variations in water depths on the runways.

The variations tested during this program will not be effective for the ROTO operation. There is a tendency for a pilot to over-speed in inclement weather and near the ground. For the ROTO operation the aircraft would be under automatic control for both touch down and braking during rollout.

Take Off and Landing Performance On Slippery Runways.

Reference (A14) is a paper presented in a DC-10 Operations Seminar. It gives the development and procedure JAL has developed and uses for take off and landing on slippery runways. They have categorized the braking action as good, medium to good, medium, medium to poor and poor and assigned measured friction readings obtained by their friction tester; then, correlated these to the friction experienced by various model airplanes on the same surfaces. This work was done by the Japan Civil Aviation Bureau (JCAB), Japan Air Lines (JAL), All Nippon Airlines (ANA) and Toa Domestic Airlines (TDA).

The categorized braking action is then used for developing landing nomograms whose elements start with the airplane weight, and continue with, braking action, wind, OAT, pressure altitude, runway slope, and ends with the landing distance. Notes on the nomograms specify aircraft configuration of full spoilers, full reverse, full brakes, and speed threshold of 1.3 V stall + 10K and maximum runway touch down distance of 2500 feet.

Turn-off Requirements

As noted earlier in the report, the airplane can be subjected to a peak lateral acceleration of 0.15 g's while turning during the ROTO operation. It seems prudent that the minimum measured coefficient of friction available on the runway would be substantially more than the peak g being experienced.

From Reference (A5), It was found for wet runway conditions the estimated aircraft braking performance from ground vehicles friction measurements was within +/- 0.1 friction coefficient value of the measured value except for some rain-wet conditions. Therefore in the vicinity of the high speed turn-off the measured friction should be above 0.25 (0.15+0.1), particularly for rain-wet conditions. However, as indicated previously, the friction in the

vicinity of the turn-off must be known at all times. This information cannot be obtained continuously with existing friction measuring equipment.

Therefore, it is suggested that correlation be developed between the friction indicated by a friction tester and the surface condition as indicated by a surface condition tester. It is probable that a highly textured surface would be desirable in the vicinity of the turn-off; notwithstanding, the extent and affects of any contamination -- water, snow, slush or ice -- must be known for safe execution of the highspeed turn-off.

CONCLUSION

The three considerations relative to the measurement of runway friction for application to high-speed ROTO have been addressed. The conclusions relative to these are as follows:

STATE OF THE ART

Much work has been done by the FAA, NASA and the International community toward the measurement of runway friction and correlation to the friction experienced by aircraft. Several different friction measuring devices have been qualified by FAA and NASA. The quality control of tires used on the equipment was found to be an important element in friction measurement This control was verified for reliability and repeatability and selected suppliers were identified. For most equipment and conditions the estimated aircraft braking performance is within +/- 0.1 friction coefficient-value of the measured values. The enables the categorization of braking conditions with reasonably accurate information, but does not provide sufficiently accurate data for regulatory stopping distance accountability.

LIMITS AND CONCERNS

For the ROTO operation, the precise prediction of stopping distance is probably not the primary concern. The two mile separation of landing airplanes precludes frequent measuring of friction with devices under tentative condition when decisions are required whether to keep the airport open of not. Also, it further precludes friction measurement with vehicles in the vicinity of the high-speed turn-off. To obtain information about the surface conditions in this vicinity, the use of the Surface Friction Condition Sensor appears to be a must. However this surface embedded device will not provide a friction value measurement. Since there is not a way to make frequent measurements under operation conditions, additional tests will be necessary to estimate the friction as indicated by the surface condition sensor reading.

PRACTICALITY OF FRICTION MEASUREMENT FOR THE ROTO

Sweden and Japan have developed procedures which have been demonstrated, through operational experience, the practicality of the using friction testers for determining the quality of braking action.

However, to accomplish the turn-off at precise locations on the runway, a minimum friction value at these locations must be known for each landing at anytime to ensure lateral control of the airplane. As indicated above additional work is required to correlated the surface condition with a measure of friction. Undoubtedly, several procedures can be developed for assuring the required level of friction exists at required locations on the runway. Highly textured surfaces and several methods of contaminate elimination are two avenues which might be explored.

REFERENCES

A1. Anon, CRITERIA FOR APPROVAL OF CATEGORY III LANDING WEATHER MINIMA, Advisory Circular No 120-28C, Federal Aviation Administration, U S Department of Transportation, 3/9/84.

A2. Anon, RUNWAY SURFACE CONDITION SENSOR SPECIFICATION GUIDE, Advisory Circular No 150/5220-13B, Federal Aviation Administration, U. S. Department of Transportation, 3/27/91.

A3. Yager, Thomas J., Vogler William A., CURRENT STATUS OF JOINT FAA/NASA RUNWAY FRICTION PROGRAM,, SAE Technical Paper Series No. 892340, SAE, 400 Commonwealth Drive, Warrendale, PA 1596-0001 USA. 9/25/89.

A4. Yager, Thomas J. Yager, Vogler, William A., and Baldasare, Paul., SUMMARY REPORT OF AIRCRAFT AND GROUND VEHICLE FRICTION CORRELATION TEST RESULTS OBTAINED UNDER WINTER RUNWAY CONDITIONS DURING JOINT FAA/NASA RUNWAY FRICTION PROGRAM, NASA TM-100506, March 1988.

A5. Yager, Thomas J., Vogler, William A. Vogler, and Baldasare, Paul., EVALUATION OF TWO TRANSPORT AIRCRAFT AND SEVERAL GROUND TEST VEHICLE FRICTION MEASUREMENTS OBTAINED FOR VARIOUS RUNWAY SURFACE TYPES AND CONDITIONS, NASA Technical Paper, February 1990.

A6. Yager, Thomas J., SUMMARY AND PROCEEDINGS DOCUMENT, FIRST ANNUAL TIRE/RUNWAY FRICTION WORKSHOP AND NASA WALLOPS FLIGHT FACILITY, NASA Langley Research Center, Hampton, VA 23681-0001, May 20, 1994.

A7. Yager, Thomas J., A SUMMARY OF RECENT AIRCRAFT/GROUND VEHICLE FRICTION MEASUREMENT TESTS, SAE Technical Series 881408, Aerospace Technical Conference and Exhibition, Anaheim, CA., 10/3/1988 to 10/6/1988.

A8. Anon, MEASUREMENT, CONSTRUCTION, AND MAINTENANCE OF SKID RESISTANT AIRPORT PAVEMENT SURFACES, Advisory Circular No: 150/5320-12B, U S Department of Transportation, Federal Aviation Administration, 11/12/91.

A9. Morrow, Thomas H., RELIABILITY AND PERFORMANCE OF FRICTION MEASURING TIRES AND FRICTION EQUIPMENT CORRELATION, Report No.

DOT/FAA/AS-90-1, US Department of Transportation, Federal Aviation Administration Washington, D. C. 20591, March 1990.

A10. Anon, AIRPORT WINTER SAFETY AND OPERATIONS, Advisory Circular AC No. 150/5200-30, U S Department of Transportation, Federal Aviation Administration, Washington DC, 4/20/88.

A11. Graul, Richard A., Lenke, Lary R., Standiford, Daniel L., RUNWAY RUBBER REMOVAL SPECIFICATION DEVELOPMENT: FINAL REPORT, New Mexico Engineering Research Institute Box 25, University of New Mexico, Albuquerque, New Mexico 87131, October 1985.

A12. Suiter, R. L., Dodge, N. A. , DC-9 SCANDINAVIAN WINTER SERVICE BRAKING TESTS, Paper No 6713, Douglas Aircraft Co., MDC, 1978.

A13. Antvik, Gunnar, Wennberg, Rolf, SWEDISH EXPERIENCE AND WORK IN MEASURING FRICTION AT AIRPORTS, PAPER PRESENTATION at NASA Tire/Runway Friction Workshop, Swedish Civil Aviation Administration, May 1994.

A14. Iwase, Capt. K. TAKE OFF AND LANDING PERFORMANCE ON SLIPPERY RUNWAYS, DC10 Operations Seminar, Japan Air Lines, Circa 1983.

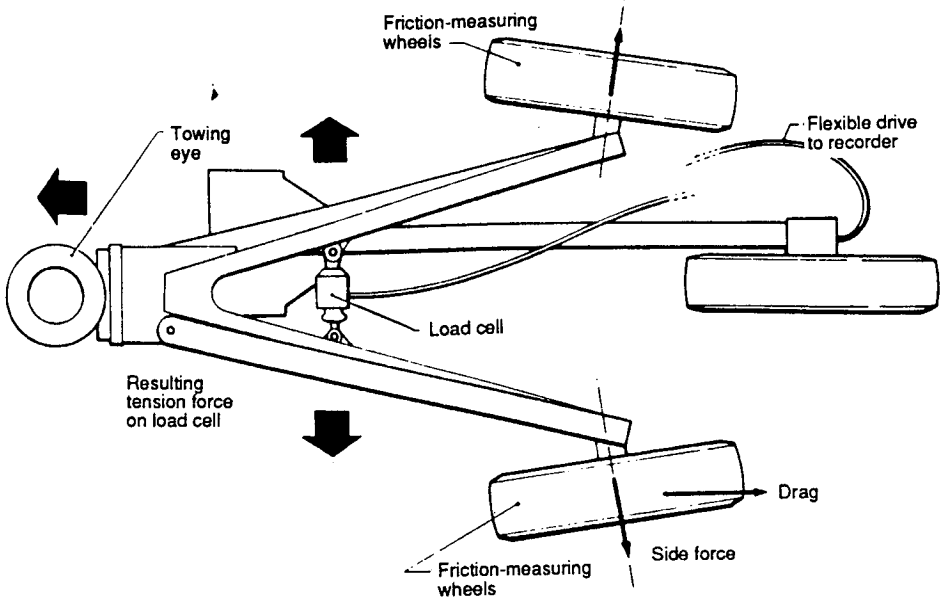

(a) Plan view without top frame.

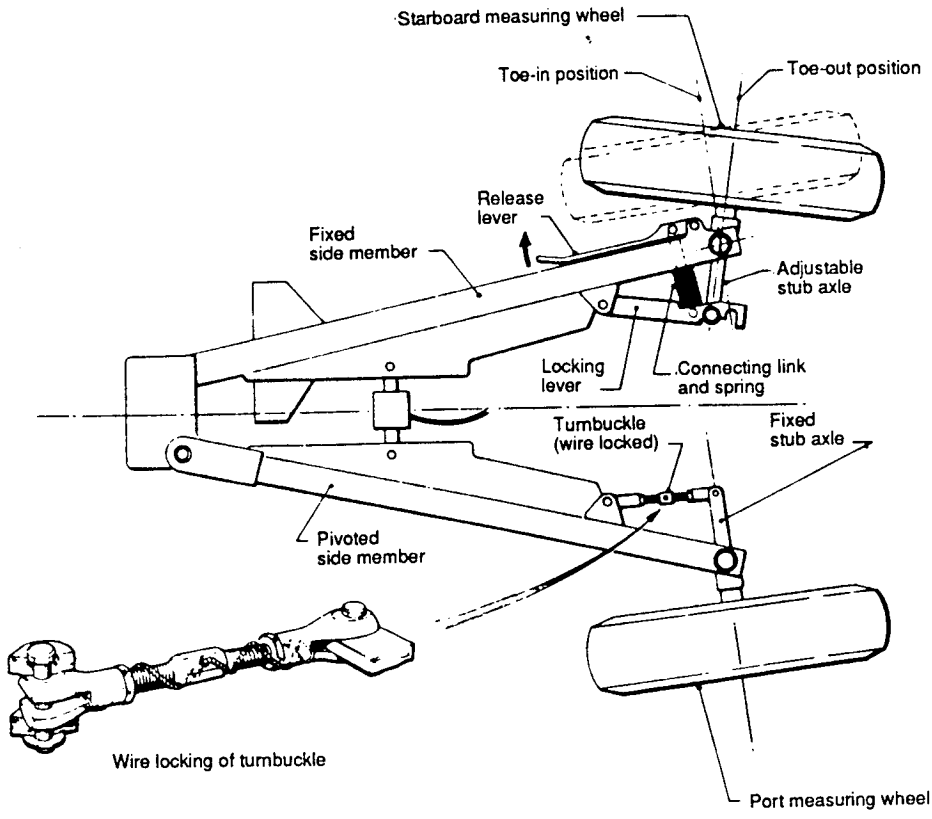

(b) Measuring-wheel settings.

Figure A 1. Features of Mu-Meter measurement system.

L-89-78

Figure A2. Runway friction tester during test run on compacted snow.

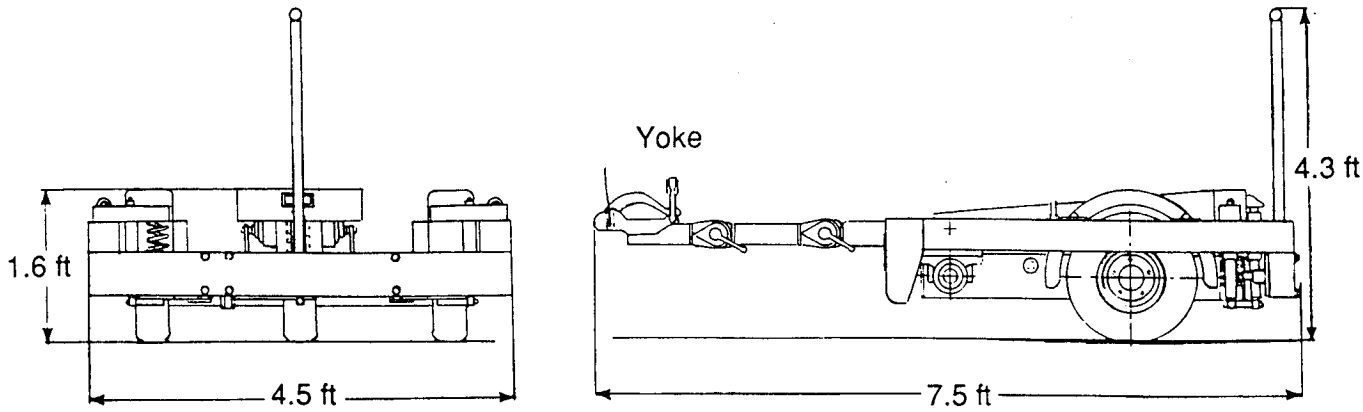

(a) Schematic.

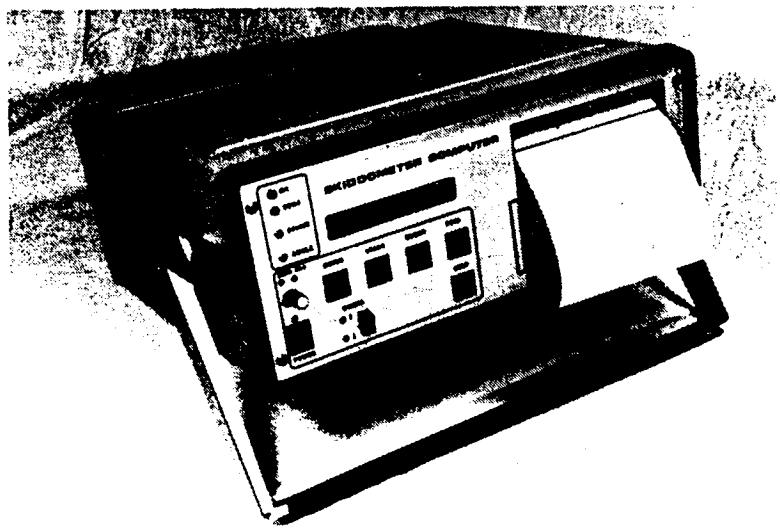

L-89-77

(b) Portable computer and recorder.

Figure A3. Trailer schematic and portable computer and recorder used with BV-11 skiddometer.

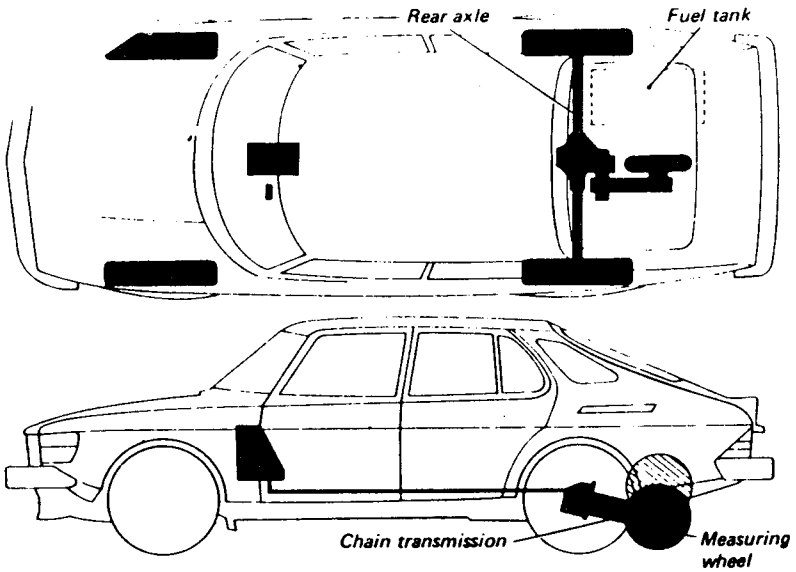

(a) Overall vehicle configuration.

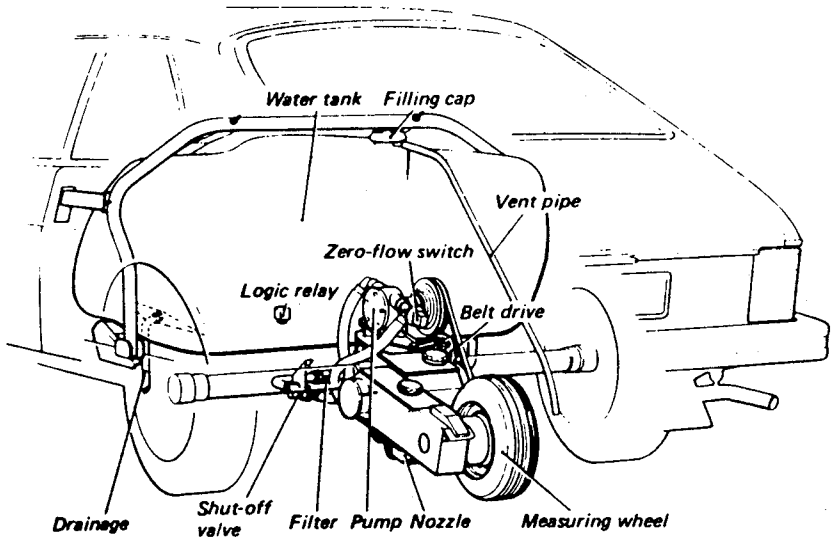

(b) Self-wetting system.

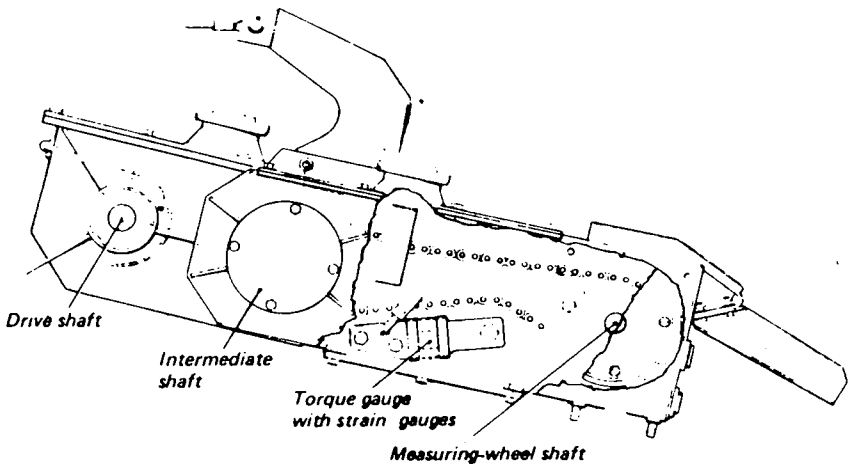

(c) Cutaway side view of measuring-wheel arm with chain drive.

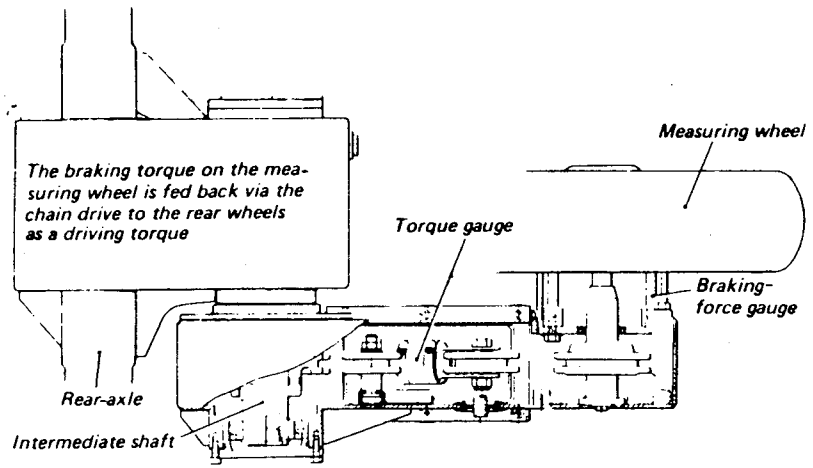

(d) Cutaway plan view of measuring-wheel arm.

Figure A4. Schematics of surface friction tester vehicle with details on self-wetting system and measuring-wheel arm.

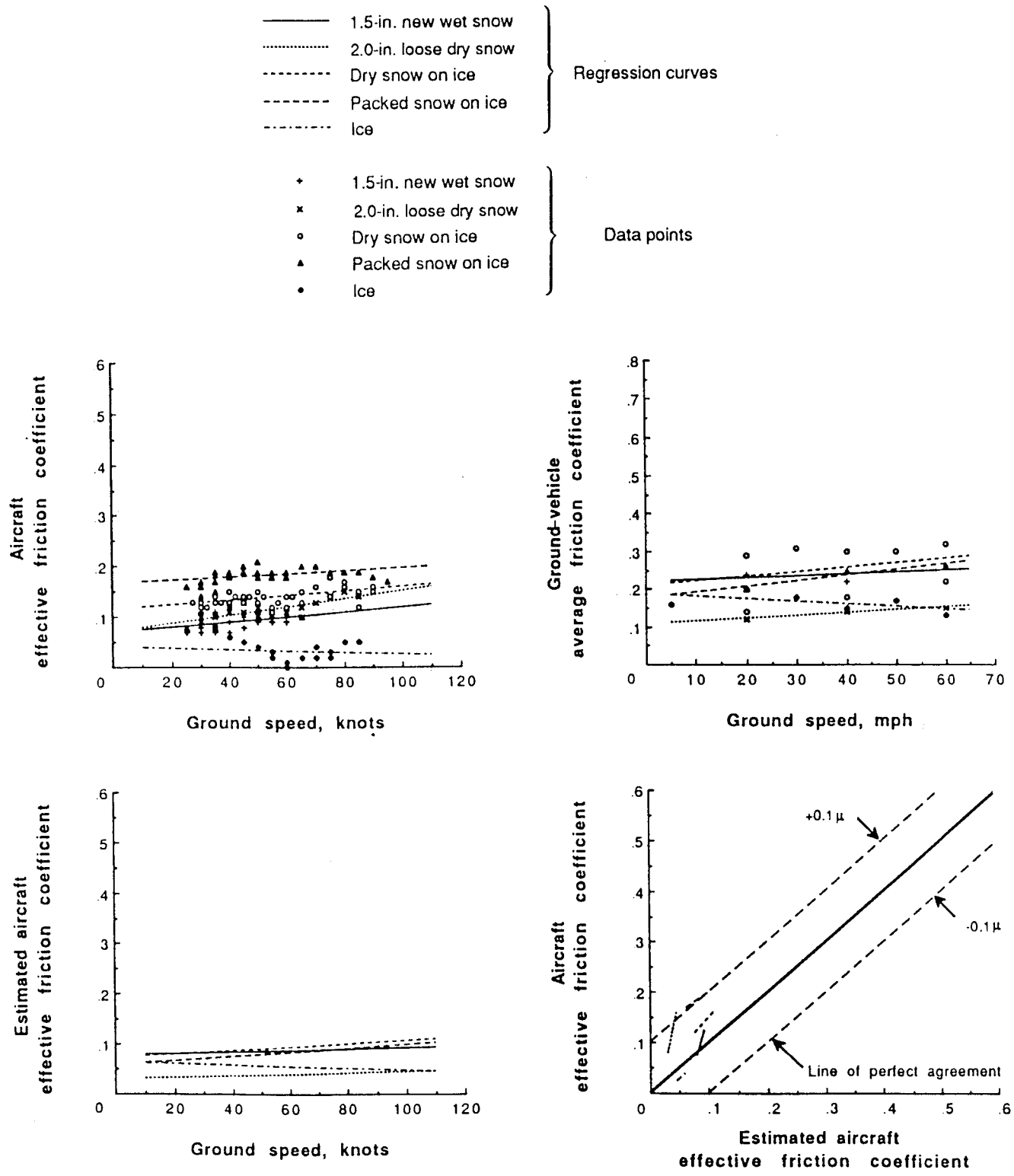

(c) BV-11 skiddometer data.

Figure A5. Variation of Boeing 727 aircraft and ground-vehicle friction data with speed and variation of estimated aircraft braking performance with actual braking performance on snow- and ice-covered runways.

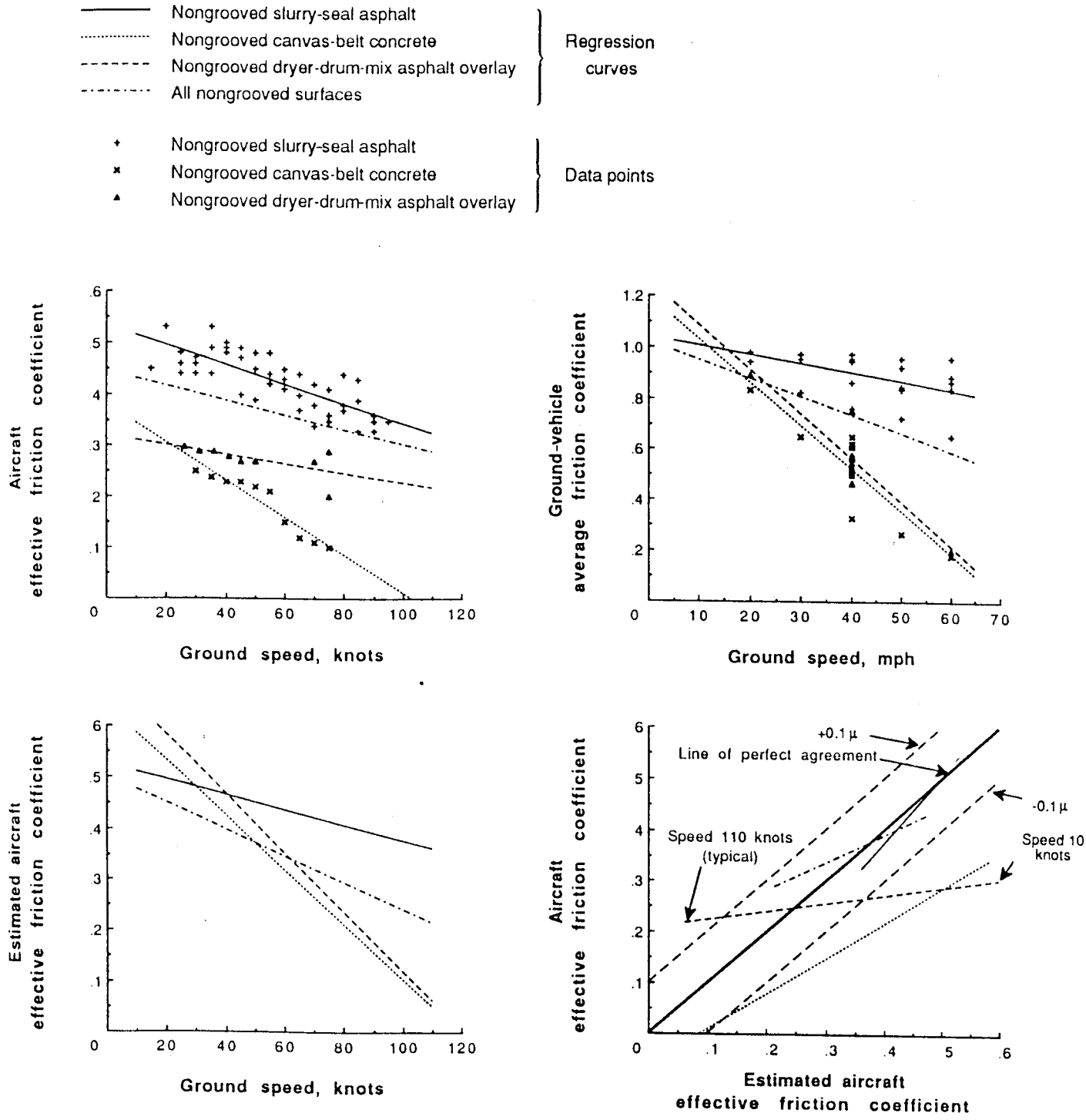

(d) BV-11 skiddometer data.

Figure A6. Variation of Boeing 727 aircraft and ground-vehicle friction data with speed and variation of estimated aircraft braking performance with actual braking performance on truck-wet, nongrooved test surfaces.

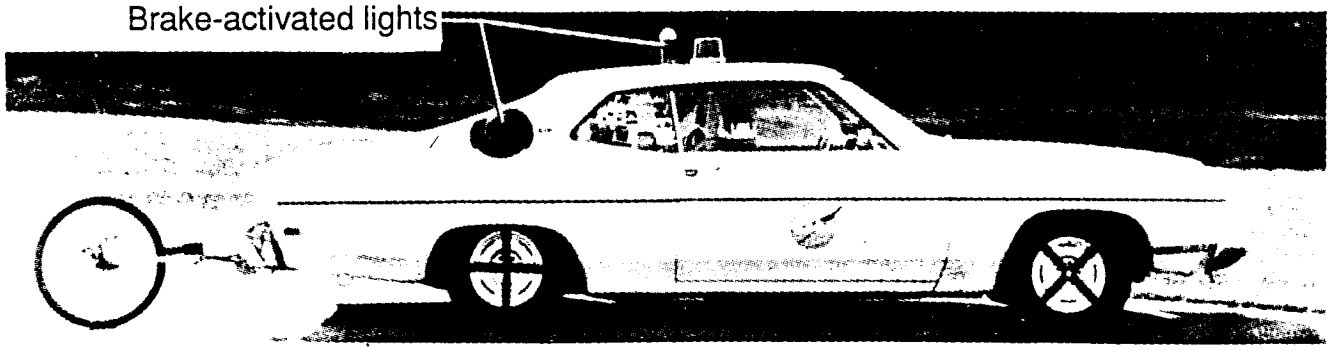

L-89-71

(a) NASA diagonal-braked vehicle.

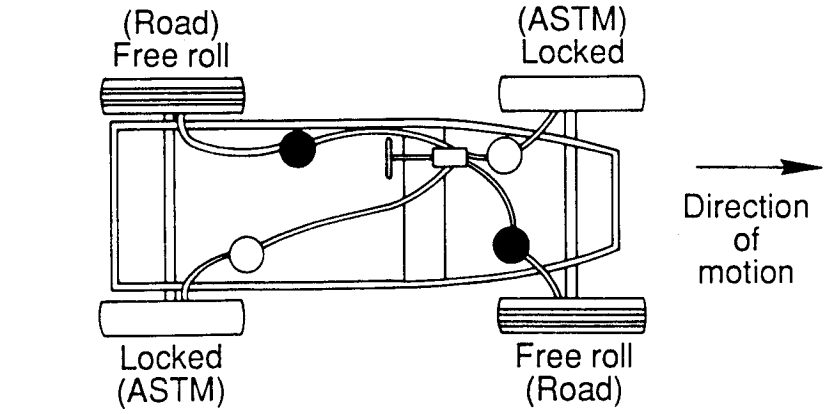

● Valve closed; brakes cannot be actuated

○ Valve open; brakes can be actuated

(b) Schematic of diagonal-braked system.

Figure A1. NASA diagonal-braked vehicle system.

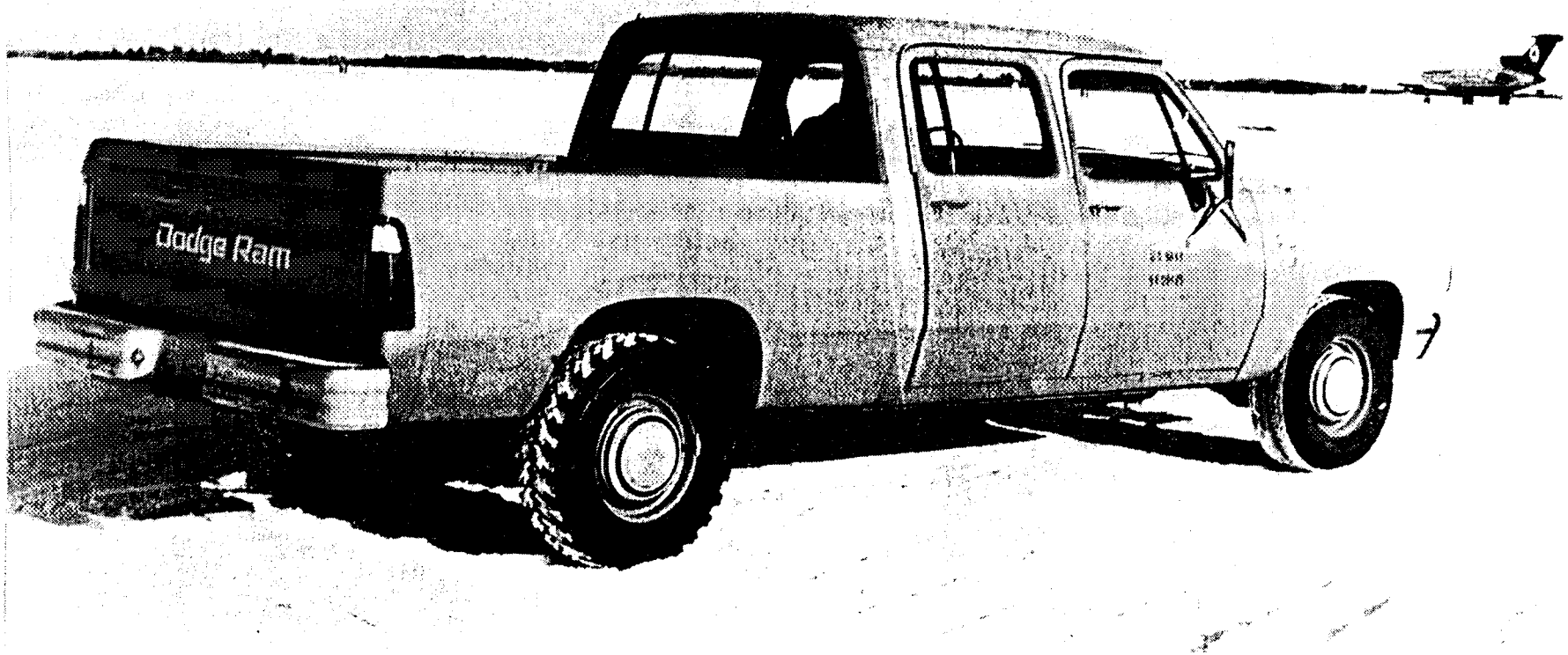

L-89-81

Figure A8. Navy runway condition reading (RCR) test vehicle.

FIGURE A9

MEASURING OF FRICTION ON CONTAMINATED R/W:S

Most types of friction measuring equipment provide unreliable results if the R/W is contaminated by any loose contamination. This is concluded by ICAO and confirmed by Swedish experience.

To overcome or at least reduce this shortcoming in the 1970's was carried out a research program in which Finland, Norway, and Sweden participated. Contractor was the Aeronautical Research Institute in Stockholm, FFA. Among airlines contributing was SAS and Braaten, Norway. Conclusion was:

Reasonably reliable friction measurement results obtained even if the R/W is contaminated by slush or snow within prescribed limits if:

1. SFT or BV-11 used for the test
2. Aero tire pressure 700K Pa (100 psi)
3. Test speed 95K m/h (60 mph)

Experience in Sweden over 15 years of operation has proved the conclusion.

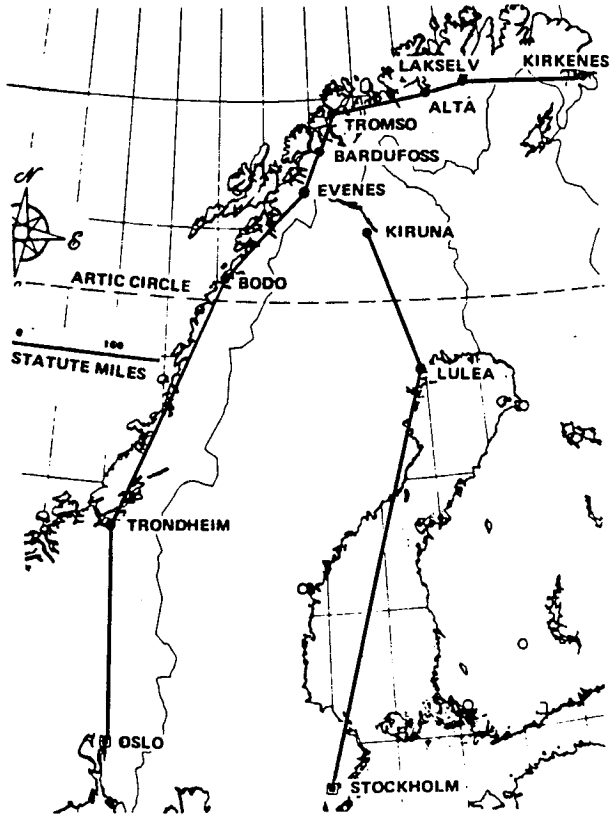

FIGURE A10. DC-9-21 SAS TYPICAL FLIGHT NORTH OF ARCTIC CIRCLE

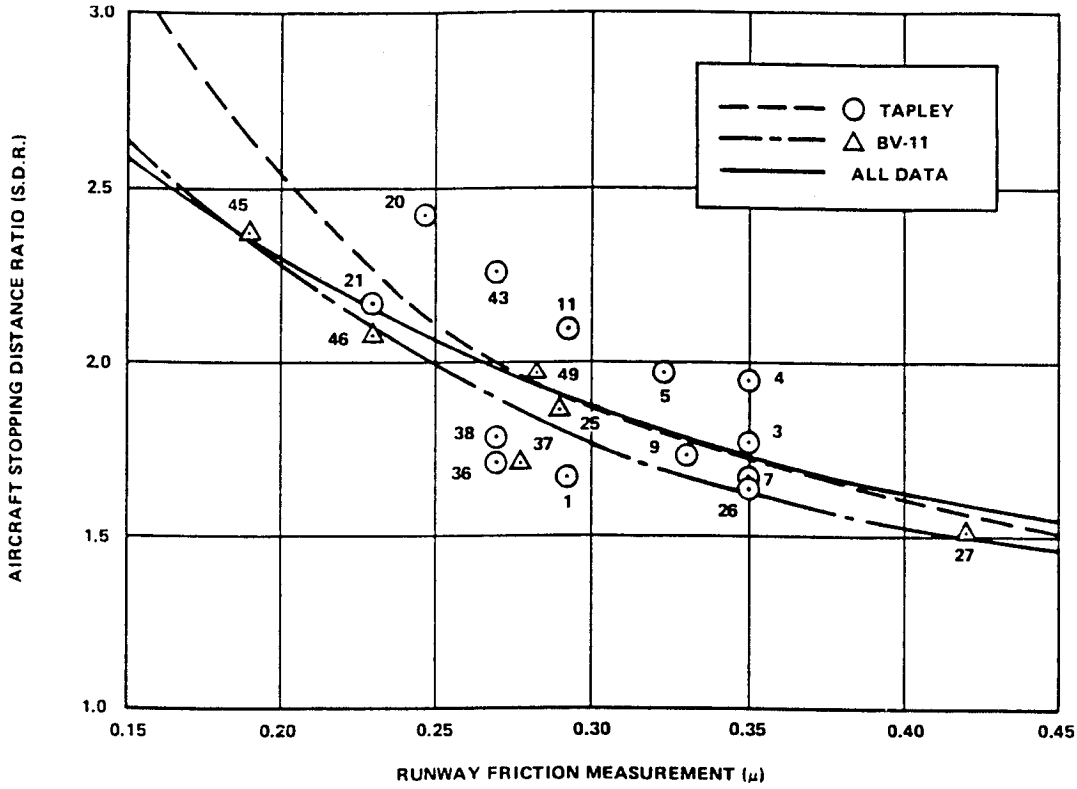

NOTE: NO. BY DATA SYMBOLS ARE ID NO. FROM FIGURE 5

FIGURE A11. AIRCRAFT PERFORMANCE CORRELATION WITH RUNWAY FRICTION MEASUREMENTS

REPORT DOCUMENTATION PAGE

Form Approved
OMB No. 0704-0188

1. AGENCY USE ONLY *(Leave Blank)*	2. REPORT DATE	3. REPORT TYPE AND DATES COVERED
	January 1995	Contractor Report

4. TITLE AND SUBTITLE
Guidance and Control Requirements for High-Speed Rollout and Turnoff (ROTO)

5. FUNDING NUMBERS
C NAS1-19703
WU 538-04-13-01

6. AUTHOR(S)
S. H. Goldthorpe, A. C. Kernik, L. S. McBee, O. W. Preston

7. PERFORMING ORGANIZATION NAME(S) AND ADDRESS(ES)
McDonnell Douglas Aerospace
1510 Hughes Way, M/C: 71-12
Long Beach, CA 90810-1864

8. PERFORMING ORGANIZATION REPORT NUMBER

9. SPONSORING/MONITORING AGENCY NAME(S) AND ADDRESS(ES)
National Aeronautics and Space Administration
Langley Research Center
Hampton, VA 23681-0001

10. SPONSORING/MONITORING AGENCY REPORT NUMBER
NASA CR-195026

11. SUPPLEMENTARY NOTES
Langley Technical Monitor: R. M. Hueschen
Final Report - Task 3

12a. DISTRIBUTION/AVAILABILITY STATEMENT
Unclassified - Unlimited
Subject Category 08

12b. DISTRIBUTION CODE

13. ABSTRACT *(Maximum 200 words)*

This report defines the initial requirements for designing a research high-speed rollout and turnoff (ROTO) guidance and control system applicable to transport class aircraft whose purpose is to reduce the average runway occupancy time (ROT) for aircraft operations. The requirements will be used to develop a ROTO system for both automatic and manual piloted operation under normal and reduced visibility conditions. Requirements were determined for nose wheel/rudder steering, braking/reverse thrust, and the navigation system with the aid of a non-real time, three degree-of-freedom MD-11 simulation program incorporating airframe and gear dynamics. The requirements were developed for speeds up to 70 knots using 30° exit geometries under dry and wet surface conditions. The requirements were generated under the assumptions that the aircraft landing system meets the current Category III touchdown dispersion requirements and that aircraft interarrival spacing is 2 nautical miles. This effort determined that auto-asymmetric braking is needed to assist steering for aft center-of-gravity aircraft. **This report shows various time-history plots of the aircraft performance for the ROTO operation. This effort also investigated the state-of-the-art in the measurement of the runway coefficient of friction for various runway conditions.**

14. SUBJECT TERMS
High Speed Rollout and Turnoff; Rollout Guidance and Control; Airport Surface Operation; Autobraking; Runway Friction Measurement

15. NUMBER OF PAGES
126

16. PRICE CODE
A07

17. SECURITY CLASSIFICATION OF REPORT	18. SECURITY CLASSIFICATION OF THIS PAGE	19. SECURITY CLASSIFICATION OF ABSTRACT	20. LIMITATION OF ABSTRACT
Unclassified	Unclassified		